

INTEGRALLY ATTACHED TIMBER FOLDED SURFACE STRUCTURES: GEOMETRICAL, EXPERIMENTAL AND NUMERICAL STUDY

THÈSE N° 8114 (2017)

PRÉSENTÉE LE 6 OCTOBRE 2017

À LA FACULTÉ DE L'ENVIRONNEMENT NATUREL, ARCHITECTURAL ET CONSTRUIT

LABORATOIRE DE CONSTRUCTION EN BOIS

PROGRAMME DOCTORAL EN GÉNIE CIVIL ET ENVIRONNEMENT

ÉCOLE POLYTECHNIQUE FÉDÉRALE DE LAUSANNE

POUR L'OBTENTION DU GRADE DE DOCTEUR ÈS SCIENCES

PAR

Andrea ŠTITIĆ

acceptée sur proposition du jury:

Prof. E. Brühwiler, président du jury

Prof. Y. Weinand, directeur de thèse

Prof. J. Schwartz, rapporteur

Dr A. Lebé, rapporteur

Prof. D. Lignos, rapporteur



ÉCOLE POLYTECHNIQUE
FÉDÉRALE DE LAUSANNE

Suisse
2017

Do not fear to be eccentric in opinion,
for every opinion now accepted was once eccentric.

— Bertrand Russell

To my parents, Ana and Franjo

Acknowledgements

First and foremost, I wish to express my deepest gratitude to my loved ones, who believed in me and encouraged me throughout my life and during my research career — my parents Ana and Franjo, to whom I owe everything I am today or ever hope to be; my sisters Monika and Sara and my brother Marko, I could not have asked for a more loving and supporting family, thank you for always being there for me.

I would also like to sincerely thank my thesis director, Professor Yves Weinand, who has given me the opportunity to do my research in a very motivating and encouraging work environment within IBOIS, EPFL. My sincere appreciation also extends to the president of the dissertation committee, Prof. Eugen Brühwiler, and the committee members, Prof. Joseph Schwartz, Prof. Dimitrios Lignos and Dr. Arthur Lebé for their valuable comments and feedback on my thesis work.

Furthermore, Monika and Sara deserve my special thanks as they so kindly spent many hours proofreading the entire text, giving me constructive and extremely appreciated advice. Monika, your support during these last four years in my both happy and sad moments meant the world to me. My wholehearted thanks also goes to Luca, for his absolute support and understanding during the writing of this thesis. To all of you, I am forever grateful.

Last but not least, I wish to thank all my colleagues and friends from IBOIS who helped me during my doctoral research with their advice and numerous constructive discussions on a wide range of topics: Ben, Sina, Christopher, Stéphane, Anh Chi, Aryan and Julien. Also, many thanks to the entire team of technical collaborators without whose assistance the experimental part of my work would have been impossible.

Lausanne, October 6, 2017

A. Š.

Abstract

In structural engineering, folded surface structures present one of the concepts for construction of self supporting column free systems. They utilize structural benefits of folding to achieve material saving and improve structural efficiency. The folding principle can be simply described as stiffening a thin surface by placing its material further away from the axis of flexure.

The application of folded surface structures in timber engineering is motivated by multiple advantages of relatively recently developed, high-performance engineered wood panel products. When used in folded systems, such panels can provide for a sustainable and lightweight solution with high load-bearing potential and high prefabrication possibilities. However, same as all timber products, these panels have limitations concerning the dimensions of the prefabricated units. These limitations are dictated by demands of transportation, assembly and, more stringently, by available manufacturing techniques. These factors influence the selection of timber structures' potential folded form, by constraining the dimensions of their discrete elements. Accordingly, structural forms with multiple elements along the span are needed for facilitating large spanning timber folded surface systems. Consisting of a large number of discrete plane elements, their realization requires proper edgewise connection details for ensuring an efficient load bearing system. For structures made of thin timber panels, this presents a great challenge when using the conventional joining techniques. For this reason, the use of timber folded structures for civil engineering applications has been very limited. However, recently, the re-discovery of *integral mechanical attachments* resulted in a new technical solution for edgewise joining of thin timber panels, which utilize digital prefabrication to integrate connectors through plate geometry.

This thesis aims to facilitate the realization of large span timber folded surface structures which use one-degree-of-freedom *multiple tab-and-slot joint* integral mechanical attachment technique. Regarding the material, the presented work concentrates on certified Kerto-Q laminated veneer lumber panels.

Taking into consideration the constraints of material, fabrication and chosen connection detail, various folded form topologies were examined for the considered application. Moreover, a relation was established between the structural form and the mentioned constraints, allowing

Abstract

for their implementation into the folded form design from the very start.

The structural behaviour of folded systems was studied by performing extensive experimental tests. The innovative test setup developed for this purpose is presented. The results of this in-depth experimental analysis provide new insights regarding the substantial influence of the semi-rigid connection details on the global behaviour of timber folded surface structures. In addition, for analysing their feasibility, the tested structures are reviewed in terms of fabrication time, assembly and on-site construction. Furthermore, based on the experimental test results, a pertinent numerical model for predicting the load bearing behaviour of the regarded structures is provided. Using finite element method the semi-rigid structural behaviour of *multiple tab-and-slot joints*, as well as the entire timber folded system, was modelled with sufficient accuracy.

Using the developed numerical models, a correlation is established between the folded surface form foldability potential and structural capacity of a static folded system. With respect to the presented findings, it is recommended that when designing timber folded surface structures, foldability of the form should be considered in addition to the previously established geometric constraints arising from material, fabrication and connection details requirements. In conclusion, a great structural potential of the proposed timber folded plate systems is recognised, and the subjects discussed within this thesis are shown to be of significant influence in establishing these structures on a building scale. The presented investigations provide a solid foundation for future works in the field of timber folded surface structures.

Key words: *timber folded surface structures, folded plate structures, timber panels, LVL, integral mechanical attachments, multiple tab-and-slot joints, folded form, foldability*

Résumé

Dans le domaine de l'ingénierie civile, les structures plissées font partie des concepts de construction ne nécessitant pas la présence de colonnes porteuses. Ils utilisent les avantages structurels du pliage pour réaliser des économies de matériaux et améliorer l'efficacité structurelle. Le principe du pliage peut être simplement décrit comme un renforcement d'une surface mince en plaçant son matériau le plus loin possible de l'axe de flexion.

L'application des structures plissées de type coque dans l'ingénierie du bois est motivée par les multiples avantages des produits récemment développés, les panneaux bois hautes performances. Lorsqu'ils sont utilisés dans des systèmes plissés, de tels panneaux peuvent fournir une solution durable et légère avec un haut potentiel de résistance et des possibilités de préfabrication élevées. Cependant, comme tous les produits bois, ces panneaux ont des limites concernant les dimensions des unités préfabriquées. Ces limites sont dictées par les exigences de transport, de montage et, plus directement, par les techniques de fabrication disponibles. Ces facteurs influent sur la sélection de la forme plissée potentielle des structures bois en contraignant les dimensions de chaque élément. Par conséquent, des formes structurelles avec plusieurs éléments le long de la portée sont nécessaires pour faciliter l'usage des systèmes plissés longue portée en bois. Composés d'un grand nombre d'éléments plans discrets, leur réalisation nécessite des détails de connexion appropriés pour assurer un système porteur efficace. Pour les structures en panneaux de bois minces, utiliser des techniques d'assemblage conventionnelles présente un grand défi. Pour cette raison, l'utilisation de structures plissées en bois pour les applications de génie civil a été très limitée. Cependant, la récente redécouverte des assemblages mécaniques intégrés a permis une nouvelle solution technique pour l'assemblage de panneaux de bois minces. Cette technique utilise la préfabrication numérique pour intégrer les connecteurs à travers la géométrie de la plaque.

Cette thèse vise à faciliter la réalisation à grande échelle des structures plissées en panneaux de bois longue portée qui utilisent des joints à rainures-languettes multiples à un degré de liberté. En ce qui concerne le matériau, le travail présenté se focalise sur des panneaux en lamibois Kerto-Q.

Compte tenu des contraintes relatives au matériau, à la fabrication et au détail de connexion choisi, différentes formes topologiques plissées ont été examinées pour l'application étudiée.

Résumé

De plus, une relation a été établie entre la forme structurelle et les contraintes mentionnées, permettant leur implémentation dans la conception de formes plissées dès le départ.

Le comportement structurel des systèmes plissés a été étudié en réalisant d'importants tests expérimentaux. Le dispositif d'essai novateur développé dans ce but est présenté. Les résultats d'une analyse expérimentale détaillée apportent de nouvelles connaissances concernant l'influence considérable des connexions semi-rigides sur le comportement global de structures plissées en bois. En outre, afin d'analyser leur faisabilité, les structures testées ont été examinées quant à leur temps de fabrication, d'assemblage et de construction. De plus, basé sur les résultats des tests expérimentaux, un modèle numérique pertinent permettant de prédire le comportement en charge de la structure considérée est présenté. En utilisant la méthode de calcul par éléments finis, le comportement structurel semi-rigide des joints à rainures-languettes multiples, ainsi que de la structure plissée en bois dans son entièreté, a été modélisé avec suffisamment de précision.

En utilisant les modèles numériques développés, une relation est établie entre le potentiel de pliability de la forme plissée et la capacité structurelle d'un système statique plissé. Selon les résultats présentés, il est recommandé pour la conception de structures plissées en bois de tenir compte de la pliability de la forme en plus des contraintes géométriques précédemment établies résultant des exigences relatives au matériau, à la fabrication et aux détails de connexion.

En conclusion, le haut potentiel structurel des systèmes plissés en bois proposés est reconnu et les sujets traités dans cette thèse ont démontré avoir une influence significative dans la conception de ces structures à grande échelle. De plus, les recherches présentées constituent une base solide pour des travaux futurs dans le domaine des structures plissées en bois.

Mots clefs : *structures plissées en bois, panneaux de bois, panneaux en lamibois, assemblages mécaniques intégrés, joints à rainures-languettes multiples, forme plissée, pliability*

Sažetak

U građevinskim konstrukcijama, složenice ili naborane pločaste konstrukcije predstavljaju jedno od rješenja za izvođenje samostojećih sustava bez stupova. Takve građevine koriste prednosti površinskih nabora kako bi doprinjele uštedi materijala i poboljšale konstrukcijsku učinkovitost. Pod principom nabiranja podrazumijevamo ukrućenje tanke površine postavljanjem njezinog materijala dalje od osi savijanja.

Mnogobrojne prednosti relativno nedavno razvijenih ploča na bazi drveta visokih performansi pokrenule su primjenu složenica u drvenim konstrukcijama. Pri korištenju u takvim sustavima, ploče na bazi drveta pružaju održiva rješenja male težine i velike nosivosti te visoke razine predgotovljenosti. Međutim, jednako kao i ostala drvena građa, spomenute ploče ograničene su dimenzijama predgotovljenih proizvoda. Navedena ograničenja određena su zahtjevima transporta, montaže, te raspoloživim tehnikama proizvodnje. Svi ti faktori utječu na odabir forme naborane površine ograničavanjem dimenzija njenih pojedinih elemenata. Shodno tome, za izvođenje drvenih naboranih pločastih konstrukcija velikog raspona potrebno je koristiti konstrukcijske forme s više elemenata duž raspona. S obzirom na velik broj pojedinačnih plošnih elemenata, ostvarivanje takvih konstrukcija zahtjeva specifične detalje rubne veze potrebne za osiguravanje učinkovitog prijenosa opterećenja. Za konstrukcije sastavljene od tankostijenih ploča izvođenje takvih detalja veza korištenjem konvencionalnih tehnika spajanja predstavlja brojne poteškoće, te je upotreba drvenih pločastih naboranih konstrukcija u visokogradnji iz tog razloga bila ograničena. Ipak, u novije vrijeme, ponovna upotreba integralnih klasičnih drvenih spojeva dovela je do novog tehničkog rješenja za rubno spajanje tankostijenih predgotovljenih drvenih ploča korištenjem veza integriranih u geometriju ploče. Cilj ove disertacije je omogućavanje izvedbe drvenih naboranih pločastih konstrukcija velikog raspona koje koriste integrirane veze na utor i pero s jednim stupnjem slobode. Materijal na koji se fokusira dani rad su certificirane Kerto-Q ploče od lameliranog furnirskog drva (LVL). Uzimajući u obzir ograničenja samog materijala, proizvodnju i izabrane detalje spajanja, ispitane su različite topologije naborane forme kako bi se bolje proučila razmatrana upotreba. Pronađen je odnos između konstrukcijske forme i spomenutih ograničenja, što je omogućilo njihovu implementaciju u dizajn površine naborane forme od samoga početka.

Ponašanje naboranih pločastih sustava pod opterećenjem istraživano je izvođenjem opširnih

eksperimentalnih testiranja. U tu svrhu razvijen je i inovativan sustav testiranja, također prezentiran u ovom radu. Rezultati ove opsežne eksperimentalne analize predstavljaju nove uvide u značajan utjecaj polukrutih spojnih detalja na ponašanje drvenih naboranih pločastih konstrukcija na globalnoj razini. Za analizu isplativosti, testirane konstrukcije promatrane su u vidu vremena proizvodnje, montaže te postavljanja na mjesto gradnje. Nadalje, bazirajući se na rezultatima testova, razvijen je i numerički model za predviđanje nosivosti razmatranih konstrukcija. Ponašanje polukrutih konstrukcija s integriranim vezama, kao i cjelokupnog konstrukcijskog sustava, modelirano je sa zadovoljavajućim stupnjem točnosti korištenjem metode konačnih elemenata.

Koristeći se razrađenim numeričkim modelima, usvojena je međuovisnost naborane površinske forme odnosno njezinog inherentnog potencijala sklapanja te nosivog kapaciteta naboranog pločastog statičkog sustava. Pri projektiranju drvenih naboranih pločastih konstrukcija preporuča se uzeti u obzir naboranost forme zajedno uz sva ostala, već spomenuta, geometrijska ograničenja koja proizlaze iz potrebe materijala, proizvodnje te detalja spajanja.

Ovim istraživanjem prepoznat je izniman nosivi potencijal predloženih drvenih naboranih pločastih konstrukcija, te su predmeti rasprave ove teze od iznimne važnosti za implementaciju spomenutih konstrukcija u visokogradnji. Predstavljeni rad predstavlja čvrst temelj za buduća istraživanja kako u drvenim tako i u ostalim vrstama naboranih pločastih konstrukcija.

Ključne riječi: *drvene naborane pločaste konstrukcije, složenice, ploče na bazi drveta, LVL, integralni klasični drveni spojevi, veze na utor i pero, forma naborane površine, sklapanje*

Contents

Acknowledgements	i
Abstract (English/Français/Hrvatski)	iii
List of figures	xiii
List of tables	xvii
1 Introduction	1
1.1 State of the Art: Folded Surface Structures	4
1.1.1 A Brief Overview	4
1.1.2 Use of Timber in Folded Surface Structures	9
1.1.3 Connection Details for Edgewise Joining of Thin Timber Panels	14
1.1.4 Experimental techniques	18
1.1.5 Structural analysis	19
1.2 Problem statement	22
1.3 Objectives	23
1.4 Scope	24
2 Topological and Structural Considerations	27
2.1 Introduction	27
2.2 Topology of the Folded Form	28
2.3 Structural Constraints	31
2.3.1 Joint Constraints	31
2.3.2 Geometry of the Structures	31
2.4 Structural Behaviour of Folded Surface Structures	34
2.4.1 Structural Analysis - Geometry of the Structures	35
2.4.2 Structural Analysis - Finite Element Model	38
2.5 Study Case - Observations on a Prototype Structure	40
2.6 Conclusions	44

Contents

3	Experimental Investigations	47
3.1	Introduction	47
3.2	Structure Design	49
3.2.1	Material	49
3.2.2	Global Geometry	49
3.2.3	Connection Details	49
3.2.4	Digital Fabrication and Assembly	52
3.2.5	Geometry Generation	52
3.2.6	Fabrication Data Generation	55
3.3	Preliminary Connection Detail Tests	56
3.3.1	Connections With Adhesive	58
3.3.2	Connections Without Adhesive	58
3.4	Large Scale Structure Tests	61
3.4.1	Test Setup	62
3.4.2	Instrumentation and Loading Procedure	64
3.5	Results	66
3.6	Discussion	77
3.7	Conclusions	81
4	Numerical Modelling	83
4.1	Introduction	83
4.2	Experimental Investigations Revisited	84
4.2.1	Results	86
4.3	Numerical Modelling	87
4.3.1	Finite Element Type Study	90
4.3.2	Mesh Convergence Study	93
4.3.3	Connection Detail Modeling	93
4.4	Results and Discussion	105
4.4.1	Comparison to the rigid connection model	109
4.5	Conclusions	109
5	Foldability of the Form with Respect to Structural Performance	113
5.1	Introduction	113
5.2	Rigid Foldability	114
5.2.1	Foldability range	116
5.3	Structural Analysis	124
5.4	Correlating Foldability and Structural Behaviour	127
5.5	Conclusions	133

6 Conclusion and Outlook	135
6.1 Conclusions	135
6.2 Outlook	139
Bibliography	148
Curriculum Vitae	149

List of Figures

1.1	Timber folded surface prototype, A. Stitic, IBOIS, EPFL	3
1.2	Folding principle explained on a paper model	4
1.3	Example of rigid-foldable origami structure by T. Tachi	6
1.4	Unesco Conference building, Paris, France	6
1.5	Miami Marine Stadium, Miami, USA	7
1.6	Folded forms as proposed by Z.S. Makowski	8
1.7	Sulphur Extraction Factory, Pomezia, Rome, Italy	8
1.8	Anette-Kahn Student Residence, Tübingen, Germany	11
1.9	International Architecture Exhibition (IBA) roof structure, Berlin, Germany . .	12
1.10	Music Rehearsal Hall, Thannhausen, Germany	13
1.11	Chapel St. Loup, Pompaples, Switzerland	14
1.12	Origami inspired plywood prototype, H. Buri, IBOIS, EPFL	15
1.13	Variations of multiple tab-and-slot joint geometry	16
1.14	Multiple tab-and-slot joint constraints	17
1.15	Examples of loading systems designed for applying surface load	18
1.16	Erection and experimental testing of a folded surface prototype realized by B.S. Benjamin and Z.S. Makowski	19
1.17	Folded surface prototype realized by P. Huybers	20
1.18	Two-way action in a folded plate system	21
2.1	Classification of folded surface structures	29
2.2	Minimal value of the apex angle, β , and the maximal value of the assembly direction deviation for the rhombus, anti-prism and trapezoid-based folded form	32
2.3	Geometrical parameters of the anti-prismatic folded form	32
2.4	Single isosceles triangle element	33
2.5	Minimal and maximal span-to-rise ratio of a regular anti-prism based form . .	34
2.6	Load bearing behaviour of a single fold, combination of the slab and plate effect	35
2.7	Transversal cross section and perspective view of the anti-prism, trapezoid and rhombus based structure	37

List of Figures

2.8	Vertical displacements along a normalised span of the anti-prism, trapezoid and rhombus based structure	39
2.9	Deviation of folded form central line from the equivalent smooth shell funicular curve	40
2.10	Connection detail in a two panel assembly	41
2.11	Edge-to-edge connectivity between the faces for anti-prism based folded form and isosceles trapezoid version.	42
2.12	Assembly of the prototype structure	43
2.13	Testing and failure of the timber folded surface prototype	43
2.14	Load-displacement curve for the tested prototype structure	44
3.1	Test setup devised for approximating uniformly distributed surface load	48
3.2	Large scale structure geometry parameters	50
3.3	Test details geometry parameters	50
3.4	MTSJ plate insertion vectors and assembly sequence of the chosen folded form	51
3.5	MTSJ generator in Grasshopper	54
3.6	Test setup for connection detail bending tests	56
3.7	Moment-rotation curves and stiffness of connection details used within experimental tests	59
3.8	Failure of adhesively bonded connections	60
3.9	Failure of MTSJ connections without adhesive	60
3.10	One-faced finger joint geometry	61
3.11	Test setup	63
3.12	DIC system setup	65
3.13	DIC system view from left and right camera	65
3.14	Speckle pattern with speckle sizes between 1 – 5mm	67
3.15	Loading procedure	67
3.16	Test loading process, separated according to the defined seven loading steps . .	68
3.17	Large scale experimental test total load vs. midspan displacement	70
3.18	Displacement fields of each of the tested structure type unfavorable replicate, shown at the moment when the total load on the structure amounted to 25kN	71
3.19	Total load vs. midspan displacement graph and failure propagation for adhesively joined structure type	72
3.20	Total load vs. midspan displacement graph and failure propagation for open slot MTSJ structure type	73
3.21	Total load vs. midspan displacement graph and failure propagation for closed slot MTSJ structure type	74

3.22 Loss of structural integrity in adhesively joined structures after point (D) and detail of edge after failure	75
3.23 MTSJ failure modes	76
3.24 Total load and rotation of supports vs. normalized time shown on the example of MTSJ open slot replicate 3	77
3.25 MTSJ with closed slots, failure along the middle of the loaded plate bottom face	78
3.26 MTSJ open and closed slot contact faces pairs	80
4.1 MTSJ closed slot large scale structure geometry parameters	85
4.2 MTSJ closed slot connection details parameters	85
4.3 Total load vs. midspan deflection of the 3 replicates and elastic part and stiffness, k , representing the entire group	87
4.4 MTSJ open slot structure, displacement and strain field of a single mid-fold plate, shown at the moment when the total load on the structure amounted to $25kN$	88
4.5 Comparison between strain gauge SG_3 e_{xx} data with the DIC strain measurements at the same point	89
4.6 Material orientation of LVL panels	90
4.7 Element type vertical displacement results for one isolated triangular plate and total computation time needed for the analysis	91
4.8 Mesh seed size convergence with respect to displacement results, relative displacement error of the consecutive refinement and total computation time needed for the analysis	94
4.9 Schematic of numerical modelling of timber plates and MTSJ details	95
4.10 Experimental setup side support detail	96
4.11 Influence of secondary moments introduced by heavy supports	96
4.12 Influence of gravity load on the rotations of the simplified curved shell structure	97
4.13 Strip model and spring model geometry representation within ABAQUS	99
4.14 Strip element model for the derivation of the bending stiffness, k_m	100
4.15 Strip element model for the derivation of the axial stiffness, k_n	100
4.16 Strip element model for the derivation of the shear stiffnesses, $k_{v,12}$, $k_{v,13}$ and $k_{v,23}$	101
4.17 Maximum vertical displacement of a spring model using different number of spring sets per group representing individual tabs of MTSJ.	106
4.18 Comparison of experimental and numerically obtained results. Total load vs. maximum vertical displacement	107
4.19 Comparison of experimental and numerically obtained results for $25kN$ total load	108
4.20 Comparison of experimental and numerically obtained strain results	110

List of Figures

4.21 Comparison of semi-rigid and rigid spring model results with experimental tests. Total load vs. maximum vertical displacement	111
5.1 Foldability and the transformation paths of a simple form including one fold unit consisting of two quadrilateral plate elements	115
5.2 Foldability range of the St. Loup Chapel form	118
5.3 Foldability range of the Thannhausen Music Rehearsal Hall form	119
5.4 Foldability range of the Thannhausen Music Rehearsal Hall modified form . . .	120
5.5 Foldability range of the Yoshimura pattern folded form and its modified version obtained by dynamic relaxation	121
5.6 Dynamic relaxation of the Yoshimura pattern connectivity	122
5.7 Global descriptor G_{Ω} values for initial and two extreme states of the observed forms	123
5.8 Geometry of the numerically modelled structures	126
5.9 Bending moment about local $-x$ axis of the plates, M_x , in the section defined by plane A	127
5.10 Bending moment about local $-y$ axis of the plates, M_y , in the section defined by plane B	128
5.11 Bending moment about local $-y$ axis of the plates, M_y , in the section defined by plane C	129
5.12 In-plane compression (-) and tension (+) forces exerted on the connection repre- senting strips, in local $-y$ axis of the plates	130
5.13 Comparison of TO and TR structure results	131
5.14 TO and TR structure reaction force and resulting rotation directions at the roof- wall interface	132
5.15 Roof-wall plate interface detail displacement in the global $-x$ axis direction . .	133
6.1 Vidy Theater Pavilion, Lausanne, Switzerland	138

List of Tables

1.1	Overview of engineered wood panels	10
3.1	MTSJ Generator Program	54
3.2	Plate Fabrication Program	55
3.3	Test geometry of connection details joined using adhesives	57
3.4	Test geometry of connection details joined without using adhesives	57
3.5	Comparison of results of three different large scale structure types	69
3.6	Fabrication and assembly time for each of the tested large scale structure type .	81
4.1	Elastic properties used for orthotropic material model of Kerto-Q 21 mm panels	91
4.2	Strip element model, estimated stiffness parameters per strip unit length	104
4.3	Spring model, estimated stiffness parameters per tab of the MTSJ closed slot connection	105

1 Introduction

The increasing necessity for clear and wide span structures during the 20th century lead to the design and development of new various forms, span systems and materials, by architects and engineers wishing to meet those needs. When deciding on the structural system for construction of a free spanning structure, not only did the width of the span or the ceiling height needed to be considered but also the architectural form and image of the building. Certain requirements and restrictions along with advantages and disadvantages of the chosen system had to be well examined. For example, shape of the structure and material characteristics, namely strength, stiffness and weight. Furthermore, taking into account erection time, transportation, workmanship and availability of the material, all of which influence the total cost of construction, was essential for the final decision.

A very general classification of free spanning structures can be done depending on their geometry, onto skeletal and surface structures [25, 30]. Skeletal structures are composed of linear or curved elements arranged in a way to form stable systems. For example, spatial structures such as grid shells, or two-dimensional systems such as beams, trusses, arches, frames etc. In such structures the dimensions of the element cross-section are small in comparison to the span. On the other hand, surface structures are characterized by a very small thickness in relation to their other dimensions. Depending on the material used, surface structures can be considered flexible or rigid. Materials such as canvas or vinyl make up flexible surface structures, usually for temporary use, while the rigid ones are used for more permanent structures and are constructed from materials such as concrete, steel and timber. Surface structures include tensile membranes, shells and folded plates, systems that can be highly efficient if designed based on their underlying structural principles. They derive their stiffness from folds or curvature, or in the case of membranes, from prestressing, which enables them to use a minimal amount of material for spanning large distances. Furthermore,

they provide an integral way of construction as they can act both as a load-bearing structure and cladding at the same time, which makes them advantageous over other structural systems. However, as opposed to flexible surface structures which have enjoyed continued interest since their introduction into architecture in the 1940's, after experiencing an initial boom in the 1960s, interest in designing and constructing rigid surface structures has been on the decline. The nondecreasing popularity of flexible surface structures can be explained by the continuous development of new materials, such as fluoropolymer films, for example, which keep broadening their design scope [14]. On the contrary, construction of rigid surface structures which were mainly designed for and realized in reinforced concrete, included a complex and labour-intense formwork for on-site casting of curved shells and problems of efficient joining technique for connecting prefabricated elements in folded plates structures [49]. Furthermore, the industrialization of the building industry and its products which brought the possibility for cost effective construction through the repeated use of industrially produced components, increased the demand for skeletal systems as they are made from discrete elements which can be easily prefabricated and connected on-site.

However, recently, as a result of latest developments of cutting-edge digital design techniques, new material technologies and powerful computer-numerically controlled (CNC) manufacturing methods, major impulses for the design and construction of rigid structural surfaces have reappeared. The hallmark of this new “digital” age is a strong tendency towards individualisation and optimised use of materials and resources. It is noteworthy that the timber sector, due to the lightweight nature of timber, its ecological advantages and high prefabrication possibilities, has been pioneering the digital age in the building industry over the last two decades [83]. According to [82] the timber construction market is continuously growing in all of Europe, even on those markets where building construction in other materials is currently decreasing. Because of its highly flexible nature, aforementioned technological developments, low cost rates and consideration of aesthetic appeal, structural timber has become a sustainable alternative for constructing medium and long span surface structures. Engineered wood panel products, such as Cross-Laminated Timber (CLT) and Laminated Veneer Lumber (LVL) can now offer a lightweight and integral way of construction, by fulfilling a supporting as well as covering function. By providing very good mechanical properties and high prefabrication possibilities, their high load-bearing potential and strength to weight ratio, combined with structural benefits obtained by surface folding, can allow for realization of very efficient structural systems.

Within this field, Laboratory for Timber Constructions (IBOIS) at Ecole Polytechnique Federale de Lausanne (EPFL) has initiated interdisciplinary research dealing with both the architectural and structural aspects of folded structures made from timber. The main objective of this

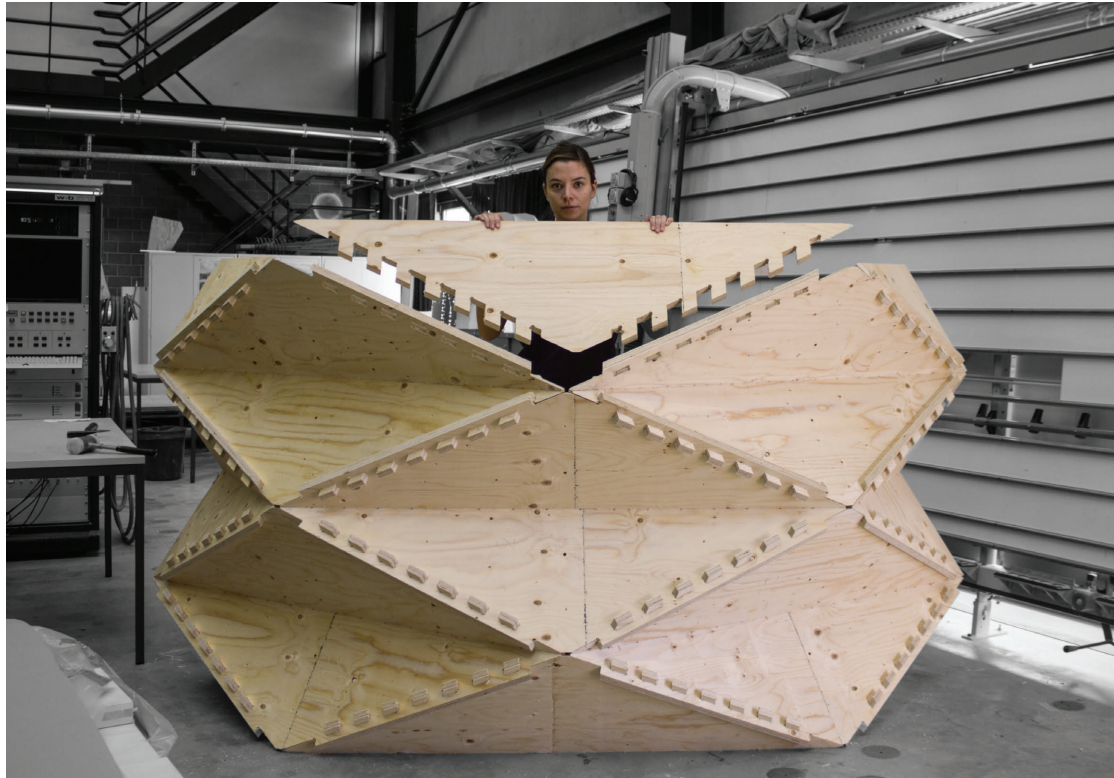


Figure 1.1 – Timber folded surface prototype with closed slot multiple tab-and-slot joints, A. Stitic, IBOIS, EPFL, 2016.

research is to explore architectural forms for timber folded systems as well as study their structural behaviour and feasible connection details. As a result, structures which to the full extent combine the structural advantages of timber panels as a material with the efficiency of folded surface structures are obtained (Fig. 1.1). Since great structural potential of timber folded surface systems has been recognized in previous studies as well as in herein performed experimental tests, the issues discussed within this research are considered to be of significant influence in establishing these structures on a building scale.

1.1 State of the Art: Folded Surface Structures

1.1.1 A Brief Overview

Within the scope of rigid surface structures, folded plate systems in structural engineering present one of the concepts for construction of self supporting, column free systems. They employ the structural potential of the folding principle with regard to material saving and structural efficiency. By placing the material further away from the axis of flexure, i.e. folding, the moment of inertia is increased which inherently leads to higher structural stiffness (see Fig. 1.2). The common terminology for describing structures which utilize the benefits of folding usually employs *folded plates*, *folded slabs* or *corrugated structures*. However, such structures are composed of discrete, inclined plane structural surfaces, where the load bearing behaviour combines both a slab and a plate mechanism. These individual surfaces are then joined together to form a globally folded surface form, which is why the terminology *folded surface structures* proposed by [78] is preferred and will be further used.

Rigid folded surface structures can be divided into two groups depending on their kinematic potential and the use of folding principle: 1) kinematic or deployable; and 2) static folded structures, both made of individual solid plates positioned at different angles in space, mutually connected along their adjoining edges.

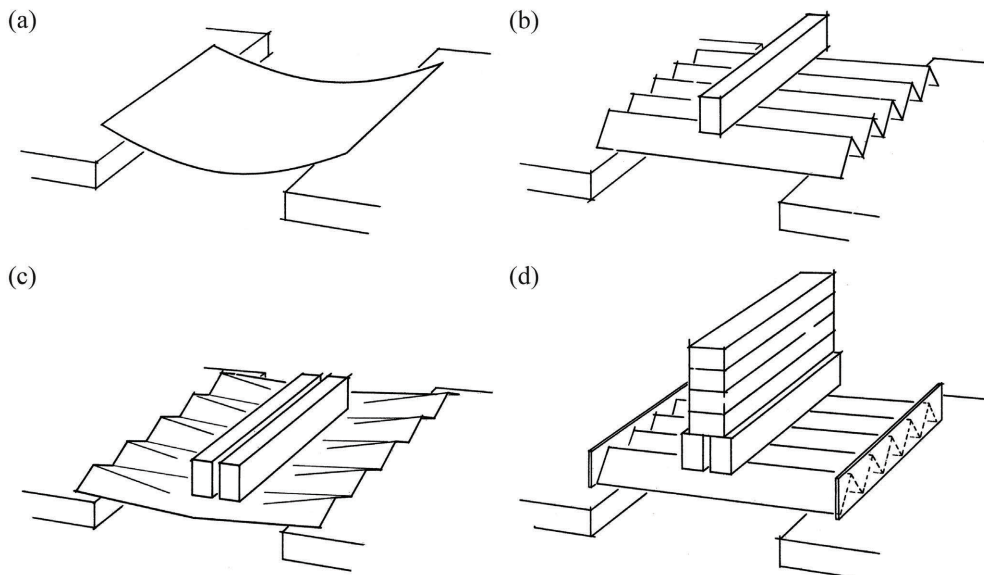


Figure 1.2 – Folding principle explained on a paper model; (a) A single sheet of paper bends without any load; (b) When folded it can support load; (c) When overloaded the folds get distorted; (d) End restrains stiffen the folds and increase the bearing strength [79].

First group containing deployable (kinematic) structures takes advantage of folding to form structures that can be transformed from a closed compact configuration to a predetermined, expanded form, in which they are stable and can carry loads [35] (see Fig. 1.3). In this regard hinged joints along the folds are realized for enabling movement by rotation. The plates themselves are rigid and during the deployment remain completely flat and their edges remain straight, i.e. only deployable structures made of rigid surface elements are considered here. As these structures are mechanisms, when reaching the designated final form they need to be blocked from further movement, by additional stabilizing elements and/or supports, in order for the folds to start behaving as load bearing.

As the folding potential and therefore the final compactness of these structures depend exclusively on the used form, their main inspiration was found in the art of paper folding, *origami*, where the transformation between an original flat form to the final polyhedral one is implemented purely via bending around the paper creases, i.e. without in-plane (stretching) deformation [62]. Many in-depth studies have been conducted on feasible forms and their geometric requirements which would allow for them to be applied to rigid deployable folded surface structures, some of the pioneering work includes [60, 31, 89, 39, 38]. Different structural applications and materials have also been studied, ranging from mobile shelter structures [87] to the ones intended to be deployed in space [61], from cardboard [46] all the way to concrete origami prototype with thin plates and a continuous steel mesh [19].

The second group contains static folded structures, which use the structural benefits of folding for achieving higher structural height and therefore better load bearing capacity while using thinner cross sections. Compared to the first group of structures, such structures have completely opposite requirements for their connection details. In order to remain stable they need to have joints which provide a certain level of rigidity to the system. First examples of static folded structures were built at the beginning of the 20th century, as a result of new constructive opportunities that arose with the appearance of reinforced concrete.

Some of the most prominent examples include *The Unesco Conference building* in Paris (1953) designed by architects M. Breurer and B. Zehrfuss, together with P. L. Nervi as the project structural engineer, as well as their 1961 project for a church at *St. John's Abbey*, a Benedictine monastery in Collegeville, Minnesota (Fig. 1.4) This kind of *structural architecture* where the optimization of single concrete plate structure is achieved by folding, is best illustrated on the example of Miami Marine Stadium (1963) which at that time, with its 100 meter folded plate roof, was the longest span of cantilevered concrete ever realized (Fig. 1.5).

Building of structures such as those shown above, presented very complex and intensive manual work which included intricate and heavy scaffolding for cast-in-place concrete and heavy erection equipment for precast concrete elements (see Fig. 1.5 right). This largely

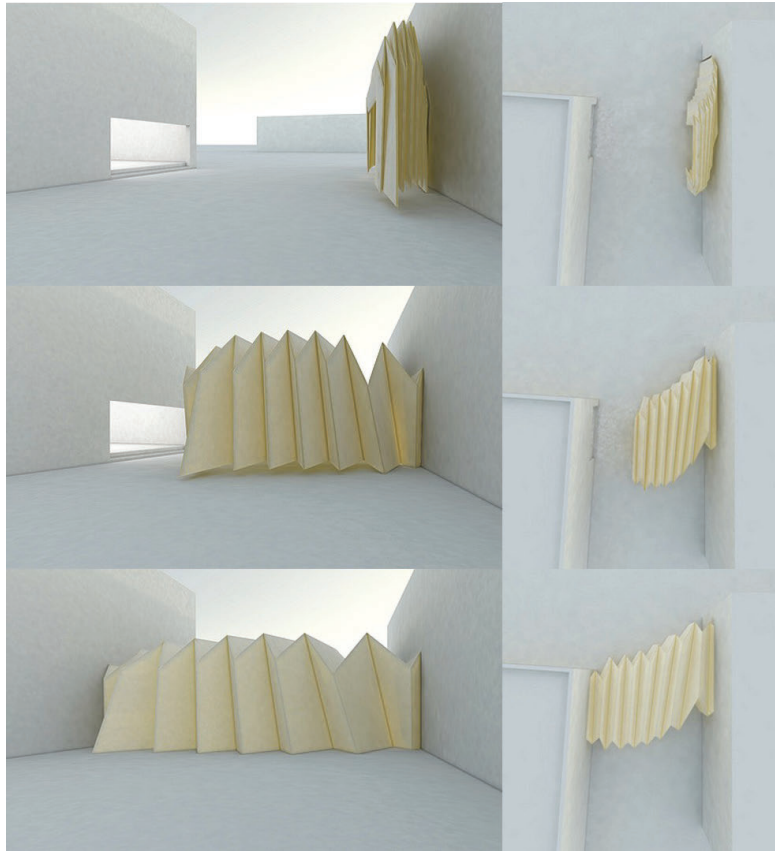


Figure 1.3 – An example of rigid-foldable origami structure as envisioned by T. Tachi [5].



Figure 1.4 – Unesco Conference building in Paris, France, M. Breurer, B. Zehrfuss (architects) and P.L. Nervi (structural engineer), 1953 [2] (left) and St. John's Abbey, Minnesota, USA, M. Breurer (architect) and P.L. Nervi (structural engineer), 1961 [3] (right).

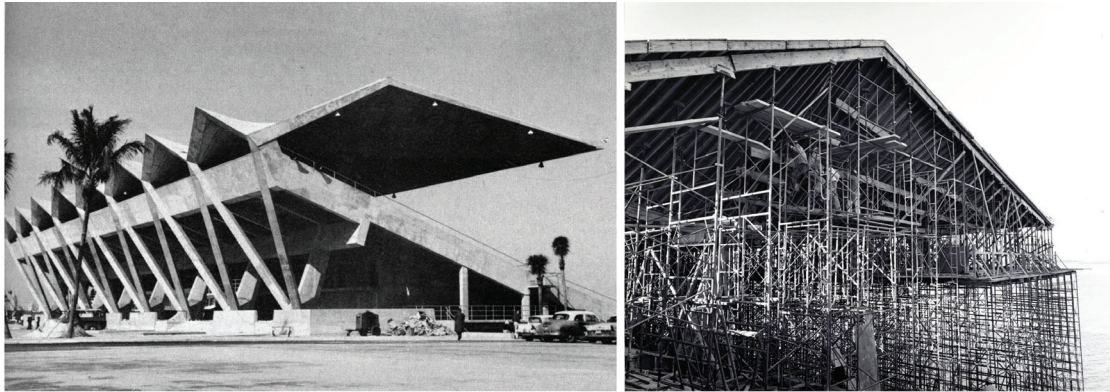


Figure 1.5 – Miami Marine Stadium designed by Hilario Candela, 1963 (left). Construction of the stadium with a large amount of formwork required scaffolding (right) [7].

influenced the used geometrical forms which were most commonly built as simple prismatic or non-prismatic systems, consisting of repeating rectangular or triangular plates. Using repetitive elements, governed by the concrete placement using a single set of forms, led to structures with uniform slope angles and connection details [44]. Even when using simple forms, the main advantage of using reinforced concrete and even more so prestressed concrete elements for constituting the folded systems, were the large achievable spans. On the other hand their main shortcoming seems to have been the laborious construction, which ultimately led to almost complete loss of interest in such systems during the 1970s [49].

In parallel, starting from the 1960s other materials were explored as an alternative to concrete for the construction of folded surface structures. Continuing until today, materials such as structural plastic, timber and even glass, were studied for this purpose. On one hand, thin plates formed from such materials, i.e. thickness/average side ratio: $t/L \leq 0.05$, have the advantage of constituting lightweight elements, however on the other hand, more complex forms are required for facilitating large spans. Due to their lower out of plane stiffness as well as maximum attainable element size limitations imposed by manufacturing constraints, forms with multiple elements across the width of the structure are necessary. In 1963 Z.S. Makowski proposed a number of folded configurations for execution in plastics (see Fig.1.6) (as cited in [43]). One of such forms was applied in a well-known structure designed by R. Piano, where modular rhomboid-shaped polyester elements were used to form a very lightweight structure covering a 10m span of a *Sulphur Extraction Factory* in Pomezia, Rome (Fig.1.7).

A very in-depth analysis of folded structures various folded form topologies and their geometric parameters for application in structural plastics was given by P. Huybers in 1972 [43]. A more general collection of forms as well as their underlying structural principles were presented by H. Engel in 1971 [24]. Both of the aforementioned studies concluded that the shape of the surface determines the load-bearing mechanism of the entire surface-active system.

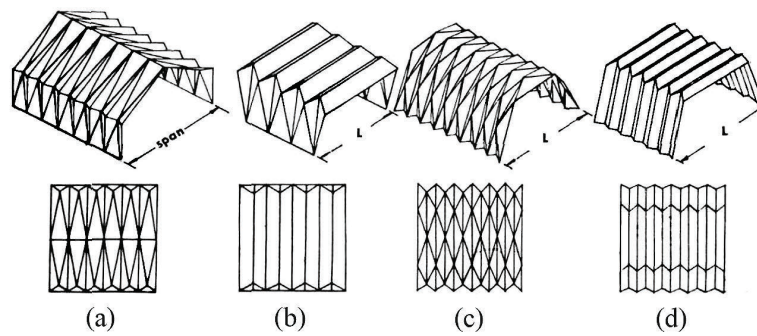


Figure 1.6 – Various folded forms proposed by Z.S. Makowski; (a) and (c) non-prismatic or anti-prismatic forms which can facilitate spans bigger than the largest occurring element; (b) and (d) prismatically folded forms with parallel creases, such forms could only be used for smaller spans as such configurations do not allow further subdivision of the surface without introducing problems of stability. Figure taken from [43].



Figure 1.7 – Sulphur Extraction Factory by R. Piano, 1966. The thin folded sheets of reinforced polyester provide strength, stiffness and stability with minimum weight and also make the covered area very bright [67].

Additionally, same as for concrete folded structures, where the realization of seamless rigid connections was recognised as one of the main requirements, already in their origins as coal bunker structures (Craemer 1929, as cited in [68]), sufficiently rigid connection details were found to be of prime importance. As more elements across the span were added and more connection details needed to be realized, achieving efficient connections has proved to be the main difficulty for structures made of lightweight materials. As a consequence, this led to structures more sensitive to deflections. A good example is found in folded surface structures made of glass plates, where a variety of folded forms have been proposed and different joint options tested [91, 58], however finding a viable connection detail for enabling the necessary jump from conception to construction is still underway.

After a more general introduction presented above and according to the main interest of this thesis, the next two subsections focus more onto the state of the art of static timber folded surface structures as well as timber panels feasible edgewise connection details.

1.1.2 Use of Timber in Folded Surface Structures

The application of timber to folded surface structures has been motivated by multiple advantages of relatively recently developed engineered wood panel products. For their production the raw wood material is milled by different processes into pieces with certain dimensions and subsequently bonded by means of adhesives. Depending on the processing type, stranding, peeling or sawing, various panel products are obtained, made out of strands, veneers or solid wood boards respectively (see Table 1.1). In contrast to natural roundwood, the engineered products have multiple advantages, which include increased dimensional stability, more homogenous mechanical properties and greater durability [45]. Their high load-bearing potential and strength to weight ratio combined together with structural benefits obtained by surface folding, allow for realization of efficient folded surface systems.

One of the earliest examples of folded surface structures built entirely out of timber panels is the *Anette-Kahn Student Residence* in Tübingen, Germany built in 1963. This 10.5 meter span roof was designed having a non-prismatic form with a series of inversely oblique folds joining at a $50^\circ - 55^\circ$ angle. Its 60mm thick plates are composed of three crosswise glued layers of wooden planks, somewhat a precursor of the 1990s developed CLT panels that we know today. At the edges the panels overlap and are glued along the interface. They are additionally reinforced from the top by nailed-in steel V-shaped plates (see Fig. 1.8) [57].

In 1976 a roof structure of 18m span was realized for the *International Architecture Exhibition* in Berlin to demonstrate this new structural concept within timber engineering. It was built in diagonally crossed two-layer panels with a simple prismatic form, composed of consecutive

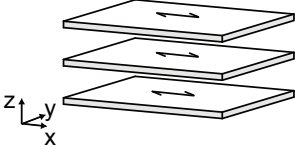
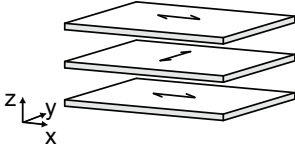
Grain orientation of components		
	Orientation of all components in one direction	Orthogonal orientation of components
Basic wood component		
Strands	Longitudinal Strand Lumber (LSL); Parallel Strand Lumber (Parallam)	Oriented Strand Lumber (OSB)
Veneers	Longitudinal Veneer Lumber (LVL)	Plywood; LVL with orientation of some layers in transverse direction
Boards	Glued Laminated Timber (GLT, glulam)	Cross Laminated Timber (CLT)

Table 1.1 – Overview of engineered wood panels depending on their basic wood components and their layer orientation.

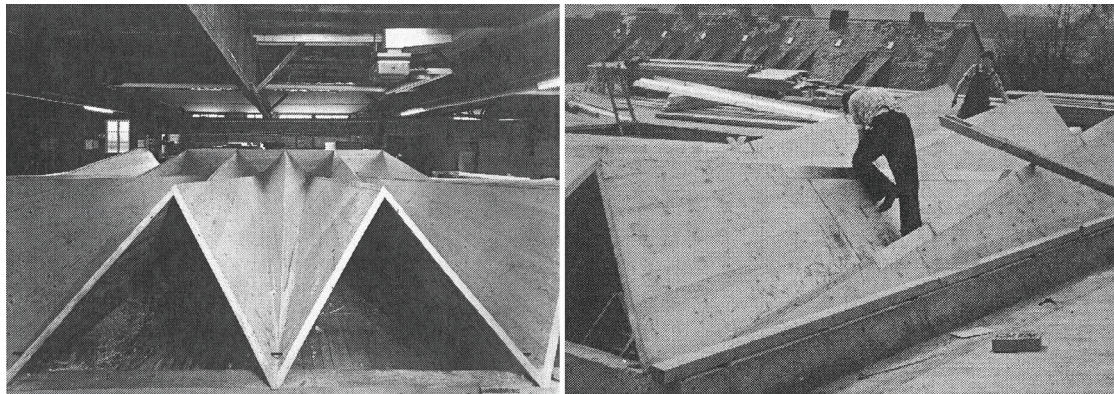


Figure 1.8 – Anette-Kahn Student Residence, Tübingen, Germany, H. Hilzinger, 1963.

parallel folds. In this example the folds provide a structural static height of 1.05m . Miter joints were realized at the plate edges, mutually connected using adhesives and bolts (see Fig. 1.9). The two above presented structures seem to be one of the rare examples realized entirely out of timber panels, forming a pure folded plate structure. In literature many other examples can be found under the folded plate structures category, however the addition of a timber truss as a second structural system makes them more of a hybrid folded plate and truss system [63], which is why they are not considered in this review. The reason behind this scarcity was most probably an insufficiently developed technology regarding the production of timber panels with adequate mechanical properties. As K. Leitner mentions in her thesis work, where she provides a comprehensive collection of built examples (both pure and hybrid timber folded structures), the problem of missing characteristic values for timber panels at that time restricted the construction of pure timber plate folded systems according to the building codes [57].

More recently, rapid proliferation in manufacturing methods within the timber industry in the 1990s enabled the development of new timber products with more homogenous mechanical properties, which led to a revival of interest in timber folded surface structures.

In 2002 *Thannhausen Music Rehearsal Hall* was built near Augsburg, Germany, where a 10m span was reached by using 100mm thick glue-laminated timber (GLT) panels 1.10. As opposed to previous examples in timber where folding was used only for roof structures, here the folding principle is applied to the side walls as well, which then together with the roof form a unique folded surface system. The geometry of the structural form is very similar to the examples found in concrete, where a simple prismatic form with parallel folds is used. However, the geometry of the individual prefabricated elements is not exactly the same, including different element widths and dihedral angles between the plates, showing a big advantage of timber over concrete for potentially more free-form geometries. The edge joining of prefabricated



Figure 1.10 – Music Rehearsal Hall, Thannhausen, Germany, R. Schineis, 2002.

modules, each consisting of two plates connected with glued miter joints and forming a V-shaped valley fold, were realized with a miter joint geometry with the addition of screws and adhesive.

Another timber folded surface structure was realized in Pomaples, Switzerland in 2008 1.11. The *Temporary Chapel St. Loup* was built using prefabricated cross-laminated timber (CLT) panels, with only 40mm thick vertical wall plates and 60mm thick roof plate elements spanning 9m. The origami-inspired form uses a reverse folding technique which enables the straight folds to change their direction in space, in this case along the span of the structure. The irregularity of the form led to plates of unique geometry and various fold angles, ranging from 104° to 130°. The chapel was entirely designed in a 3D CAD software and the plates geometry could be directly transferred to fabrication, without modifications [18]. This project once again emphasized the prefabrication advantages of timber panels as well as the increasing use of computer-aided tools for generating architectural forms. Together with computer-controlled machine (CNC) technology, this substantially expanded the future prospects of timber folded surface structures and led to architectural form experimentation, which enabled the overcoming of the timber panel size limitations and facilitating the realization of larger spans.

K. Leitner explored various folded forms for application in deployable timber folded structures [57]. H. Buri found inspiration in origami and studied different architectural forms derived from paper folding [18], resulting in the realization of the above presented *Chapel St. Loup*. A. Falk and P. von Buelow study concentrated on folded vaults made from cross-laminated timber panels. They varied the geometric parameters of the chosen form and examined their influence on structural stiffness. To that extent a computer tool was developed, which compared the forms of the obtained structures by performing a modal analysis [28].



Figure 1.11 – Chapel St. Loup, Pompaples, Switzerland, Local Architecture and SHEL, 2008.

1.1.3 Connection Details for Edgewise Joining of Thin Timber Panels

Even though the previously mentioned architectural design exploration resulted in many interesting and creative forms, all of the conducted studies seem to have had a common difficulty in finding adequate edgewise connection details for thin timber panels (thickness/average side ratio: $t/L \leq 0.05$ [65]), which would be able to facilitate a large span construction. In timber engineering, the issue of designing adequate thin panel, edgewise joining details presents a major challenge, as it is difficult to address by using standard state-of-the-art joining techniques. The performance of folded surface structures depends on linear edge-to-edge connections between the panels, which is why these joints are considered a key component for their design.

In the previously mentioned examples it can be seen that the connection details were usually realized by using a combination of adhesives and metal fasteners for achieving the needed rigidity at the folds. However, on-site gluing is generally considered not feasible due to the lack of constant conditions for curing of the adhesives. In the case of *Thannhausen Music Rehearsal Hall* a special permission needed to be acquired for performing the adhesive joining on-site. On the other hand, in the *Anette-Kahn Student Residence* project it was reported that realizing glued joints was hard even in the controlled factory conditions [57]. Also, achieving a strong enough connection when gluing along the faces of a butt or miter joined thin plate edges, meeting end-grain to end-grain in certain layers, which meets the requirements of ordinary service using conventional bonding techniques is considered practically impossible [32]. Therefore, joining of timber panels is more commonly realised by using metal fasteners, such as in the example of *Chapel St. Loup*. However, for realizing larger structures consisting of multiple elements along the span, this has shown to be an unfeasible solution. H. Buri preformed an experimental test on a prototype built from plywood panels (see Fig. 1.12), connected with screwed miter joints, where he concluded that such connections were not sufficiently resistant to withstand the resulting transverse bending moments, and that the



Figure 1.12 – Origami inspired plywood prototype testing and connection failure, H. Buri, Laboratory for Timber Constructions, EPFL, 2010.

joints for large panel assemblies needed to be improved (see Fig. 1.12). Also, connecting a large number of non-orthogonal line joints with screws showed to be quite difficult to realize [18]. Moreover, according to the current regulations, the minimal distance from the screw to the panel edge is set to $4d$ (d = diameter of the screw) which restricts the minimal value of the panel thickness depending on the size of the fastener [27]. Consequently, the final panel thickness usually needs to be dimensioned according to the minimal requirements imposed by the connection detail. This results in use of thicker panels and increased dead weight of the structure, without it being conditioned by the structural requirements regarding the load-bearing capacity.

Recently, the re-discovery of *integral mechanical attachments* resulted in a new technical solution for edgewise joining of thin timber panels, inspired by traditional woodworking joints [80, 52, 72]. Rather than using additional connectors, these connections utilize digital prefabrication to integrate connectors through the plate geometry. While this was not a very efficient solution with the earlier machine-tool-technology, it is no longer the case with multiple axis computer-controlled machines (CNC), common even in medium scale carpentries [83]. A very comprehensive study on the influence of fabrication techniques on the development of the integral mechanical attachments, as well as their different types, is given in [68].

A particularly interesting integral mechanical attachment technique are the so called one-degree-of-freedom *multiple tab-and-slot joints* (MTSJ) proposed by C. Robeller and S. Roche [68, 75]. They can be realized both with an open slot or closed slot geometry (see Fig. 1.13). Such joints offer multiple advantages: in addition to their load bearing function (connector feature) they also integrate features for the fast and precise positioning of thin elements (locator feature); they do not impose any constraints on the panel thickness and they can be integrated into any plate geometry.

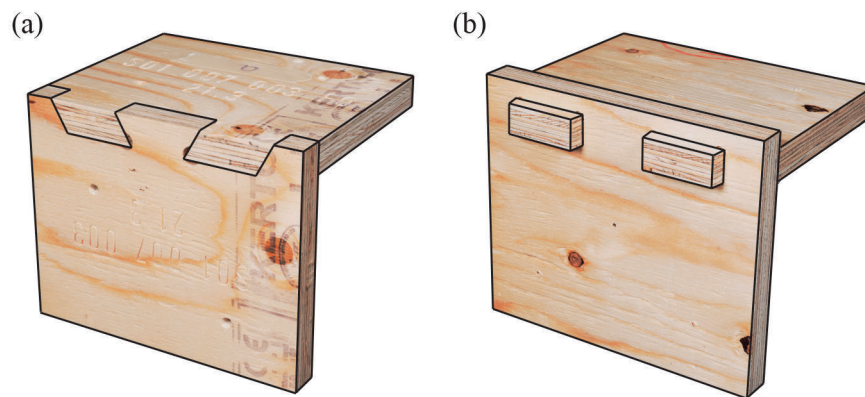


Figure 1.13 – Multiple tab-and-slot joint realized with 21mm thick Kerto-Q LVL panels joining at a 90° angle; (a) with open geometry; (b) with closed geometry [74].

Nevertheless, there exists a certain number of constraints that need to be taken into consideration, particularly within the domain of folded surface geometry. The MTSJ geometry is described with a set of three angles which define the inclination of their locking faces and determine the unique assembly direction, which needs to be chosen within the intersection of the so called *individual edge rotation windows* (see Fig. 1.14a). This further defines the feasible range of angles between the plates as well as the number of edges which can be simultaneously assembled, all having an influence on the design of the final form. Additionally, the machine tool limited inclination needs to be taken into account as well, and the fold angles between the plates, φ , need to be constrained accordingly (see Fig. 1.14b). The first realized large scale structure application of 1 DOF open slot MTSJ was a 13m span pavilion in Mendrisio, Switzerland built in 2013. Constructed with 77mm thick CLT panels, the joints showed a very promising structural behaviour as well as great benefits considering ease in fabrication and assembly [71]. A more in-depth study of their local mechanical behaviour was performed by S. Roche [76, 75, 74, 21]. The performed experimental tests, examining open and closed slot MTSJ rotational and shear load bearing behaviour, suggested that they provide a suitable degree of bending as well as shear stiffness for structural applications. Their behaviour was found to be highly dependent on the combination of the locking faces angle values, where the weakest ones were those with all three angles equal to 0°, i.e. this combination of angles results in a regular three-degree-of-freedom finger joint. With a certain combination of angles, MTSJ semi-rigid behaviour was found to be competitive to that of screwed connections, confirming that they can provide a highly feasible alternative to standard joining techniques.

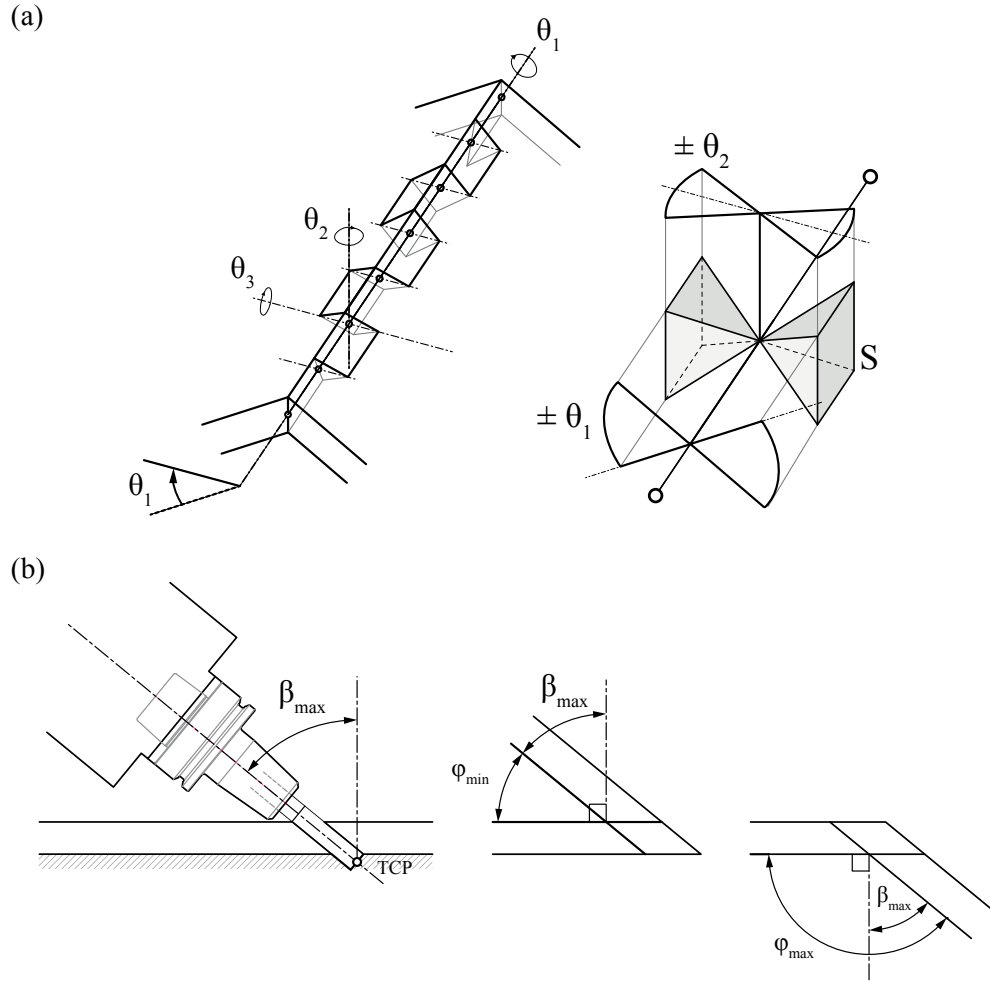


Figure 1.14 – MTSJ constraints; (a) Three angles describing the joint geometry, θ_1 , θ_2 and θ_3 , as well as the intersection, S , of their *individual edge rotation windows* which defines the domain of possible insertion vectors; (b) Fabrication constraints caused by the maximum tool inclination, β_{max} [68].

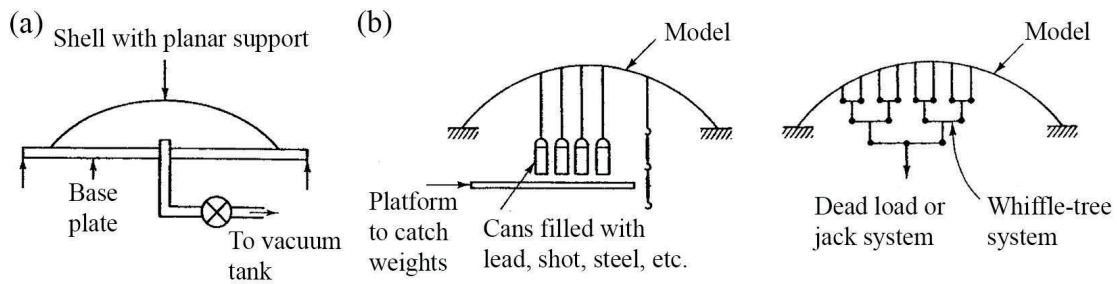


Figure 1.15 – Loading systems for applying surface load as shown by H. G. Harris and G. M. Sabnis [41]; (a) Vacuum loading of shell models ; (b) Discrete loading systems: suspended dead weights and a whiffle-tree system.

1.1.4 Experimental techniques

Experimental testing of any complex structure poses a major challenge, especially when larger scale is considered. This is particularly true for surface-active structural systems designed for taking surface loads, such as shells, vaults and folded structures, where designing and constructing the loading apparatus for realistically applying the load has proven to be quite complicated [42]. There exist two different loading techniques developed for applying surface load on such structures: pressure or vacuum loading where the load is introduced by applying an air bag pressure or vacuum to the enclosed space, defined by the shell and the base plate; and discrete load systems where the uniform load is replaced with discrete suspended weights (see Fig. 1.15). The choice between the two systems is usually dependent on the equipment available and the size of the model.

One of the first recorded examples of experimental tests on a folded plate prototype was the one performed by B.S. Benjamin and professor Z.S. Makowski in 1965 [15] (see Fig. 1.16). The realized glass-fibre reinforced plastics structure with a $6m$ span, was entirely prefabricated and assembled of equally shaped and sized units, mutually connected by bolts. The load was suspended on four points, i.e. for each prefabricated valley fold unit, by steel cables supporting wooden platforms loaded with bricks. The wooden platforms were placed on steel beams which were resting on hydraulic jacks. An equal distribution of load on each loaded point was enabled by lowering the jacks until the platforms hung freely from the structure (see Fig. 1.16 right). In this way a total load of $\sim 1400N/m^2$ was applied. A shortcoming of the presented load application seems to be the fact that only a predefined amount of load can be applied. Increasing the load further, even to a such amount that failure is reached, by simply adding more bricks is not practical as it cannot be done simultaneously for each loaded point.

A different type of loading system was applied in 1970 by P. Huybers on his prototype shell structure, also realized in glass-fibre reinforced plastic [43] (see Fig. 1.17). By means of 14

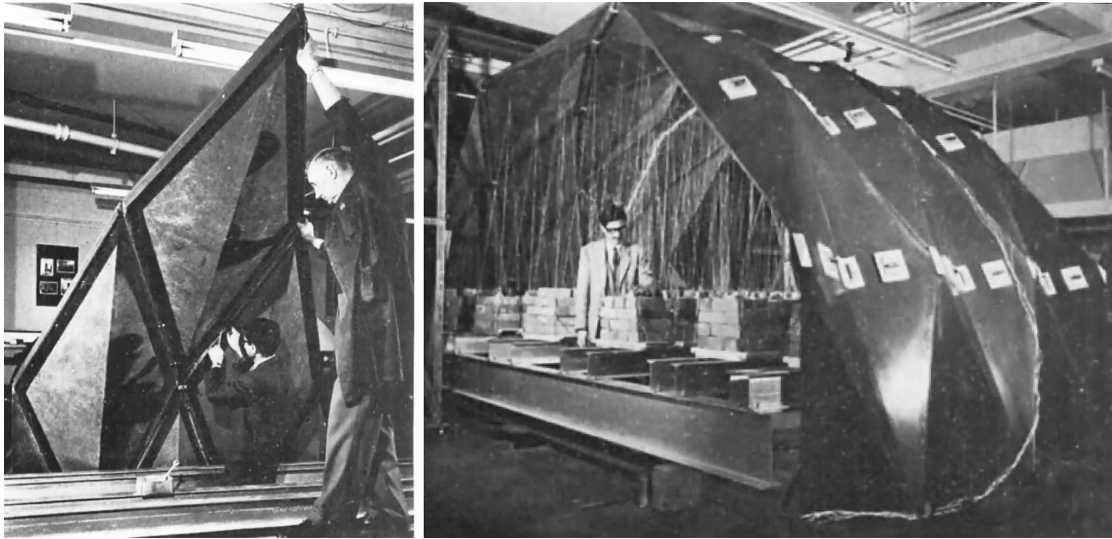


Figure 1.16 – Erection (left) and experimental testing (right) of the folded surface prototype realized by B.S. Benjamin and Z.S. Makowski [15].

hydraulic jacks, placed in a row and attached to the uppermost central points of the cross-section and the concrete floor, a row of concentrated loads was applied. Similarly but with a less sophisticated setup, H. Buri tested his plywood folded prototype shown in Fig. 1.12. The load was introduced by hydraulic jacks placed above the structure, which were pressing on wooden beams resting on the structure top surface. In this way the load was introduced simultaneously onto several edges in the length equal to the wooden beams width. In the two previous presented examples increasing of load until complete failure is achievable, however the results showed that applying the load in such a way results in a distorted impression of the structural behaviour, as opposed to that expected in actual practice. It is assumed that the structures would behave considerably different under a more uniformly distributed load.

1.1.5 Structural analysis

In 1930, first work on structural analysis of concrete folded plates, applied for large coal bunkers, was published by G. Ehlers [23]. In his approach the membrane solution assuming negligible displacements of the joints was used. The plates were regarded as hinged to each other so that the transverse moments at the joints were ignored. Two years later, E. Gruber presented a more rigorous theory where he took into account the rigidity of the connections as he established that large errors could occur if the rigidity of the joints is ignored [37]. In succeeding years many engineers have made their contributions to this subject and established methods for solving folded plate problems. These methods were generally very complex and too arduous for design use [97]. However, in the late 1950's when concrete folded plate

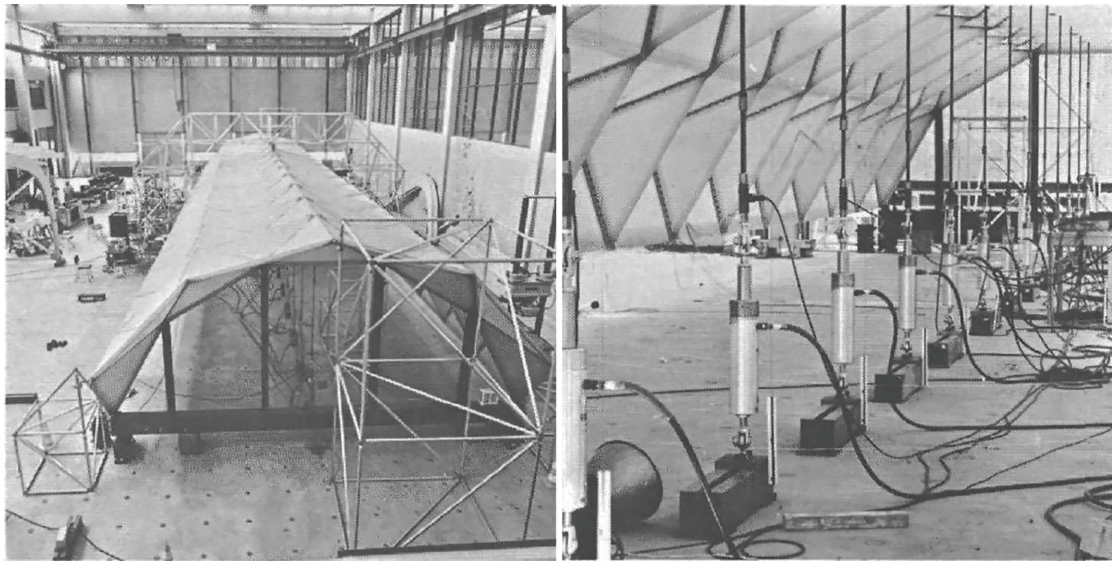


Figure 1.17 – Folded surface prototype realized by P. Huybers (left) and its experimental testing load introduction system by 14 hydraulic jacks positioned under the structure (right) [43].

structures gained increasing use and popularity, simplified analysis methods were developed, which were much more applicable for practical use. These methods were mostly concerning geometrically simple rectangular elements forming prismatic forms with parallel folds and rigid diaphragms at the end, where the structural action was separated into slab (bending) and plate (membrane) component (see Fig. 1.18) [29]. An excellent and very detailed report of all available methods at that time can be found in 1963 Phase I Report by the Task Committee on Folded Plate Construction, assigned by ASCE [64].

However, as noticed by B.S. Benjamin and Z.S. Makowski and later also by L. Kollar, the proposed approaches were only suitable for long folded plates where the span/width plate ratio is greater than 2. For short folded plate elements with the span/width plate ratio smaller than 2, a type of construction not economical in concrete, but both economical and feasible in plastics, i.e. as well as timber, such analysis would yield erroneous results [15, 53]. Additional difficulty was recognised in large deflections that could occur in less stiff plate elements, meaning that small-deflection theories no longer apply, and geometric non-linearity has to be taken into consideration, leading to a considerably more involved problem. Therefore, a full slab action needed to be determined, i.e. not only as a transverse strip.

Depending on the structure, various theories developed for plate and shell problems could be used for analysing the individual plate full slab action, resting on a combination of fixed, simply supported or free edges. Such theories include: General thick and thin plate and shell theory, Membrane theory of shells, Moment theory as well as Approximate Shell theories [93]. The global assembly is then achieved by introducing edge deformation, shear and

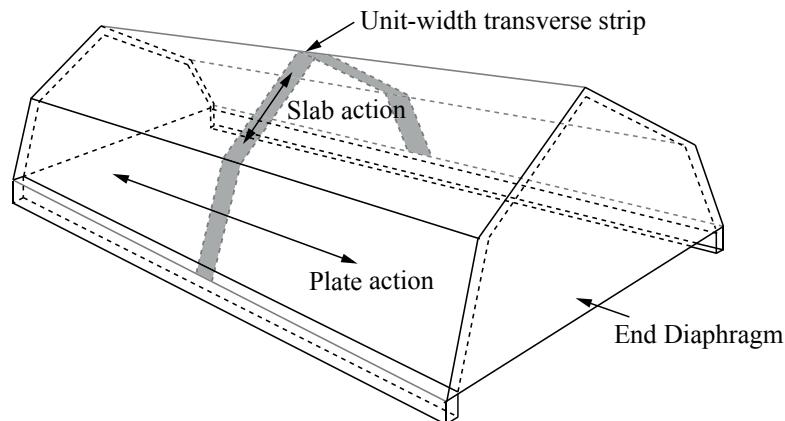


Figure 1.18 – Two-way action in a folded plate system. Across the folds in a unit-width transverse strip the plates act as a continuous slab where each fold acts as a support, in the longitudinal direction the plates act as deep beams resting on fixed supports.

bending compatibility equations. The mathematical formulation of such approach leads, as a rule, to a system of partial differential equations. Solving these equations analytically involves cumbersome computations, especially when complicated effects associated with material anisotropy and geometric non-homogeneity have to be taken into account [88, 98]. Additionally, the analytical solutions of shell structural problems are also limited in scope and, in general do not apply to arbitrary shapes, loading, irregular plate geometries and plate semi-rigid edge conditions. For example, the governing partial differential equations can be solved analytically for homogeneous and isotropic rectangular plates, isosceles right triangular plates, equilateral triangular plates and some cases of skew plates [93]. On the other hand, the development of numerical formulations over the past 50 years, notably the finite element method (FEM), has enabled a more fast and efficient analysis of a wide-range of folded structural forms, by solving partial differential equations by numerical approximate methods and discretization of the continuum. Taking into consideration the complexities of the geometry, boundary conditions, heterogeneous material properties etc., accurate results could be obtained in case when finding an analytical solution would be close to impossible [65, 93]. Today, the structural analysis of folded surface systems is mainly based on such numerical methods, performed with the use of sophisticated computer softwares.

Regarding the numerical models implemented for timber folded structures specifically, a particular emphasis has been put on the joint semi-rigidity representation, which has shown to have an important influence on the global structural behaviour. In the studies presented in [57, 18, 68] the joints were either modelled as completely rigid or as hinges, leading to highly inaccurate estimations of structure displacements.

1.2 Problem statement

Based on the state of the art review presented above, the following steps are recognised as necessary for facilitating the realization of timber folded surface structures on a building scale:

- A synthesis is required of the performed research considering folded surface structures forms in general and the research within the timber engineering domain, concerning various constraints imposed by the material, fabrication and edgewise connection details. This would aid in recognising the extents of feasible forms applicable for timber folded surface structures.
- Concerning the structural behaviour of timber folded surface structures with MTSJ connections, no detailed relevant scale experimental tests have been performed for exploring their structural potential. For performing such tests it is necessary to improve the state-of-the-art techniques, to enable the application of uniformly distributed surface loads as well as allow the incremental load increase for testing until structure failure. Moreover, the state-of-the-art performed small scale tests on MTSJ details concentrated on individual loading cases, i.e. bending and shear, imposed locally on the connection. However in the global structure context, where the edge connections are subjected to combined influence of bending, shear, tension and compression, the potential feasibility of such semi-rigid connections has not been studied. It has been demonstrated, regardless of the material, that the connection behavior has a very large influence on the structural performance of civil engineering structures [40, 13]. Therefore, the characterisation of the MTSJ semi-rigidity within a global system is considered to be of crucial importance for establishing timber folded surface structures on a building scale.
- The numerical models proposed for structural analysis of timber folded surface structures with semi-rigid connections have shown highly inaccurate estimations of structure displacements. Therefore more rigorous models are required for the reliable structural analysis of timber folded structures with MTSJ connections.
- The necessity for large spans precipitated the need for forms with multiple elements along the width of the structure. In timber, the state-of-the-art mentioned difficulty of realizing edgewise connections between thin timber panels (see Section 1.1.3), initiated a search for new ways of increasing structural rigidity. For now, this search has mainly focused on developing more suitable connections which would be able to provide sufficient rigidity to the system, where recently a very promising outcome is presented by the one-degree-of-freedom MTSJ. However, a complementary approach could be found in exploring the influence of form on the structural behaviour of the folded

structure as well as its connection details, and understanding how additional stiffness can be provided to the structure by modifying its geometry. It is noticed that even though the connection detail requirements for kinematic and static structures are completely opposite, the forms used for both structure types seem to be very similar. This might not be an issue when concrete structures are considered, due to a high rigidity of their connections, however in timber folded structures it presents a potential disadvantage.

As stated in [62], for the forms used in origami, i.e. deployable structures, the transformations from the initial state to the folded one occurs with relatively little energy (and therefore unexpectedly), meaning that the phenomenon can be dangerous when it occurs. This is especially true for static folded structures, where foldability of the form is not a requirement, and can therefore be potentially disadvantageous. In this regard, the relation seems to be lacking between the static form geometry, its foldability and the connection detail requirements, as well as their mutual influence on global structural performance.

1.3 Objectives

The main objectives of this research are to study timber folded surface structures feasible folded forms and structural behaviour, to observe the relation between their structural performance under load and global form, as well as local connection detail requirements, and to provide a pertinent numerical model for their structural analysis. With respect to the presented problem statement, this is accomplished through four following research steps:

- Studying the topology and main geometrical parameters of the folded form within the scope of timber folded structures. Exploring in detail the interrelation of various constraints imposed by the material, fabrication and MTSJ connections on the overall structural form. Explaining the structural behaviour of timber folded surface structures and highlighting the importance of its folded form as well as connection detail within the global system. Presented in Chapter 2.
- Performing relevant scale laboratory tests for examining the structural behaviour of the chosen folded form system under realistic load. Additionally, the influence of the connection detail semi-rigidity on the structure overall behaviour is examined. The performed tests are also used for verifying the feasibility of the designed form, concerning its fabrication and assembly constraints. Presented in Chapter 3.
- Developing a pertinent yet simplified numerical model which includes the semi-rigid behaviour of the connection details, and which can be used to adequately represent the

structural behaviour of the considered structures. The presented model is validated by the experimental test results obtained in the previous step. Presented in Chapter 4.

- Studying the relation of the forms topological characteristics, with regard to its foldability range and performance under load by focusing on the level of connection detail participation in the overall load bearing mechanism. This step is performed only within the framework of MTSJ timber folded surface structures by using validated numerical models from the previous step. Presented in Chapter 5.

1.4 Scope

Scope of this research is defined regarding the material, connection detail and structural analysis:

Material

Among the diverse innovative engineered wood panel products, the presented work focuses on certified Kerto-Q laminated veneer lumber (LVL) panels [94]. Kerto is produced from 3 mm thick, rotary-peeled softwood veneers that are glued together to form a continuous sheet. Prior to lamination, the veneers are dried and the grains of each veneer are oriented in the same direction. This makes LVL stronger, straighter and more uniform than solid timber. It also overcomes some of timber's natural limitations such as strength-reducing knots. The added durability of being an engineered wood product also means LVL is less prone to shrinking or warping. Depending on the application, various types of Kerto panels have been developed. Kerto-Q is a cross-bonded Kerto. This means that one fifth of the veneers are glued crosswise. This improves the lateral bending strength and stiffness of the panel. With cross-bonded veneers, there is also an essential reduction in moisture-dependent variations across the width of the panel. Considering the dimensions, timber engineered panels, same as all timber products, have limitations concerning the dimensions of the prefabricated units. Currently, planar elements with maximum dimensions of 23 m in length, 2.5 m in width and a thickness varying from 21 mm to 69 mm in steps of 6 mm, can be acquired for LVL panel elements [94]. Furthermore, standard transport sizes according to Swiss regulations include elements up to 13.50 m x 2.50 m x 2.60 m. Finally, the available 5-axis MAKKA MM7S CNC router, used for formatting the panels, can accommodate a maximum panel size of 2,5 m x 1,25 m. The latter was taken as the constraint for the size of the used individual panel elements. Panels of 21 mm thickness and 2,5 m x 1,25 m dimensions were supplied by Metsä-wood Germany and were used for all the experiments presented within this thesis.

Connection detail

This research concentrates on one-degree-of-freedom *multiple tab-and-slot joints* (MTSJ) which integrate into the timber plate geometry. The generation of the MTSJ geometrical parameters, as well as their fabrication, is enabled by using custom developed programs by C. Robeller [68]. All fabrication is performed on a 5-axis MAKA MM7S CNC machine by using automatically generated G-code.

Structural Analysis

As mentioned in the state of the art, the structural analysis of folded surface systems is mainly based on numerical, finite element methods performed with the use of sophisticated computer softwares. This enables more parameters to be included in the modelling, analysis, optimization and evaluation procedures of such structures. Respectively, within this research, numerical, ABAQUS-based finite element method is used for analysing the structural behaviour of the regarded timber folded surface structures.

2 Topological and Structural Considerations

This Chapter is based on: A. Stitic and Y. Weinand, Timber Folded Plate Structures - Topological and Structural Considerations, *International Journal of Space Structures*, Vol. 30, No. 2, 2015, pp. 169-177.

2.1 Introduction

Several structures made from timber engineered panels have been realized in building scale, such as *Chapel St. Loup* and *Thannhausen Music Rehearsal Hall* structure presented in Chapter 1 Section 1.1.2 (see Figs. 1.11 and 1.10). In these examples simple prismatic folded forms were used, where the width of the structure is spanned with a single element. Such forms restrict the span of the structure as timber elements are only available in limited sizes, due to manufacturing and transportation constraints. In order to achieve larger spans, a folded surface system consisting of multiple elements along the width of the structure was proposed by H. Buri with his *Origami inspired prototype* (see Fig. 1.12). In this case the chosen folded form geometry was based on folded rhombus elements. However, the joints were found to be insufficiently resistant to withstand the resulting transverse bending moments.

With respect to the above mentioned examples, two components seem to be required for achieving large spans by using timber folded surface structures: 1) folded forms with multiple elements along the span of the structure; and 2) efficient connection details between adjacent plane elements. This Chapter explores the feasibility of using one-degree-of-freedom MTSJ in large span timber folded surface structures. It examines various folded form topologies, established in timber engineering as well as in other material domains, and inspects their

structural potential for the aforementioned application.

The Chapter is structured as follows:

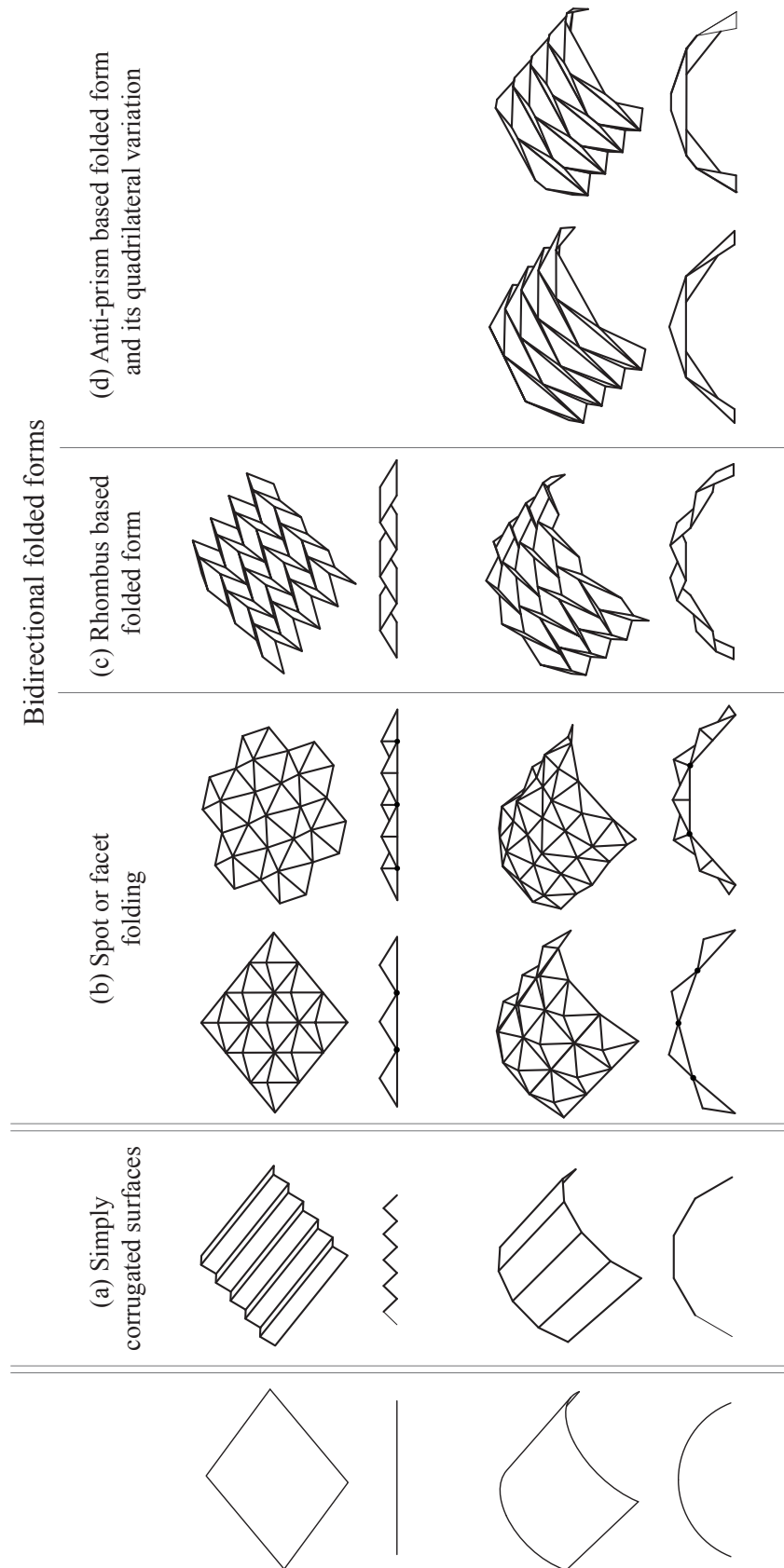
- Section 2.2 presents a classification of folded form topologies;
- Section 2.3 examines the found feasible forms geometry with respect to the structural constraints derived from MTSJ connections, including fabrication and assembly;
- Section 2.4 explains the structural behaviour of timber folded plates and compares the distinct feasible forms by means of Finite Element Analysis;
- Section 2.5 presents a case study of a built prototype together with important observations regarding the used material, fabrication and element assembly;
- Section 2.6 summarizes the main conclusions.

2.2 Topology of the Folded Form

In Fig. 2.1 various folded form topologies are classified by their ability for discretizing flat and singly curved surfaces. In order to describe these forms we will use the terminology derived from computer graphics where a surface is represented by a polygon mesh [17]. The topology of such a mesh is defined with a set of vertices and additional information on how they are connected. This connectivity further determines the bounding edges of the form's constituting faces. The spatial arrangement of vertices as well as their connectivity can be regular or irregular, thus creating a form which is either composed of identical or diverse base polygon geometry.

The first group (Fig. 2.1a) contains simply corrugated surfaces. They are composed of quadrilateral faces whose bounding edges form a succession of either parallel or oblique lines. Such folded forms are most commonly used in practice. However, due to the timber panel element size constraints, the covered surface area of such structures is limited. In order to overcome this restraint, topologies where vertices and their connections form a spatial grid are used. By doing so, bidirectional folded forms are obtained (Fig. 2.1b, c and d). Such forms consist of multiple elements in two distinct directions of the structure.

The first bidirectional folded form considered (Fig. 2.1b) includes spot or facet folded forms, which consist of vertices where several faces intersect like a bunch in one single spot [90]. Such forms are obtained by taking a basic polygon and vertically rising its centroid point. This vertex is then connected to the ones of the initial polygon, consequently forming triangular faces. For such forms there are only three types of polygons which enable regular tessellations



of a surface: equilateral triangles, squares and regular hexagons. Others require either the use of semi-regular tessellations or irregular polygon geometry. In the presented classification only regular tessellations are shown, as irregular ones offer a manifold of possible different topologies. The following group (Fig. 2.1c) consists of rhombus based folded surface forms. In origami paper folding literature this form is also known as the Miura Ori or Herringbone pattern. The final bidirectional folded form considered is the anti-prism based one. It is composed of isosceles triangle faces and is also known as Yoshimura or Diamond pattern. A variation of this form where quadrilateral faces are used is also included (Fig. 2.1d). It is obtained by duplicating the anti-prism form vertices and introducing an additional connection line between them, resulting in trapezoid faces. Both of these forms cannot discretize a flat surface and are limited to curved cross-sections [33].

The above classified bidirectional folded forms are further compared according to their utilization of the folding principle, making them more or less feasible for structural application in timber folded surface structures. To that extent all structures are considered to have pinned supports at the sides, while connections between the plates are regarded as line hinges, allowing rotations about the face edge direction. A cutting-plane is positioned perpendicular to the longitudinal axis and the obtained transverse cross section profile is observed (see Fig. 2.1). It can be noted that for quadrilateral based facet folded form, both flat and singly curved, a continuous longitudinal hinge line is formed in every second vertex of the transverse cross-section. Even with a sufficient rise to span ratio of the structure, the number of such hinges must not exceed three (including the ones at side supports) [43]. If so, the system transforms into a mechanism and is no longer stable for more than two quadrilateral polygons per span. Also, the static height of the structure at this section point is very low and equal only to the panel thickness.

Concerning other polygonal facet folded forms, due to the offset of each transversal string of polygon elements according to the previous one, the system remains stable regardless of the number of hinges. Each individual string is still a mechanism by itself, but kept stable by the neighbouring string of elements. Furthermore, as the number of polygon sides in facet folded forms increases, the dihedral angle between the faces surrounding the raised centroid point increases as well. These dihedral angles become extremely obtuse already for five-sided polygons. Since it is considered that angles close to 90° work particularly well for folded surface systems whereas the system will lack in stiffness when incrementally increasing the angle [14], and that in integrally attached timber structures the dihedral angle values are constrained between 50° and 130° by the connection detail choice (see Section 2.3.1), the above presented facet folded forms are regarded as unsuitable for the studied purpose.

Respectively, only the rhombus base folded form and the anti-prism based one, together with

its trapezoid variation, are further considered. These three forms offer a particular structural advantage by having adjacent folds both in longitudinal and transversal direction, which together provide the necessary structural height along the entire cross section.

2.3 Structural Constraints

Structural constraints concerning the chosen bidirectional forms geometrical parameters are presented hereafter.

2.3.1 Joint Constraints

The integral attachment technique, chosen for connecting the adjacent panels, imposes a certain number of constraints which need to be taken into consideration when designing the folded surface geometry. One of the main constraints considered is robotic accessibility, where due to the limited tool inclination the dihedral angle between the connecting panels, φ , is restrained between 50° and 130° (see Fig. 1.14b). Furthermore, due to the local joint geometry the orthogonal as well as non-orthogonal assembly of individual elements also presents specific restrictions concerning the geometry and the number of panel edges which can be simultaneously connected. The simultaneous assembly of multiple edges requires the panel assembly direction to be chosen within the intersection of the so called *individual edge rotation windows* (see Fig. 1.14a). These *windows* represent all possible assembly directions for each edge. The range of this intersection depends on the number of assembled edges, tool inclination limitation and the dihedral angle between the plates [59]. In order to ensure that the assembly is possible, i.e. that respective rotation windows intersect, the geometry of the panels is chosen in a way that the final assembly direction does not deviate from the plane normal to each assembled edge, for more than 20° (see Fig. 2.2).

2.3.2 Geometry of the Structures

Considering the previous insights, the study of main geometrical parameters is performed on a regular anti-prism based form (see Fig. 2.3). A large number of parameters can be used to describe the observed form: span, S ; height, H ; dihedral angle, φ ; transversal folding angle, γ ; total central angle, ψ ; radius of curvature, R ; thickness, t ; apex angle, β ; discrete element width, w ; element height, h ; the element width horizontal projection, w_s ; and the element height vertical projection, which is equal to the maximal static height of the system, h_s . However, all of the listed parameters are mutually related and only in a certain range meet the requirements of both geometric and connection detail related constraints.

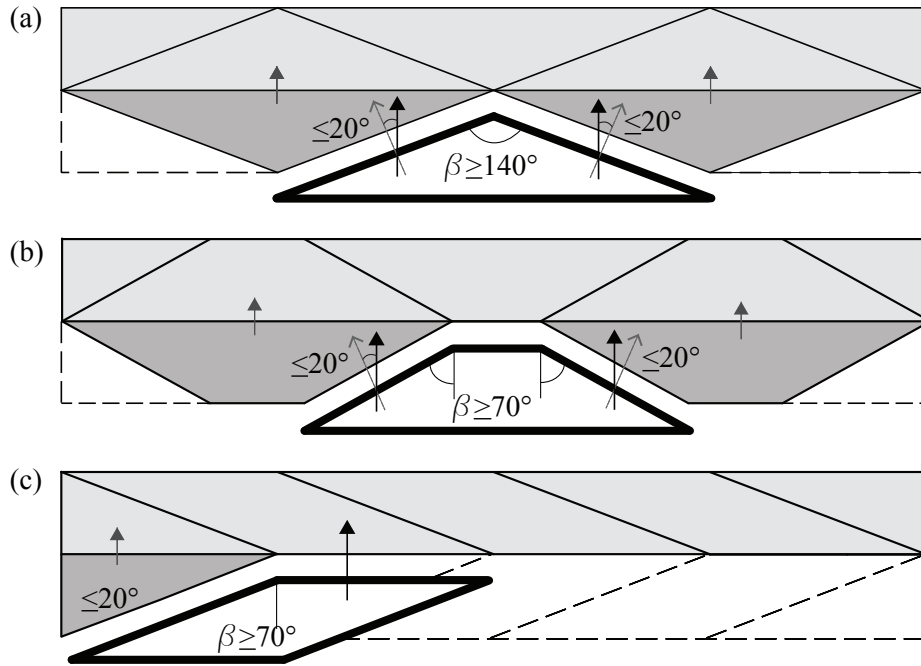


Figure 2.2 – Minimal value of the apex angle, β , and the maximal value of the assembly direction deviation from the plane normal to the assembled edges for the (a) anti-prism; (b) trapezoid; and (c) rhombus-based folded form.

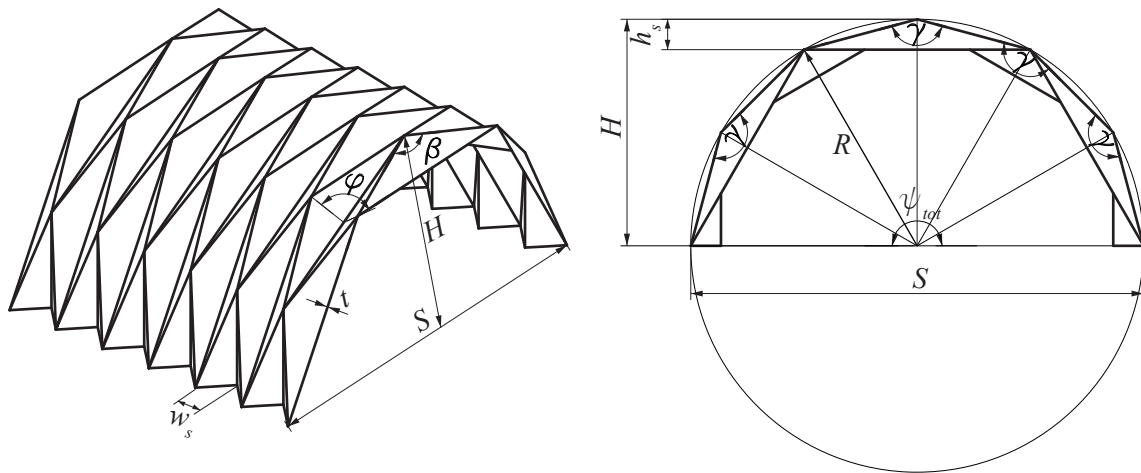


Figure 2.3 – Geometrical parameters of the anti-prismatic folded form.

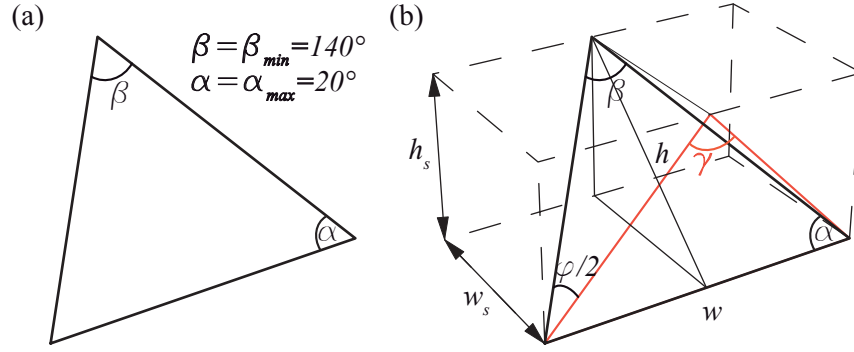


Figure 2.4 – Single isosceles triangle element (a) and its vertical projection (b).

If a single isosceles triangle element is observed, it can be seen that for any dimensions it is defined by the two interior angles, α and β (see Fig. 2.4a). Value of the apex angle, β , is constrained by the connection detail assembly. In order to enable simultaneous, multiple edge assembly, β must be larger than 140° . To avoid very acute angles for α , minimal value for β is chosen. Next, from the vertical projection of the inclined element, transversal folding angle, γ , and the dihedral angle, φ , are obtained (see Fig. 2.4b). Value of the dihedral angle, φ , is constrained by the connection detail fabrication possibilities. Consequently its value is restricted between 50° and 140° [72]. Furthermore, the value of the transversal folding angle, γ , can be expressed as a function of the dihedral angle, φ , and the apex angle, β , as follows:

$$\frac{\gamma}{2} = \tan^{-1} \left(\tan \frac{\beta}{2} \frac{1}{\cos \frac{\varphi}{2}} \right) \quad (2.1)$$

Since the apex angle is taken as a fixed value of 140° the value of the transversal folding angle, γ , only depends on the value of the dihedral angle, φ (see Eq. 2.1). From the previously defined dihedral angle range, minimal and maximal value for γ can be obtained. Discrete element width and height as well as their horizontal and vertical projection, can further be reached through basic trigonometric functions and are defined as:

$$h_s = 2 \cos^2 \left(\frac{\gamma}{2} \right) R \quad (2.2)$$

$$w_s = \tan \left(\frac{\varphi}{2} \right) h_s \quad (2.3)$$

$$h = \frac{h_s}{\cos \varphi / 2} \quad (2.4)$$

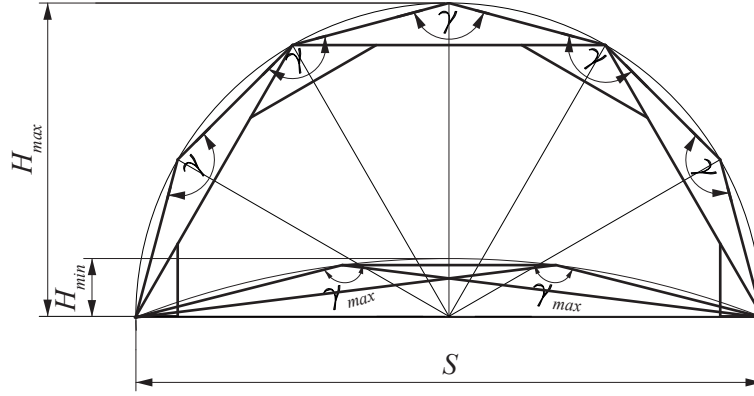


Figure 2.5 – Minimal and maximal span-to-rise ratio of a regular anti-prism based form.

$$w = 2h \tan \frac{\beta}{2} \quad (2.5)$$

Through the set interrelations, three main parameters which can be used for defining the complete system geometry, as well as their ranges, are recognised as follows:

1. $S/h = [S/h_{max}, S/h_{min}(\gamma_{max})]$
2. $\varphi = [50^\circ, 140^\circ]$
3. $t = [21mm, 69mm]$

Regarding the span-to-rise ratio, the maximal value is taken as half a circle with the corresponding height of the system equal to half the span, while the minimal one is a function of the maximal allowed value for the transversal folding angle, γ (see Eq. 2.1 and Fig. 2.5). Dihedral angle range is constrained, as aforementioned, between 50° to 140° . Finally, the available thickness's for Kerto-Q panels range from 21 to 69 millimeters [94]. Panel thickness can be considered as an independent parameter. It neither influences nor is it influenced by any other geometrical parameter. Nevertheless it has to be taken into consideration, as it certainly has an effect on the system's structural performance.

2.4 Structural Behaviour of Folded Surface Structures

Bidirectional folded surface structures carry the load by a mixture of extensional and flexural action. The relative proportions of extensional and flexural effects depend on several factors: the overall form of the structure, connection detail stiffness, support conditions and the

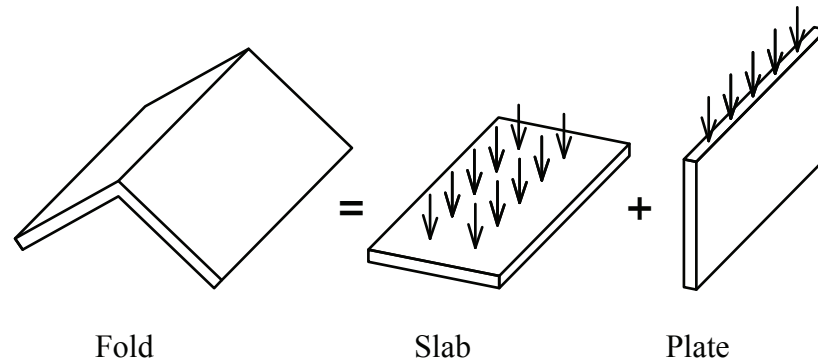


Figure 2.6 – Load bearing behaviour of a single fold, combination of the slab and plate effect.

loading configuration. Extensional or shell action resists the external transverse loading through the action of in-plane forces. This is a result of the overall shell-like form of the structures but also the individual position of the plates in relation to the acting force. The structural behaviour of such an inclined plate is divided into two different mechanisms of resistance and their combinations: plate mechanism, where the component of the acting force directed parallel to the surface is resisted by in-plane forces, and slab mechanism, where the component of the acting force directed at right angles to the surface is resisted by bending and twisting moments (see Fig. 2.6). The latter mechanism of local plate bending forms the flexural part of the overall structure's load resisting action.

The transformation of out-of-plane external load into in-plane extensional action is explained hereafter. The load normal to the plate is transferred by bending to the edges where it is resolved into components lying in the planes of the joining plates. When these in-plane forces are not in equilibrium the resulting force is further transferred to the supporting plates by in-plane shear along certain edges. The size of this in-plane shear depends on a number of factors, such as the uniformity of the dihedral angle between the observed plate and its supporting plates, stiffness of the plates as well as the edge connection detail and the nature of the load. The local plate bending behaviour also depends on the same factors. However, the values of the edge bending moments which cause edge rotation primarily depend on the rotational stiffness of the connection detail.

2.4.1 Structural Analysis - Geometry of the Structures

With respect to the recognised three main parameters describing the bidirectional folded form topology (span-to-rise ratio, dihedral angle and thickness of the panels), three topologically different forms were generated with the aim of comparing their structural behaviour. The forms are laid out so that their constituting plate elements discretize a hollow cylinder segment

with a set of predefined parameters. The cylinder outer radius was set to $R_{ext} = 2.5m$ and the cord length, i.e. span, to $S = 3m$ in order to obtain an optimal structure height of $H = 0.5m$, as well as a favourable height to span ratio of 1/6. Additionally, for restricting the maximal static height of the folded system, h_s , the inner radius of the cylinder was set to $R_{int} = 2.3m$.

While discretizing the described cylinder the main parameters were preserved in all forms. Their values were set as invariants from which the rest of the form geometry was obtained. For each folded form the base element geometry was kept the same throughout the whole system so that the form remains regular. Apex angles, β , were kept within the limits imposed by assembly constraints and restrained to a minimum of 140° for the anti-prism based folded form, and a minimum of 70° , for the rhombus and trapezoid based ones (see Fig. 2.2). The panel thickness, t , widths of elements, w , and the dihedral angle, φ , were also taken as invariables for all forms. The number of individual elements along a transverse cross-section, which can be used to approximate a set curvature with a defined maximal static height and structure span, was determined for the anti-prismatic and trapezoid-based folded forms according to:

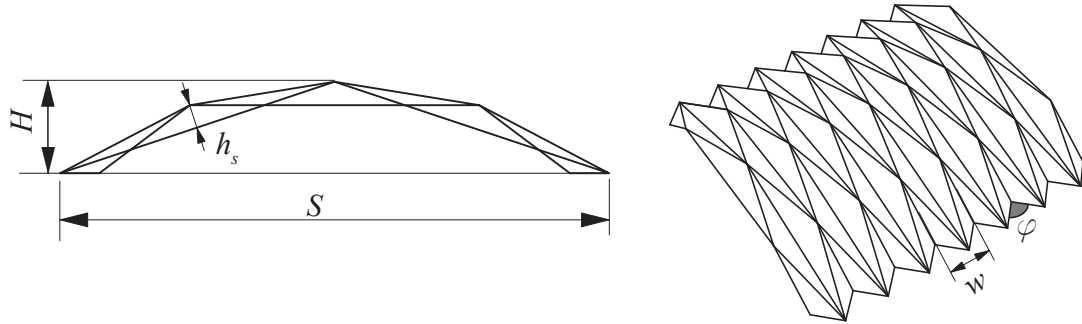
$$n = \left\lceil \frac{\psi_{tot}}{\cos^{-1}\left(\frac{R_{ext}-h_s}{R_{ext}}\right)} \right\rceil \quad (2.6)$$

and for the rhombus-based folded form according to:

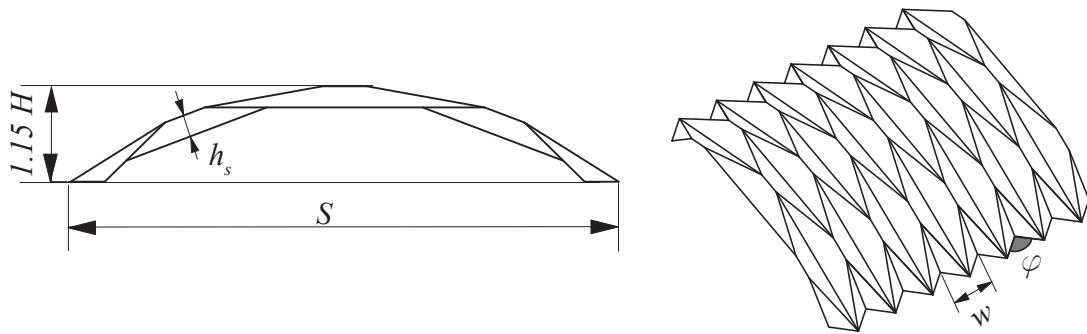
$$\tilde{n} \geq \left\lceil \frac{\psi_{tot}}{\cos^{-1}\left(\frac{R_{ext}-h_s}{R_{ext}-(h_s/2)}\right)} \right\rceil, \quad \text{where} \quad n \geq \begin{cases} \tilde{n} & \text{if } \tilde{n} \text{ is even} \\ \tilde{n} + 1 & \text{if } \tilde{n} \text{ is odd} \end{cases} \quad (2.7)$$

where ψ_{tot} is the central angle of the circular segment observed, R_{ext} the outer radius of approximated hollow cylinder and h_s the static height. For anti-prism and trapezoid based forms, Eq. 2.6 provides a unique result for a required number of whole, uncut triangular elements. On the other hand, for rhombus based folded forms the result is defined as the minimal number of elements necessary for discretization. Additionally, only an even number of elements is considered, as any odd number results in end segments of different orientation, leading to a height difference between side supports. Therefore, the result is to be rounded up to the first greater even number (see Eq. 2.7). For the set parameters, three segments for the anti-prism and trapezoid based form and a minimum of six segments for the rhombus based form were obtained (see Fig. 2.7). It is noted that approximating the same curvature with a defined height by using the rhombus based folded form resulted in a slightly smaller span, as well as reduced maximal static height of the system. In case of the trapezoid based form the overall height of the system had to be increased in order to keep the side cross-sectional

(a) Anti-prism based folded form



(b) Trapezoid based folded form



(c) Rhombus based folded form

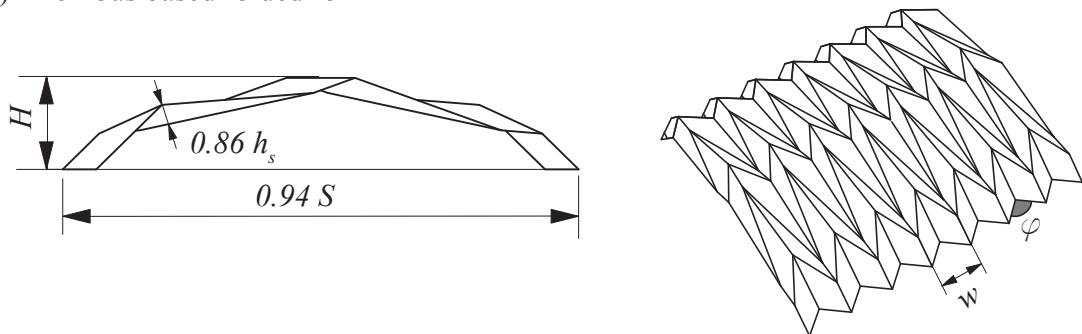


Figure 2.7 – Transversal cross section and perspective view of the anti-prism, trapezoid and rhombus based structure.

segments uncut and avoid unnecessary corrugations at the supports.

2.4.2 Structural Analysis - Finite Element Model

The three obtained structures were modelled in finite element analysis software ABAQUS and their performance under structural self-weight was observed.

Concluding that the local structural behaviour of the system and inherently the global structure stiffness highly depend on the connection detail capacity to transfer the occurring shear forces and bending moments between the adjacent plates, it was decided to model the actual semi-rigid behaviour of the joints as completely rigid. This simplification enabled obtaining maximal values of the occurring edge forces in each folded form for their mutual comparison. Furthermore, the boundary conditions were modelled as pinned, allowing rotations but no movement in all three directions. The plates were modelled as conventional shell elements (ABAQUS element type S4R) and their geometry was defined at the reference surface which is coincident with the plates' mid surface. Material properties of simplified linear elastic, orthotropic, 21 mm thick, structural LVL timber panels were implemented into the model with values according to [94]. Finally a linear finite element analysis was performed.

Fig. 2.8 shows vertical displacements along a normalised span of the mid transversal cross-section of the observed structures. The overlay plot of the deformed and undeformed structure shape, uniformly scaled for all three forms, is shown below. The lowest vertical displacements under dead load were found for the anti-prism based structure. The ratios between the values obtained for the other two observed structures and the anti-prism based one were equal to about 1.05 for the trapezoid and up to 3.5 for the rhombus based structure. Even higher discrepancies were found in values of the bending moments about individual edges. The ratio between the rhombus and the anti-prism based structure amounted to 5. Values for shear forces were again the highest for the rhombus based structure with a ratio of 3 to 1, when compared to the anti-prism one. The ratio between the trapezoid and the anti-prism based structure was equal to about 1.3. A distinct distribution of shear forces was found comparing the rhombus based with the other two structures. The shear forces appear on all edges of the rhombus based structure while in the anti-prism as well as trapezoid one they are present only at the edges which are not parallel to the main axis of the structure. Compared to the anti-prism based structure, these edges are shorter in the trapezoid based one which accounts for the aforementioned increase in shear.

As a result of the presented analysis it is concluded that the choice of the folded form has a large influence on the edge connection load-bearing requirements and that the joint semi-rigidity

2.4. Structural Behaviour of Folded Surface Structures

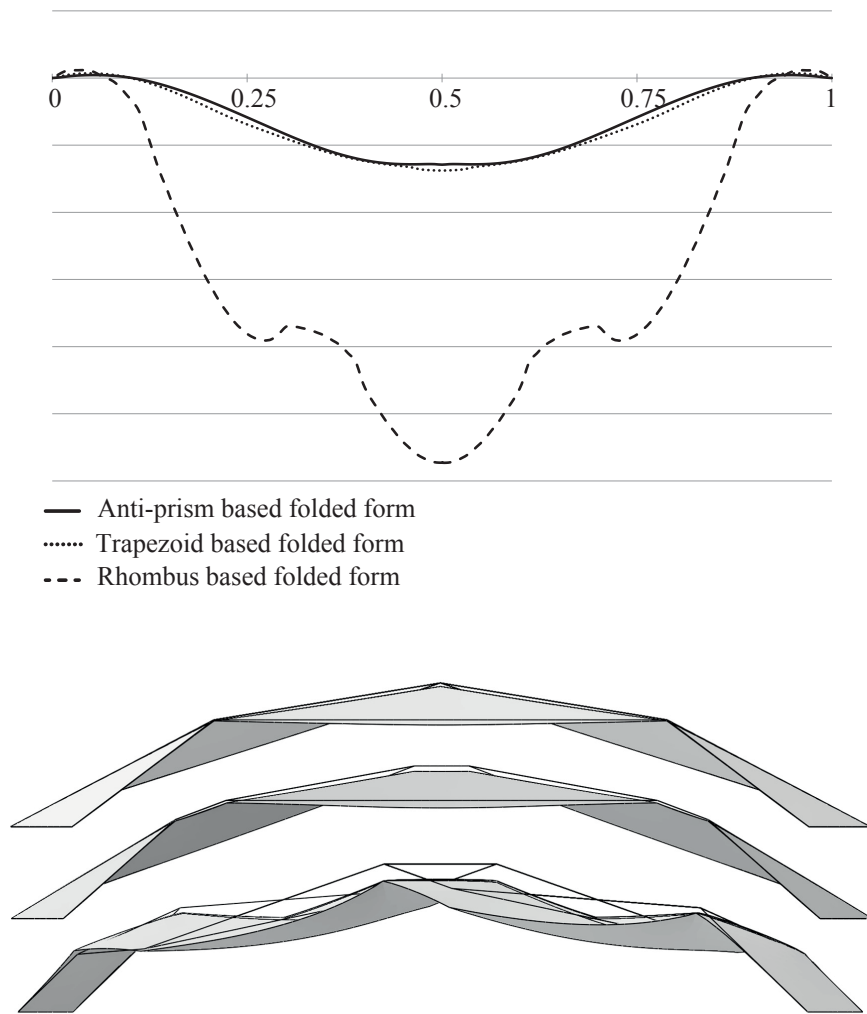


Figure 2.8 – Vertical displacements along a normalised span (above) and an overlay plot of the deformed and undeformed state, uniformly scaled for all structures (below).

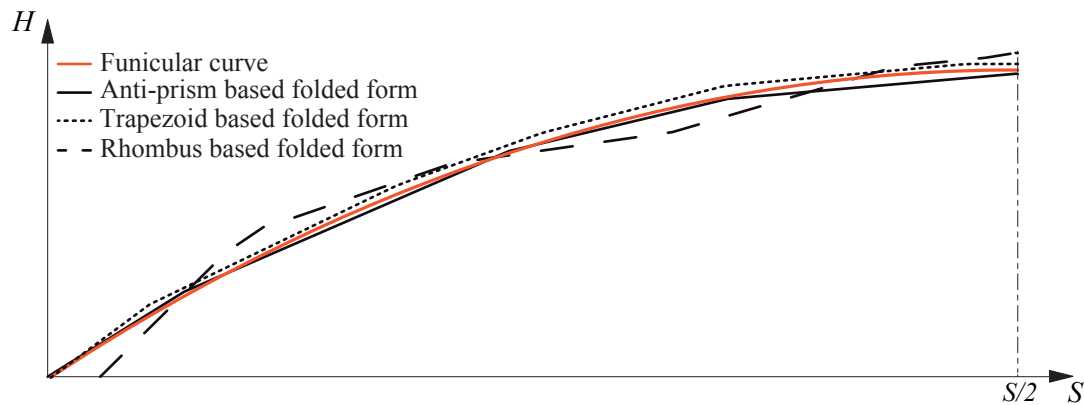


Figure 2.9 – Deviation of folded form central line from the equivalent smooth shell funicular curve.

will surely play an important role in the actual behaviour of such systems. Furthermore, the best structural performance of the folded surface structure is found when the external load is resisted mostly by shell-like extensional action. This can be enabled by choosing a form which approximates best a corresponding hollow cylinder segment, i.e. a smooth shell solution. To that end a comparison is done between each folded form transverse cross section central line and a funicular curve of the equivalent smooth shell. It can be seen that the central line of the anti-prism form is the one closest to the funicular solution (see Fig. 2.9). The amount of flexural action generated in order to resist the load depends on the degree of deviation of the folded form central line from the funicular. A substantial difference that can be noticed between the rhombus based form and the other two structures is a result of their fundamental topological distinction. The rhombus based form consists of quadrilateral faces with vertices alternately lying on the outer and inner surface of the discretized hollow cylinder, i.e. the distance between these two surfaces is equal to the maximal static height of the system. On the other hand, the anti-prism and the trapezoid based form consist of faces where all vertices lie on the outer surface. This topological difference makes the latter two forms structural height more uniformly distributed along the transverse cross-section consequently providing a higher overall effect of stiffness.

2.5 Study Case - Observations on a Prototype Structure

A prototype structure was constructed and tested in order to explore timber folded surface structures behaviour under load and collect first experiences concerning the fabrication and assembly of its constituting elements. Integral mechanical attachments were used as connection details and their geometry was designed according to [71, 59, 76].

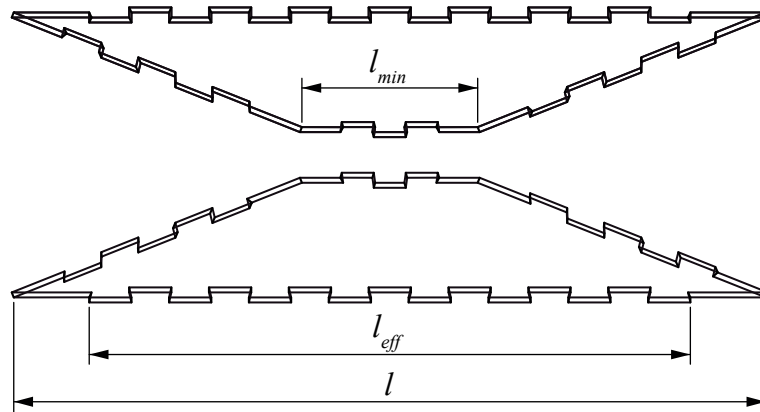


Figure 2.10 – Connection detail in a two panel assembly.

Regarding the material, two types of engineered wood products were considered, Kerto-Q structural grade Laminated Veneer Lumber (LVL) and Cross-Laminated Timber (CLT) panels. It was noticed that the more homogenous and mechanically strong peeled-veneer laminates offer particular advantages compared to CLT panels. Firstly, considerably thinner cross-sections are possible enabling for more lightweight structures. Secondly, an important shortcoming of CLT was recognised while milling the panel edges. As CLT panels consist of several layers of longitudinal timber planks which are not mutually glued on the sides, depending on the angle of the joint with respect to the individual layer plank orientation, there is a risk for considerable pieces of the joint simply chipping off after manufacturing.

Another issue of using integral mechanical attachments was recognised very early in the prototype design process. Due to specific joint geometry the effective connecting length of each edge, l_{eff} , is always shorter than its total length, l (see Fig. 2.10). This can pose a problem when trying to achieve an efficient connection of a number of plane elements which meet at one vertex. In order to reduce the vertex valence number, the prototype was designed using the isosceles trapezoid based folded form (vertex valence = 4) rather than the anti-prism based one (vertex valence = 6). The minimal edge length, l_{min} , of the trapezoid element was restricted in order to secure minimum connection between the panels and provide at least one pin on each adjoining plate edge (see Fig. 2.10). As a result an additional benefit of the trapezoid based folded form was recognised. In such a form, the edge-to-edge connectivity is realized between every element along the span and the neighbouring transversal string element (see Fig. 2.11b). As opposed to that, in the isosceles triangle solution this connection is achieved only for every second element (see Fig. 2.11a). Additionally, by using isosceles trapezoids a wider span can be realised with the same number of elements along a transverse cross section.

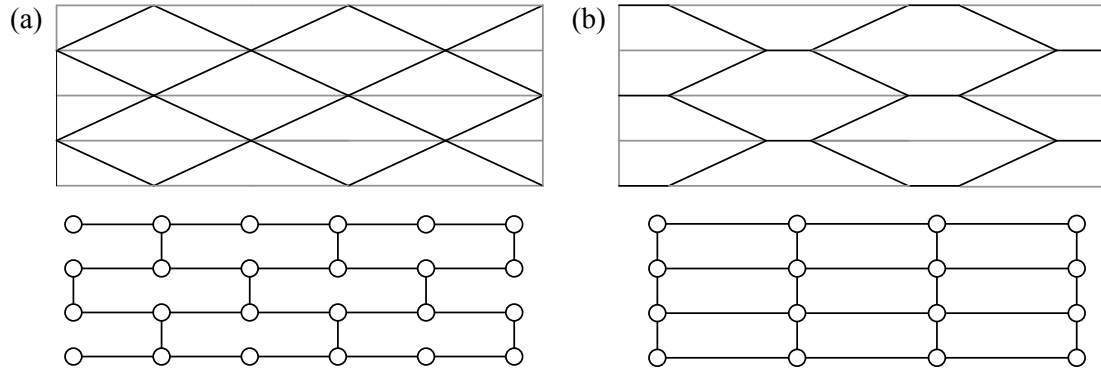


Figure 2.11 – Edge-to-edge connectivity between the faces for: (a) anti-prism based folded form; and (b) isosceles trapezoid version.

Using the RhinoPython application programming interface, a computational tool was developed which instantly generates both the geometry of the individual components and the machine G Code required for fabrication. Exploiting this geometrical freedom, we have tested our computational tool by designing a doubly curved folded surface prototype with alternating convex-concave transversal curvature (see Fig. 2.12). The built structure spanned 3 meters and was constructed with 21mm thick, Kerto-Q structural grade LVL panels (7-layer, I-III-I). The structure's total weight amounted to only 192kg. Boundary conditions that restrain displacements of the supports in the transversal direction were applied on both sides. This was achieved by fabricating form fitting lateral timber supports which enabled straightening of the edges in order to position two large concrete blocks at each side of the structure. A longitudinal line load was introduced gradually by applying pressure to a levelled steel beam placed on top of the structure (see Fig. 2.13 left). Vertical displacements were measured at the centre point of the transverse cross-section. Fig. 2.14 shows the load-displacement curve obtained from the test. Dashed line presents the first applied load cycle where the maximal load reached up to the approximated proportional limit of the curve. It can be seen that the load of 20kN corresponds to a vertical displacement of 18mm. Next, a load up to the failure of the structure was applied. This displayed a high structural efficiency (ratio of the maximal load over the dead weight of the structure) of the tested prototype, which reaches 23.44 when loaded with 45kN.

The failure of the structure occurred in the connection details, when the out of plane rotation of the edges closest to the applied line load exceeded the joint capacity (see Fig. 2.13 right). This kind of failure mode indicated that the connections used can provide a certain ductile capacity of the folded surface system made from brittle timber members. In order to assess the overall ductility of the structure and the influence of the joint semi-rigidity, the prototype was modelled in the FE analysis software with completely rigid joints, in the same way as

2.5. Study Case - Observations on a Prototype Structure

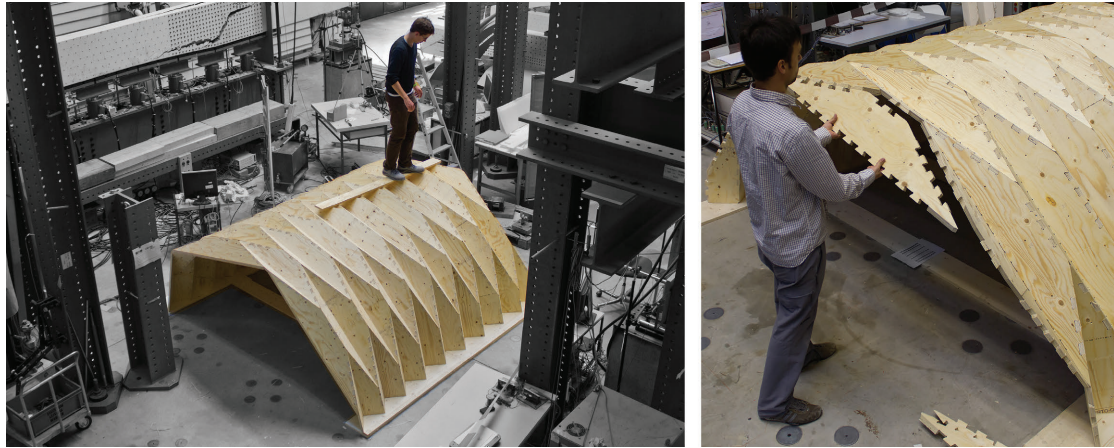


Figure 2.12 – Assembly of the prototype structure.

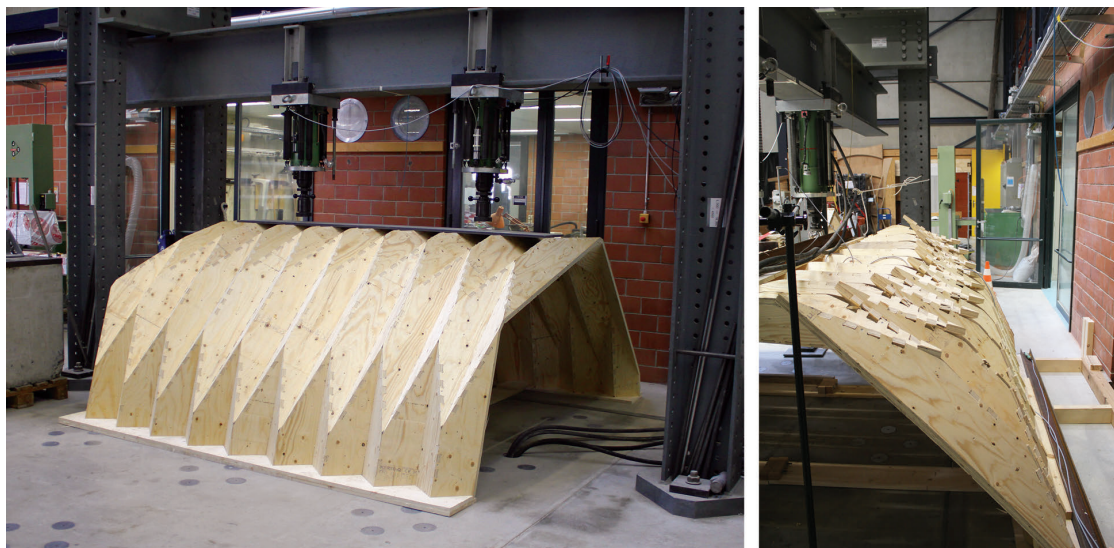


Figure 2.13 – Testing (left) and failure (right) of the timber folded surface prototype.

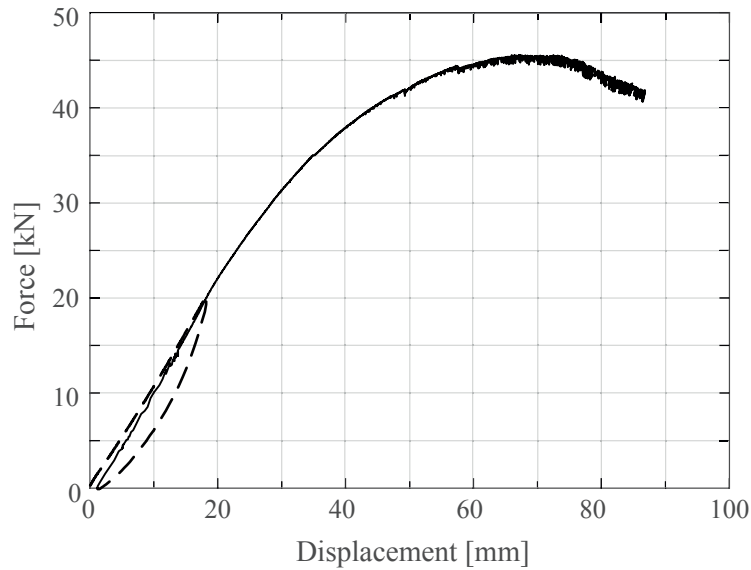


Figure 2.14 – Load-displacement curve for the tested prototype structure.

previously explained (see Section 2.4). The load was applied in the same manner as in the test, to the limit of 20 kN , which resulted in 2 mm vertical displacement. Such results suggest that the introduction of semi-rigid connections has a large influence on the overall structural behaviour and can potentially provide a beneficial ductile behaviour of timber folded surface structures under load. Further studies regarding the physical connections used within multiple panel structures, which confirm their mechanical behaviour and influence on the global load-bearing capacity, are presented in subsequent Chapters.

2.6 Conclusions

This Chapter explored the feasibility of using one-degree-of-freedom MTSJ connection details in large span timber folded surface structures. Based on the obtained results and observations, the conclusions are as follows:

- In the presented classification of folded surface structures' forms, rhombus, anti-prism and trapezoid- based bidirectional folded forms are recognised as feasible for application in timber folded systems;
- Structural constraints derived from MTSJ connections are found to have a substantial influence on the presented feasible forms geometric parameters;
- Span-to-rise ratio, dihedral angle and the panel thickness are identified as the three main parameters which govern the folded form geometry;

- The FEM structural analysis results indicate that the folded form has a large influence on the internal load distribution, where the anti-prism based form showed the most favourable structural performance under load;
- Regarding the material, LVL engineered wood panels exhibit significant advantages when compared to CLT panels. Their application seems to be more suitable considering the integrated connections fabrication as well as the total weight of the structures;
- The comparison of maximal vertical displacements measured on the prototype structure and those obtained from the FE rigid model suggests that the semi-rigid behaviour of MTSJ connections has a significant influence on the overall structural behaviour of the system.

In conclusion, the realized prototype demonstrates the realization of a very lightweight structure with a weight to surface area ratio of only $11.5\text{kg}/\text{m}^2$. It successfully combines the structural advantages of timber panels with the efficiency of folded plates, while conforming to the constraints of integrated mechanical attachments. Furthermore, it shows high structural capacity of the chosen folded form and verifies the fabrication and assembly methods used for its construction.

3 Experimental Investigations

This Chapter is based on: A. Stitic, C. Robeller and Y. Weinand, Experimental Investigation of the Influence of Integral Mechanical Attachments on Structural Behaviour of Timber Folded Surface Structures, *Thin-Walled Structures*, xx, pp. xx-xx, 2017.

3.1 Introduction

The preliminary study based on the prototype presented in Chapter 2, Section 2.5, demonstrated the potential of 1DOF open slot MTSJ timber folded surface structures to form very efficient lightweight structural systems. However, a more sophisticated experimental testing is needed for performing an in-depth analysis of their structural behaviour and validating the capacity of such structures. Additionally, the influence of the MSTJ connection detail type, i.e. open or closed-slot, and their semi-rigidity on the structure overall behaviour needs to be examined. The experimental testing of MTSJ mechanical behaviour performed by [75, 21] suggested that they provide a suitable degree of bending as well as shear stiffness. These tests concentrated on individual loading cases, i.e. bending and shear, imposed locally on the MTSJ connection detail. However in the global structure context, where the edge connections are subjected to combined influence of bending, shear, tension and compression, the potential feasibility of such semi-rigid connections has not been studied.

In the interest of examining the influence of the type of connection detail on the global behaviour of folded surface system, in this Chapter, multiple plates assembled within a large scale structure are tested. For this purpose, an innovative test setup that simulates a uniformly distributed surface load is introduced (Fig. 3.1). Additionally, since the angles defining the MTSJ locking faces inclination have to be chosen specifically to enable the assembly of the

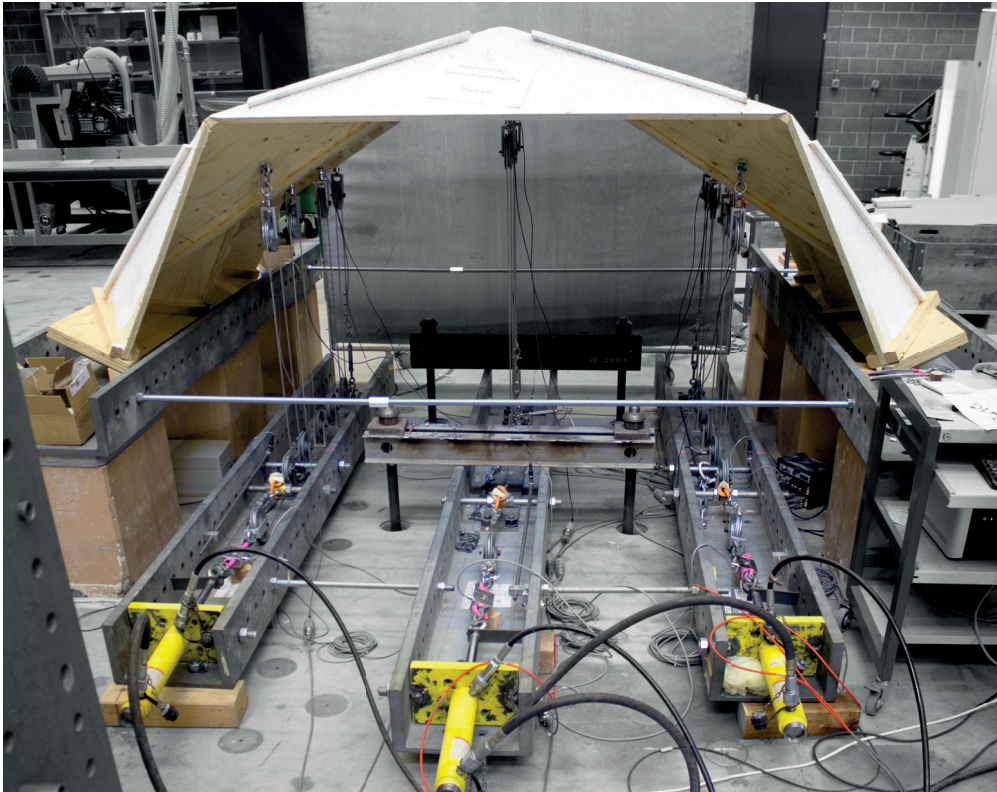


Figure 3.1 – Test setup devised for approximating uniformly distributed surface load.

tested large scale structure, preliminary small scale bending tests for establishing their detail parameters are also preformed.

The Chapter is structured as follows:

- Section 3.2 presents the structure design including material, global geometry, connection details and the fabrication process;
- Section 3.3 includes preliminary experimental tests on connection details, together with the obtained results and final choice for use in large scale structures;
- Section 3.4 presents the test setup and three types of tested large scale structures;
- Section 3.5 outlines the obtained results;
- Section 3.6 provides a discussion on the preformed large scale tests and the obtained results;
- Section 3.7 summarizes the main conclusions.

3.2 Structure Design

Detailed geometry of the test structures was defined considering a series of constraints regarding material, fabrication, connection details and element assembly.

3.2.1 Material

Panel material was chosen as 21 mm thick Kerto-Q structural grade Laminated Veneer Lumber (LVL). It consists of seven 3 mm thick spruce peeled-veneer laminates from which one fifth is glued crosswise in a lay-up $| - ||| - |$. This kind of composition improves the lateral bending strength and stiffness of the panel. Also, in this way very homogenous and mechanically strong panels are obtained, which can be assumed as having orthotropic material properties [94].

3.2.2 Global Geometry

It has been established that material, fabrication, connection details as well as element assembly constraints, dictate the range of feasible folding angles between adjacent plates, φ , as well as individual plate geometry [75]. Respectively, the final design of the folded surface was chosen as a regular *Yoshimura* pattern with maximum fold angles equal to 115° and a transversal cross section following a constant curvature, $R = 1,6m$. It consists of twenty discrete elements with maximal plate size of $1,7m \times 0,45m$, which form a structure with $3m$ span in the transversal direction ($-x$ axis, see Fig. 3.2) and $1,5m$ length in longitudinal direction ($-y$ axis, see Fig. 3.2). The height of the structure in its midpoint is equal to $1m$.

3.2.3 Connection Details

In the experimental tests presented in this paper, three different types of structural plate connection details were considered: 1) MTSJ with open slots; 2) MTSJ with closed slots; and 3) adhesively bonded connections (see Fig. 3.3). The use of metal fasteners was not considered relevant, since their application either highly restricts the requirements for minimal plate thickness, or a large amount of fasteners is necessary for achieving a sufficient connection stiffness [27]. Therefore, in the presented case of edgewise connections between 21 mm thin plates, such detailing was not feasible.

MTSJ with open slots

These prismatic connections consist of interlocked tabs and slots assembled along a specified vector of insertion. Their geometry can be described by using a set of three Bryant angles,

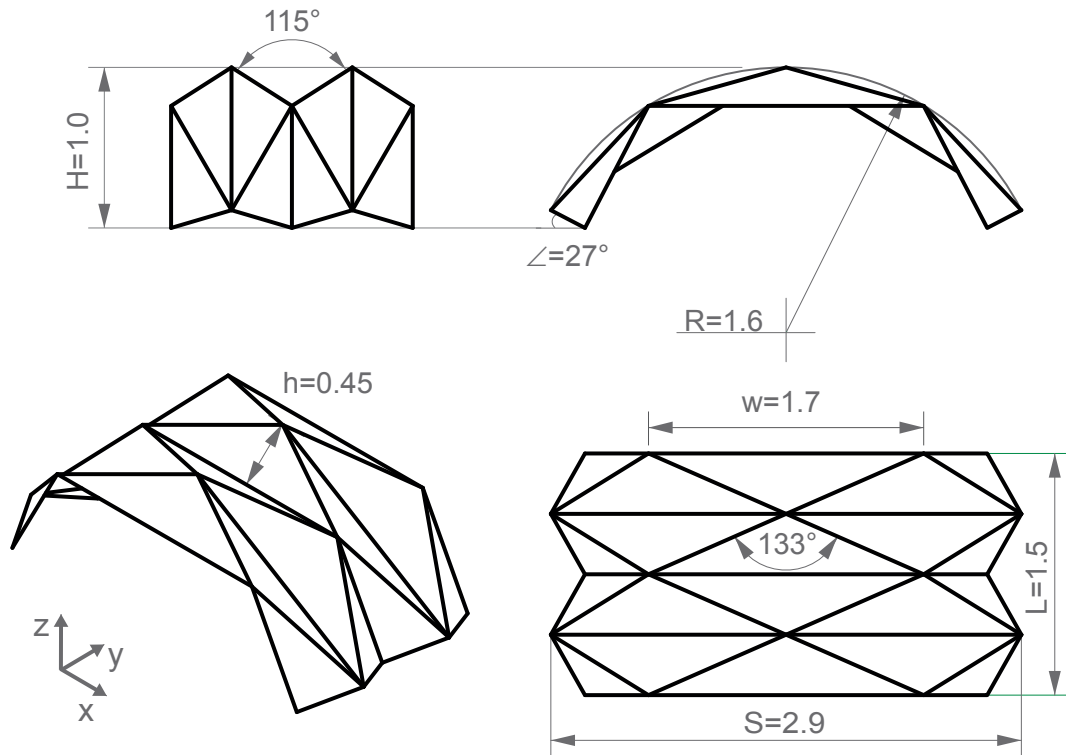


Figure 3.2 – Large scale structure geometry parameters

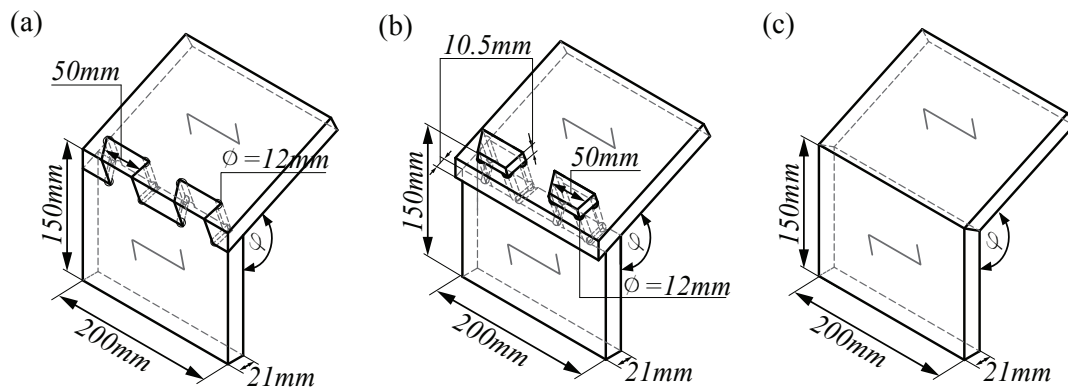


Figure 3.3 – Test detail geometry parameters, $\varphi = 115^\circ$; (a) MTSJ with open slots; (b) MTSJ with closed slots; (c) Miter joint.

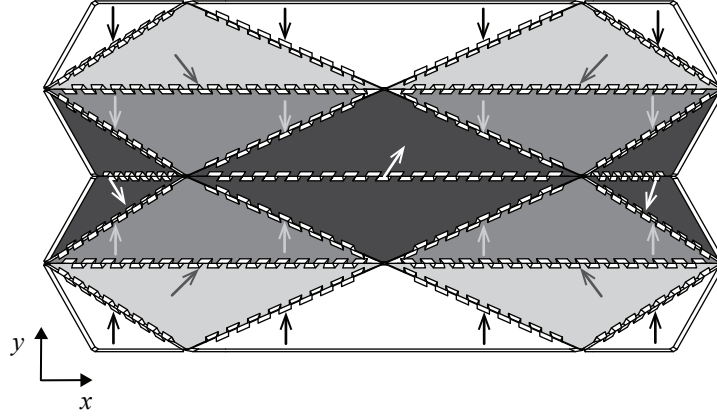


Figure 3.4 – MTSJ plate insertion vectors and assembly sequence of the chosen folded form. Plate grayscale range illustrates the order of assembly, black represents the first and white the last plates to be put in position. Arrows display the insertion vectors.

θ_1 , θ_2 and θ_3 . They further define the contact locking faces of adjacent edges, as well as the three-dimensional subset of feasible insertion vectors [75]. Their load bearing capacity, i.e. stiffness, greatly depends on the mentioned set of geometrical parameters. Bending and shear load tests, performed on two plate assemblies with various geometries, showed that the highest stiffness of such joints can be expected for the following set of angles: $\theta_1 = 0^\circ$, $10^\circ \leq \theta_2 \leq 30^\circ$, $15^\circ \leq \theta_3 \leq 30^\circ$ [75, 21]. These values are further constrained by the requirement for simultaneous assembly of two plate edges where the individual edge insertion vectors have to be parallel [72]. Finally, for such edges, i.e. skewed edges of the triangular plates, angle values were chosen so that they result in insertion vectors parallel to the structure's $-y$ axis; $\theta_1 = 0^\circ$, $\theta_2 = 27^\circ$, $\theta_3 = 20^\circ$. Concerning the remaining straight edges, i.e. those parallel to the structure's $-x$ axis, there existed two possibilities for governing the values of their Bryant angles: 1. either the insertion vector of the straight edges is chosen equal to those of the skewed edges, resulting in different values for the straight edges Bryant angles set, $\theta_1 = 0^\circ$, $\theta_2 = 0^\circ$, $\theta_3 = 20^\circ$; or 2. Bryant angles set values are kept equal to those of skewed edges, resulting in different insertion vector directions for the straight edges. The latter option was chosen in order to maintain equal joint geometry within the entire structure (Fig. 3.4).

MTSJ with closed slots

In literature, these kind of joints are also referred to as *through type joints*. Their geometry can be defined in a similar way as for the open slot ones [74], main difference being that their insertion vector is constrained to a two-dimensional subset. This is a result of the slots offset from the plate edge, making all feasible edge insertion vectors lie within the plane of the plate which is being inserted. In the presented case, their assembly sequence is equal to the one of MTSJ with open slots. Additionally, for both MTSJ the length of tabs and slots at the

intersection of the plates mid-planes was fixed at 50 mm , to achieve equal distribution along the edges, leaving a maximum of 10% of the edge length unconnected at the ends.

Adhesively bonded connections

In this detail adhesive was used for realizing edgewise connections which can typically be considered as rigid. This was further used to serve as a reference for determining the level of MTSJ structures semi-rigidity. For achieving the highest possible stiffness various types of edge geometries were tested in combination with 1C PUR glue (Collano Semparoc Rapid-V). The pressure required during curing of the adhesive, for forming the bond between two joining elements, was applied by inserting screws along the edges. The screws were removed before testing and had no influence on the mechanical behaviour of the connections.

3.2.4 Digital Fabrication and Assemblyⁱ

Manufacturing of individual parts, including the automatic generation of joint geometry with the desired parameters, was done using a digital fabrication tool for generating the 5-axis MAKKA MM7S CNC machine G-code. This allowed for the rapid creation of specimens with variable geometry parameters as well as their fabrication data, which would have been impossible with state-of-the-art CAD software tools. These functions were implemented through two custom developed programs, using the programming language Visual C# and the Rhino Common Software Development Kit (SDK)[1]. A realtime preview of the output geometry was realized through the implementation as a CAD Addon for the visual programming software Grasshopper®. Panels of $2,5\text{ m} \times 1,25\text{ m}$ dimensions were supplied by Metsä-wood Germany. They were cut with a 12 mm diameter shank-type milling cutter and $0,05\text{ mm}$ tolerance, creating a tight fit with $0,1\text{ mm}$ assembly clearance between the adjoining plates. In order to have a smooth assembly, it was necessary to ensure constant 21 mm thickness of the plates along the edges. As the thickness within one panel may vary up to $\pm 1\text{ mm}$ [94], each one was planarized along the plate edge joining area before the cutting process. With respect to the defined insertion vectors and the interlocking advantage of the chosen single-degree-of-freedom MTSJ, it was necessary to follow a specified sequence for assembling individual parts into the global structure (Fig. 3.4).

3.2.5 Geometry Generation

The generation of the plate geometry with MTSJ connectors is based on a target surface S_{target} . This surface is required in the form of planar facets, as a doubly-connected edge list

ⁱThe described digital fabrication tool was developed by the publication co-author, C. Robeller.

(DCEL) data structure [17]. This is a standardized structure for planar graphs, available in various software packages and software development kits. It allows for neighborhood request management, which is crucial for the program to generate the plate geometry. Additional input parameters are listed in Table 3.1. They include the width of the tenons w_{tenon} , the thickness of the plates t_{plate} , and a text string which sets the parameters for individual joints. This is possible through the identifiers of the edges in the polygon mesh data structure. Each of the edges is assigned a number, which is visualized by the program. Individual joint parameters for each of these edges can then be manually set by adding a line of comma separated values to the input string *Jconfig*. Each line sets the parameters for one edge, beginning with the identifier number of the edge (0) and the joint type (1). The next three values are used to set the X (2), Y (3) and Z (4) components of the joint insertion vector. If no custom configuration is specified for an edge, it is processed by default as a miter joint. The same applies to joints where the dihedral angle φ lies outside of the possible range for 1DOF MTSJ. As its primary output, the program generates a pair of contour polylines for each of the plates. It consists of a top and bottom contour, which are joined together from the polylines of the individual edges of each polygon facet. A transition segment is required at the start and end of each joint, towards the vertices of the polygons. The length of these segments is set through the input parameter L_{trans} , as a percentage of the edge length. Two additional, optional outputs can be generated through two boolean switches. The *Flatten* option will create a 2d copy for each pair of plate contours, where the geometry is transformed from the 3d plane of the target surface mesh facet it is based on, to the 2d XY plane of the world coordinate system. This optional 2d output is used for fabrication, where the plate contours need to be nested onto the timber plates. The *BREPs* option will create 3d boundary representation elements (BREP) for each plate. These solids are collections of connected surface elements, based on the plate contour polygons. They are generated by the algorithm through a combination of two trimmed surfaces for the top and bottom contour polyline, and a loft surface in between the two contour polylines. The optional output of BREPs is needed for Finite Element based calculations and for visualization purposes.

Input		Output	
Parameter	Type	Parameter	Type
S_{target}	double	Plateconts 3d	Polylines
w_{tenon}	double	Plateconts 2d	Polylines
t_{plate}	double	Platebreps	BREPs
Jconfig	string		
L_{trans}	double		
Flatten	bool		
Breps	bool		

Table 3.1 – MTSJ Generator Program.

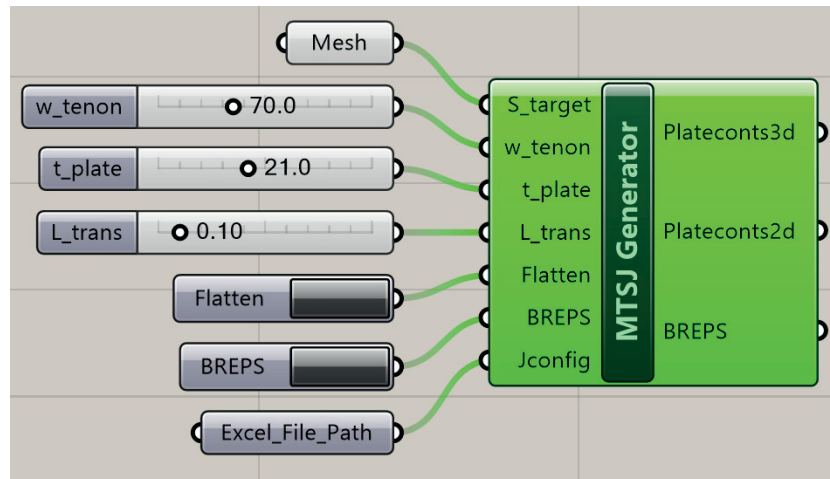


Figure 3.5 – MTSJ generator in Grasshopper.

Input		Output	
Parameter	Type	Parameter	Type
Platecontours	double	G-Code	string
Z return	double		
Z security	double		
r_{tool}	double		
n_{infeed}	integer		
$F_{cutting}$	integer		
F_{axial}	integer		
Notches	bool		

Table 3.2 – Plate Fabrication Program.

3.2.6 Fabrication Data Generation

The Generation of the ISO6983 G-Code is created with a second program, which was custom developed for the MAKKA mm7s 5-axis CNC router. This program generates the output string that contains the sequence of machining instructions based on the *Platecontour* polyline pairs, which are created with the geometry generation program from Section 3.2.5. The number of segments in the top polyline and bottom polyline within a contour pair must be equal, as they define the quadrilateral polygon facets for the cutting. The triangular facets, which are required at the transition from MTSJ to miter joints, are generated as quadrilateral faces with two points at the same location. In the case of closed-slot MTSJ, a plate definition contains multiple pairs of top and bottom polylines. Each additional pairs defines a slot, which is differentiated from the primary pair of plate contours through an inverted orientation. While the orientation of outside contours is counter-clockwise, inside contours are oriented in a clockwise rotation. This is later reflected in the direction of the cutting tool path. Finally, corresponding lists of consecutive tool path points and machining head cardan rotation angles in the output text string *G-Code* are calculated based on input parameters listed in Table 3.2. They include the tool radius r_{tool} , the number of vertical passes n_{infeed} , machine feed rates for the cutting velocity $F_{cutting}$ and F_{axial} , and Z values for the definition of retreat and security planes, to which the tool moves during the fabrication. The input parameter *Notches* will automatically create tangential notches [73] on all concave corners, which is an essential part of the fabrication of integral timber plate joints. This feature can be deactivated for pre-passes, also called roughing, commonly used when machining thick plates.

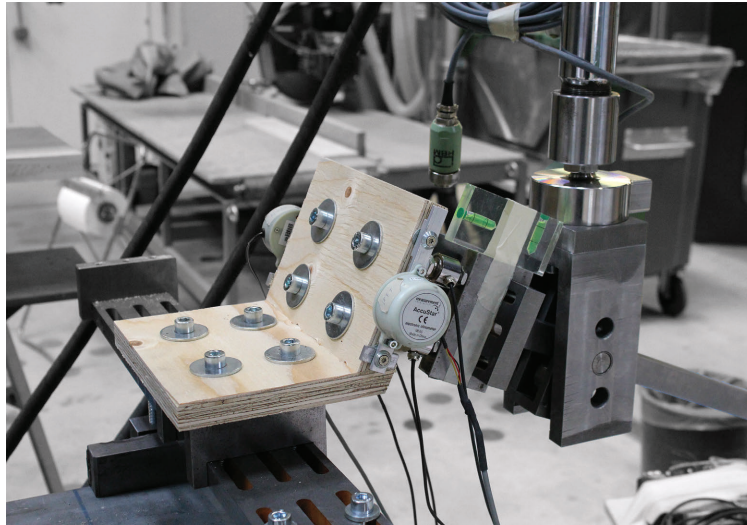


Figure 3.6 – Test setup for connection detail bending tests.

3.3 Preliminary Connection Detail Tests

Small scale bending tests were performed on two plate assemblies in order to establish the detailed parameters of connections to be used in large scale structures. Dimensions of the assembled plates were $200\text{mm} \times 150\text{mm}$ (Fig. 3.3). The length of the tabs and slots at the intersection of the plates mid-planes was fixed at 50mm . The plates were positioned under the angle of $\varphi = 115^\circ$ in a test setup consisting of a fixed part restricting the movement of one plate and a lever arm pushing the other plate (see Fig. 3.6). This causes rotation around the central axis of the joined edge and thus closing of the two-plate sample. The details were tested only in the closing mode as it has shown to be less stiff compared to the opening one [75].

Three types of adhesively bonded edge geometries were tested for determining the most rigid one: 1) miter joint with the cut face lying in the internal bisector plane of the joint angle; 2) regular finger joint; and 3) MTSJ with open slots with parameters as explained in Section 3.2.3 (Table 3.3). 1C PUR adhesive (Collano Semparoc rapid V) was applied along the edges of adjacent plates and constant pressure during curing was ensured by adding crosswise screws. After 24 hours the screws were removed and the samples tested.

In the interest of examining their failure modes, as well as the level of their semi-rigidity with respect to the glued rigid details, three details without applying adhesive were also tested: 1) MTSJ with open slots with parameters as explained in Section 3.2.3; 2) MTSJ with closed slots and the same parameters; and 3) MTSJ with closed slots where the influence of θ_3 angle was studied (Table 3.4).

3.3. Preliminary Connection Detail Tests

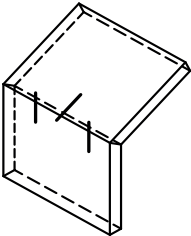
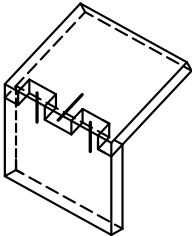
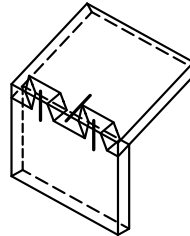
Connections with adhesive:				
		Miter joint	Finger joint	MTSJ open slots
θ_1	-		0° 	0° 
θ_2	-		0°	27°
θ_3	-		0°	20°

Table 3.3 – Test geometry of connection details joined using adhesives. Three bold lines on adhesively joined details mark the positions of screws used for applying pressure.

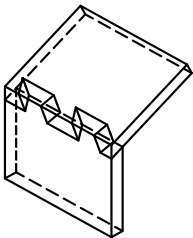
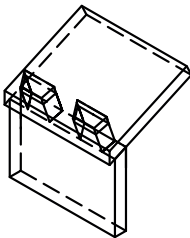
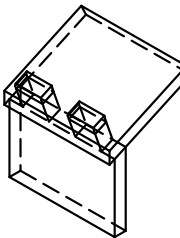
Connections without adhesive:			
	MTSJ open slots	MTSJ closed slots	MTSJ closed slots
θ_1	0° 	0° 	0° 
θ_2	27°	27°	27°
θ_3	20°	20°	0°

Table 3.4 – Test geometry of connection details joined without using adhesives.

3.3.1 Connections With Adhesive

Fig. 3.7 shows the corresponding sample moment-rotation curves obtained from the adhesively bonded test details. The different slopes of the ascending parts of the curves show that the miter joint exhibited the most rigid behaviour. This is contrary to the initial assumption that the combination of adhesive with finger joint or MTSJ geometry would bring benefits with regard to enlarged glued surface area, and therefore stiffness. It is concluded that these benefits are lost due to fabrication constraints as well as necessary tolerances, such as: the tab and slot sides of two bonded plates cannot be machined precisely enough to achieve the perfect fit needed to distribute pressure uniformly over the entire joint area; moreover, milling sharp corners with a circular tool results in circular notches at the ends of each tab and slot which additionally reduce the adherent's surface length, l_a (see Fig. 3.8).

As shown in Fig. 3.8 the miter joints exhibit highly brittle cleavage failure, which takes place at the bonded interface. It first occurs in the plate, due to tension perpendicular to the grain in the five layers with grain orientation parallel to the joined edge. The observed failure was very shallow, where only a few wood fibers remained attached to the glue, and it was instantly followed by the adhesive failure in the remaining two layers with opposite grain orientation. On the other hand, failure of the remaining two glued joints happened entirely within the panel, naturally resulting in lower stiffness. In these details the bonding interface is situated between the edges and faces of mutually connected plates, making the bond strength higher. The failure happens due to delamination caused by tension acting perpendicular to the plate plane.

Compared to the glued finger joints, the MTSJ ones exhibited lower stiffness but also a certain level of ductility after failure. This is a result of interlocking due to the introduced θ angles, where additional compression forces appear between the inclined tab and slot edges. On one hand, this reduces the effective tab length, l_{eff} , for resisting delamination in the top layers (see Fig.3.8), on the other hand it is responsible for the exhibited post-failure load capacity. Based on the results presented above, the detail with the highest stiffness, i.e. adhesively bonded miter joint, was chosen for application in larger scale structures.

3.3.2 Connections Without Adhesive

Moment-rotation curves of non-glued connection details are also shown in Fig. 3.7. They can be generally divided into three parts: 1) first part of the curve shows the relative slip at the joint interface; 2) after coming into full contact the ascending part of the curve describes the joint stiffness; and 3) the descending part describes post-failure behaviour. With respect to MTSJ with open slots, the ones with closed slots showed higher stiffness and a considerably

3.3. Preliminary Connection Detail Tests

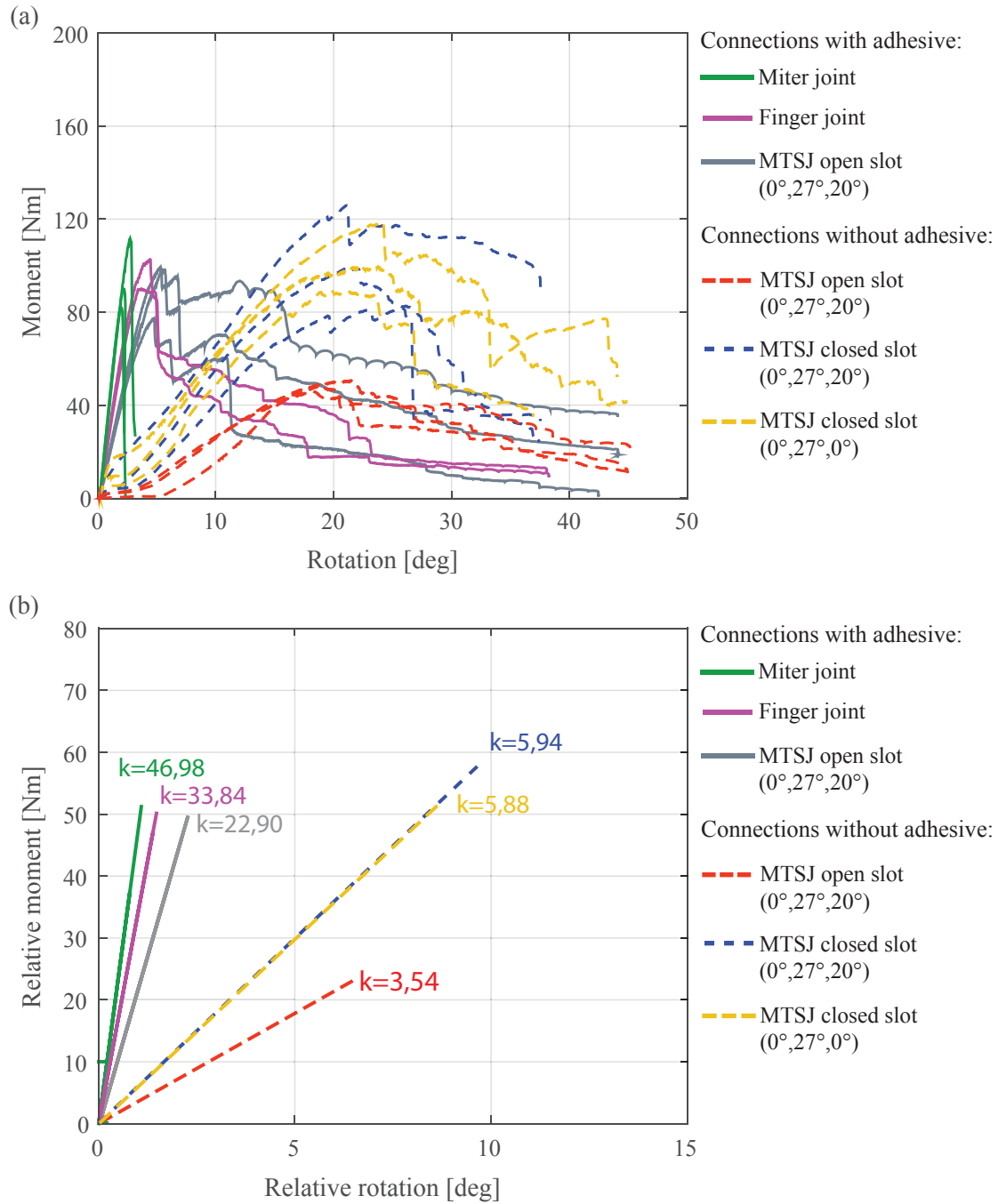


Figure 3.7 – (a) Moment-rotation curves of 6 connection details. A group of three experimental replicates was produced for each connection detail type and each replicate was fitted with a single curve. Triplets of curves of the same group are marked with the same color; (b) Stiffness, k , for each respective group. The coefficient k is determined by fitting a linear regression model to each of the 6 groups containing 3 replicates, in the elastic region of the M-R curve $[0.1M_{max}, 0.6M_{max}]$. The lower bound of the elastic region, $0.1M_{max}$, was chosen in order to exclude the initial slip while the upper bound, $0.6M_{max}$, was determined by imposing $R^2 > 0.95$, where R^2 is the coefficient of determination of the linear regression.

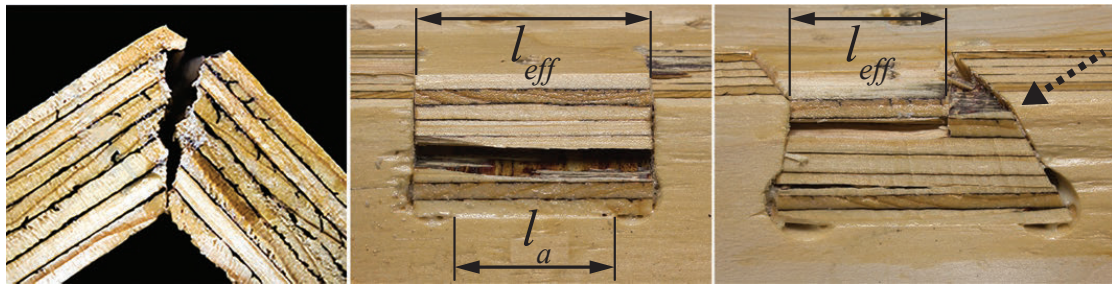


Figure 3.8 – Failure of adhesively bonded connections. From left to right: miter joint, finger joint, MTSJ with open slots. In MTSJ with open slots dashed arrow points to the surface where additional compression occurs.

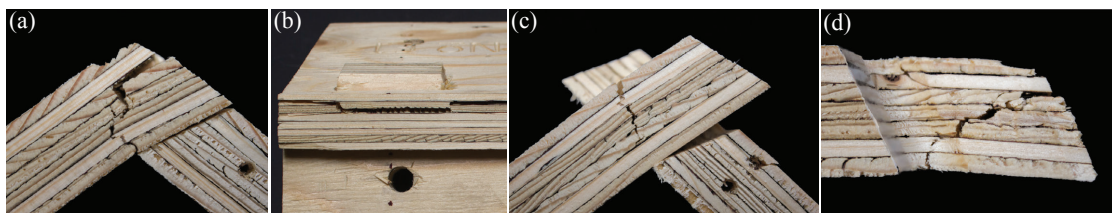


Figure 3.9 – Failure of MTSJ connections without adhesive; (a) MTSJ with open slots showing the side view of tab failure. In two top layers contact is not achieved due to initial slip causing delamination at the interface between 2nd and 3rd layer. The rest of the cross section fails due to tension perpendicular to main plate grain orientation; (b) MTSJ with closed slots, $\theta_3 = 0^\circ$. Delamination failure occurs at the interface between differently oriented layers, and failure due to tension perpendicular to grain in layers which are in the direction of plate main grain orientation, i.e. layers 1,3,4,5 and 7; (c) MTSJ with closed slots, $\theta_3 \neq 0^\circ$. Failure at the weakest longitudinal cross section of the slot plate, propagating from the top face due to tension perpendicular to the main plate grain orientation; (d) MTSJ with closed slots, $\theta_3 \neq 0^\circ$. Second type of failure mode, where the tabs fail due to tension perpendicular to the main plate grain orientation.

lower amount of initial slip. This slip is a result of fabrication and assembly tolerances and is significantly reduced for closed slots due to their protrusion geometry. The main failure modes of MTSJ details without adhesives are shown in Fig. 3.9. For more details on the mechanical behaviour of the MTSJ with open and closed slots the reader is referred to [76, 75] and [74], respectively. The average stiffness values of the connection detail types were obtained by fitting linear regression to the moment-rotation experimental results of all three tested replicates and by measuring the slope of the estimated line. With respect to the adhesively joined detail results, bigger experimental scatter was observed in the moment-rotation curves of the MTSJ connections without the applied adhesive (see Fig. 3.7). This seems to be a result of the inherent variability of the timber panel properties which effects are more emphasized as the failure takes place in both areas of the tab and outside of it.

Concerning the influence of θ_3 angle in MTSJ with closed slots, the results suggest that it has

no considerable impact on the stiffness as well as on the strength of the detail. This could be a result of the small plate thickness in respect to relatively large sized notches, where the intended beneficial compression surface at the inclined sides of the joints with $\theta_3 \neq 0^\circ$ was simply too small to make any significant difference in its load-bearing capacity. Consequently, for reasons of simplicity in large scale structures the MTSJ with closed slots was taken with $\theta_3 = 0^\circ$.

3.4 Large Scale Structure Tests

Three groups of distinct large scale structures consisting of three replicates were tested, each group with a different connection detail. The details were chosen with respect to the obtained small scale results; 1) miter joint with adhesive applied along the adjoining edges representing a rigid connection; 2) MTSJ with open slots with $\theta_1 = 0^\circ$, $\theta_2 = 27^\circ$, $\theta_3 = 20^\circ$; and 3) MTSJ with closed slots with $\theta_1 = 0^\circ$, $\theta_2 = 27^\circ$, $\theta_3 = 0^\circ$. Additionally, certain adjustments were made concerning the miter joint edge geometry, having seen that already in small scale samples aligning plate edges and inserting screws presented difficulties. One-faced finger joints were added along the edges for ensuring precise positioning during assembly of plates (see Fig. 3.10). They provided space for inserting screws perpendicular to the plate normal direction as well as avoiding sliding while doing so. The specific geometry of these joints allowed for the joint cut face to remain at the internal bisector plane of the dihedral angle, making it possible to integrate with the miter joint edge geometry.

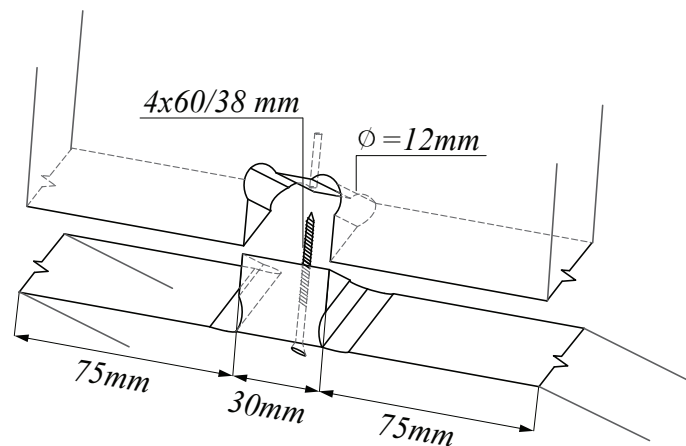


Figure 3.10 – One-faced finger joint geometry shown with a screw for applying pressure. Joint spacing along the edge was taken as 180mm. In this figure pressure area of one screw is shown.

3.4.1 Test Setup

As all surface-active structural systems, folded structures are designed for taking surface loads. Due to the fact that their surface is corrugated the application of continuous load in a controlled manner for performing experimental work has proven to be a challenging task. Similar structures have been tested by applying line and point loads on the structure edges and vertices, where the results showed that in this way a distorted impression of the structural behaviour is obtained, as opposed to that expected in actual practice. It was also assumed that the structures would behave considerably different under a uniformly distributed load [43, 18]. For that, inspiration for alternative experimental methods was found in shell structures. Such methods include the use of pressure as well as vacuum loading techniques or the application of a discrete load systems for simulating uniformly distributed load [42, 41]. Due to the size of our structure as well as its corrugated surface, the use of first two mentioned methods was excluded, due to accuracy issues in constructing an efficient testing apparatus. Finally, it was decided to represent the uniform load with discrete concentrated loads applied at the geometrical center of each plate. For reference, 1 kN of load applied at each of the 10 concentrated points, amounting to 10 kN of total load, was equivalent to 2.63 kN/m^2 uniform load. For simplicity, the structure was designed following a singly curved surface in order for all the constituting elements to be of the same shape and size, i.e. surface area. This enabled for all the discrete loads to be of equal size as well. Additional issues arose from the fact that in bidirectional folded surface structures individual plates lie in different planes, so the direction and the amount of the plate displacement varies depending on its position in a global assembly. As a solution, a load application setup was devised, which enables simultaneous, continuous loading of discrete plates while compensating for their differential displacements (Fig. 3.11). A system of pulleys with a steel wire running through, was positioned at each of the three longitudinal lines of loaded elements and the displacement-controlled load was introduced at the end of each system (see Fig. 3.11c). Loading system energy losses due to friction and other causes were not taken into account in the performed experiments. Fitting a cubic polynomial regression model to the preliminary test data, showed that the forces exerted onto each plate during the course of the experiment resulted in a coefficient of determination equal to 0,99. This confirmed that the uniform load was well approximated and that all the point loads applied on the structure could be considered equal over time.

Boundary conditions that allow rotation about $-y$ axis were used along the two supporting sides (see Fig. 3.11b). The structure was inserted into the 18mm deep slots in the timber part of the supports and fixed using additional timber slats and self-tapping screws placed crosswise.

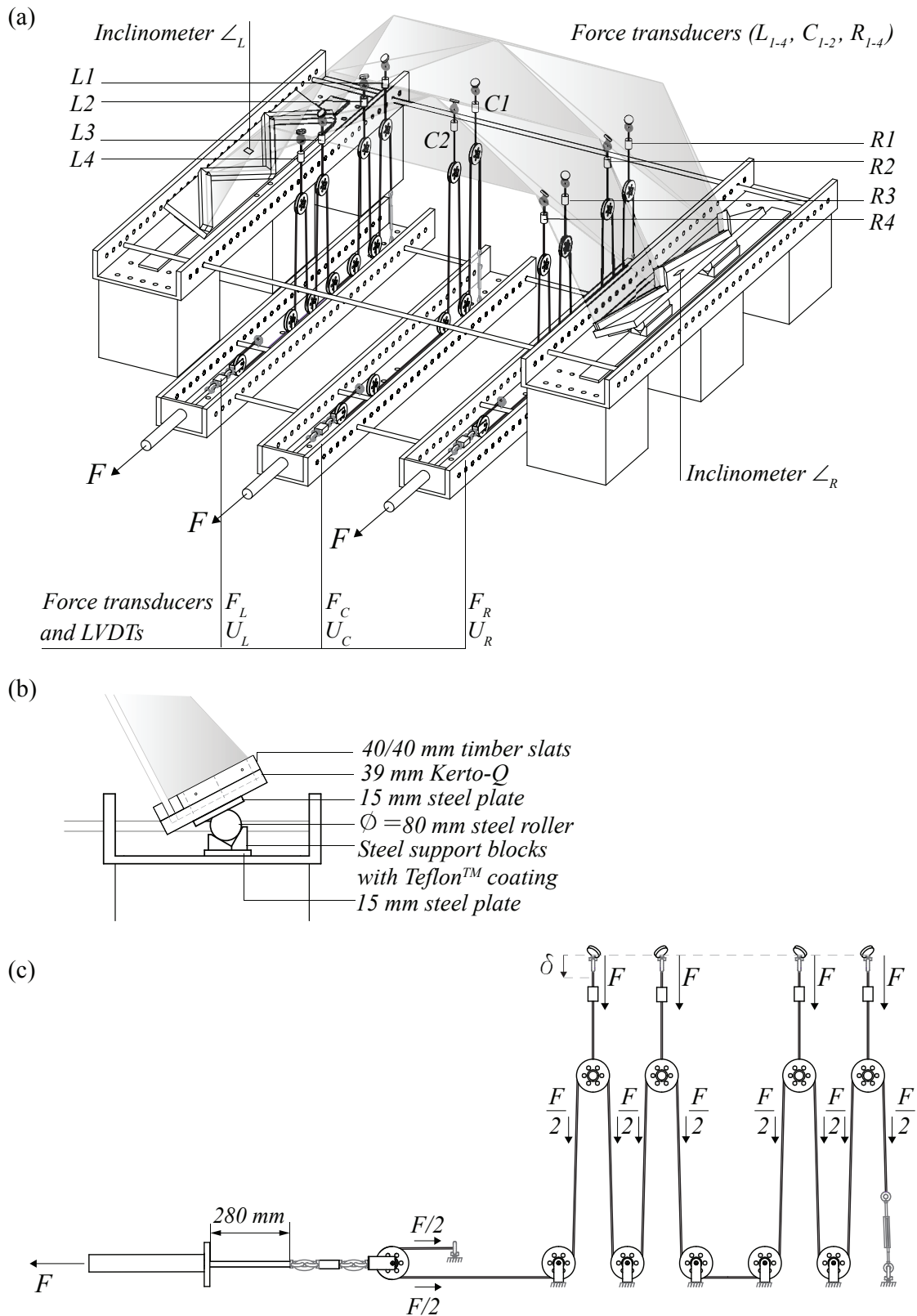


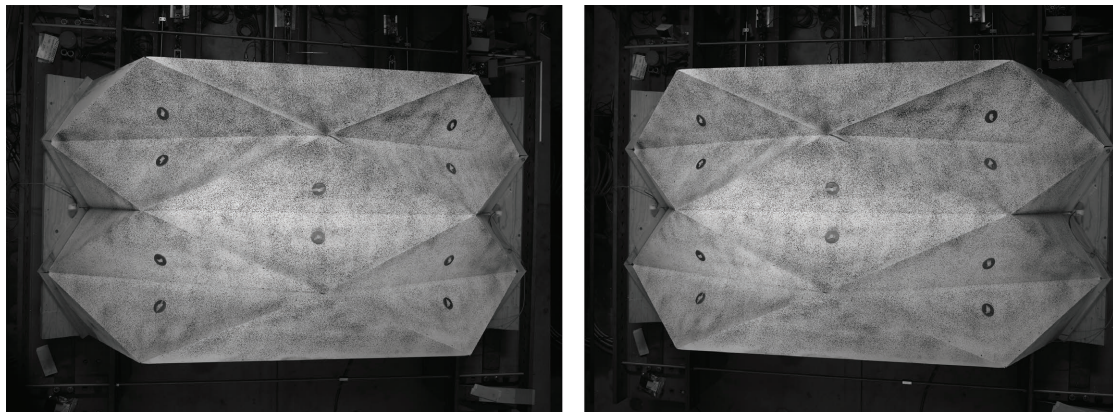
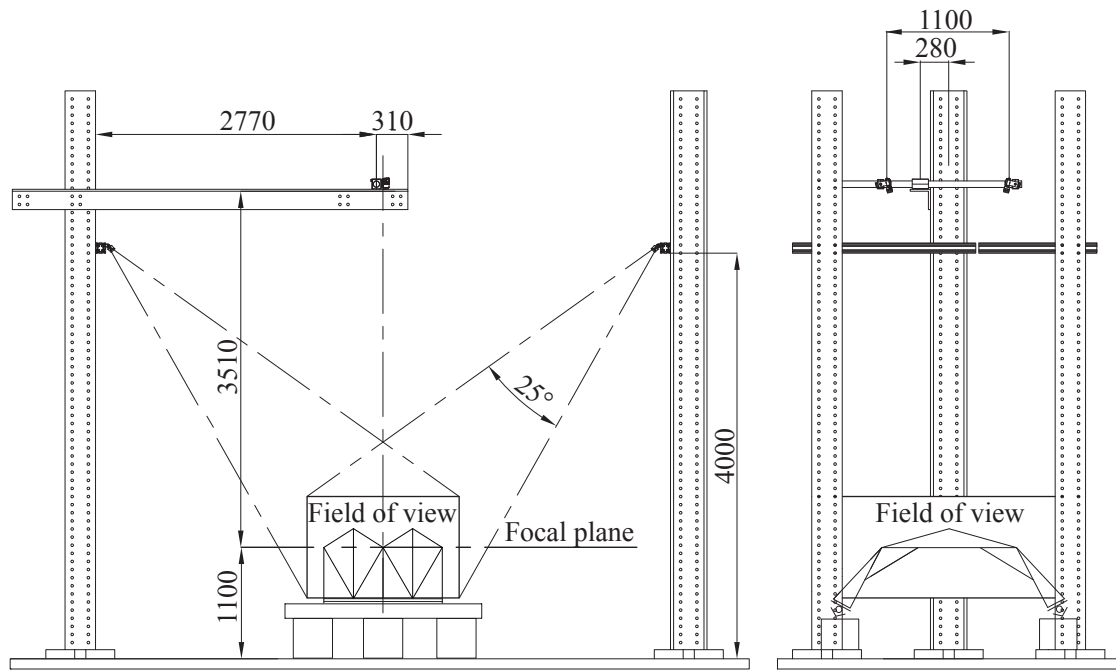
Figure 3.11 – (a) Test setup with marked measurement instrumentation; (b) Side support detail; (c) Load application setup schematic.

3.4.2 Instrumentation and Loading Procedure

Force transducers, LVDT's and inclinometers were placed as shown in Fig. 3.11a and marked as follows:

- $L_{1-4}, C_{1-2}, R_{1-4}$: HBM U9C force transducers of $20kN$ nominal force were placed above the pulleys at the centroid of each loaded plate.
- U_L, U_C, U_R : Linear variable differential transformers (LVDTs) were positioned at the end of each cable for measuring the overall system displacements.
- F_L, F_C, F_R : The total applied force is measured by HBM S9M force transducers of $20kN$ nominal force, which are positioned at the hydraulic cylinders.
- \angle_L, \angle_R : For controlling the rotation of the supports two AccuStar® electronic inclinometers with a $\pm 60^\circ$ sensing range were fixed onto the slotted $39mm$ timber plates.

Additionally, a three-dimensional digital image correlation (DIC) system was used for obtaining strain and deformation fields of the entire structure. A set of two SVCam-HR29050 29 Megapixel GigE VISION cameras was fixed on a cantilever above the setup for securing a clear view of the entire structure's top surface. The angle between the cameras was equal to 21° (Fig. 3.12). The cameras were used with a Zeiss 35mm, f/8 Distagon ZF-I lenses and BP525 Green Bandpass Filters. The cameras focal plane was set at the bottom level of the two central plates fold. Even though the whole structure was within the cameras field of view, equal to approximately $3 \times 2m$, some regions of the structure were difficult to capture. Particularly the half-size plates close to the supports, due to their high inclination with respect to the cameras position (Fig. 3.13). The structure was symmetrically illuminated by two pairs of green LED Effilux light bars with a semi-opaque diffuser and a diffusion angle of 25° . The bars were mounted on the vertical steel columns. The speed of image acquisition was set at $0,1Hz$ and the exposure time was equal to $35000\mu s$. DIC system control was performed by Correlated Solutions VIC 3DTM software. The structure's top surface was painted matte white after which a random speckle pattern was applied with a pneumatic paint sprayer containing black paint (Fig. 3.14). This allowed for the analysis software to easily track the deformation of the top surface to sub-pixel accuracy. The calibration target of $12 \times 9 - 50mm$ size and uniformly spaced markers was used. The structure shape easily facilitated the positioning of the target at different locations and various angles. It was important to keep the orientation of the target constant at all positions. Around two positions per plate at different angles were taken to obtain a good score after calibration (between 0,2 and 0,3) with order of distortion set to 2. Half-sized plates on the support sides were not included in the calibration process. The DIC



system was calibrated for each test individually in order to ensure the accuracy of measured values. First, for every experiment five images were taken to test the reliability of the setup. Generally, the vertical displacement V was considered the main indicator, and projection error values less than $0,01\text{ mm}$ were targeted when taking into consideration the entire area of interest. This area did not include the half-size plates close to the supports due to previously explained insufficiently clear view. Values less than $0,005\text{ mm}$ were targeted for the two plates of the central valley fold, where higher accuracy could be achieved. A system of pulleys was positioned at each of the three longitudinal lines of loaded elements. It consisted of pulleys attached to the structure at 10 plate geometrical centers, and those attached onto the steel U-beams, which were fixed through the concrete floor slab for keeping the system in position. As shown in Fig. 3.11a, two naked edge triangular plates were not loaded during the experiments. This was done in order to avoid high deformations and buckling of long unsupported edges which could lead to unwanted early failure at these regions. Additionally, half triangle plates along the supports were also not loaded, in favour of reducing the complexity of the setup. This decision was supported by the fact that their high inclinations, reduced surface and proximity to the supports would lead the forces directly into the supports, not having much influence on the global spatial structural behaviour. A steel cable, $\phi = 5\text{ mm}$, weaving through each of the three systems was fixed at one end and at the other connected to a hydraulic linear cylinder, Enerpac RD-910, through which a displacement-controlled load was introduced. The preliminary test for evaluating the mechanical components of the test rig showed that the available piston stroke of 280 mm was not sufficient for the planned tests. For that, an extra pulley was added to each of the systems (see Fig. 3.11c) to reduce the amount of generated displacements at the cylinder by half. The loading procedure was established according to [4]. Load was applied in a quasi-static rate using a combination of displacement control and load control methods (see Fig. 3.15). According to this, seven loading steps were established and implemented automatically by using a PCS 8000 control system by *walter+bai ag* together with DION7 software package. A detail flowchart of the loading process is presented in Fig. 3.16. Data acquired from the tests was analysed using both VIC 3DTM and custom algorithms developed within Matlab®. Within the Vic-3D software, the subset size was set to 29 to give an optimal match confidence of 0,01 pixel for a given noise level. The noise level was taken as default of 8 which is suggested to work well for most cameras [84].

3.5 Results

Total load vs. midspan displacement curves of three types of tested structures are shown in Fig. 3.17. Maximum displacements corresponding to the applied loads were obtained from the DIC system at points as shown in Fig. 3.18. Each of the three groups consisted of three



Figure 3.14 – Speckle pattern with speckle sizes between 1 – 5 mm.

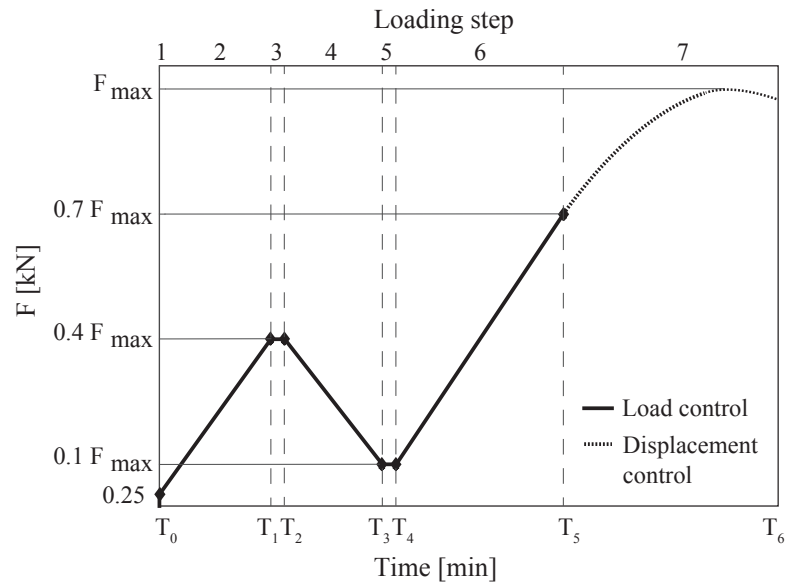


Figure 3.15 – Loading procedure.

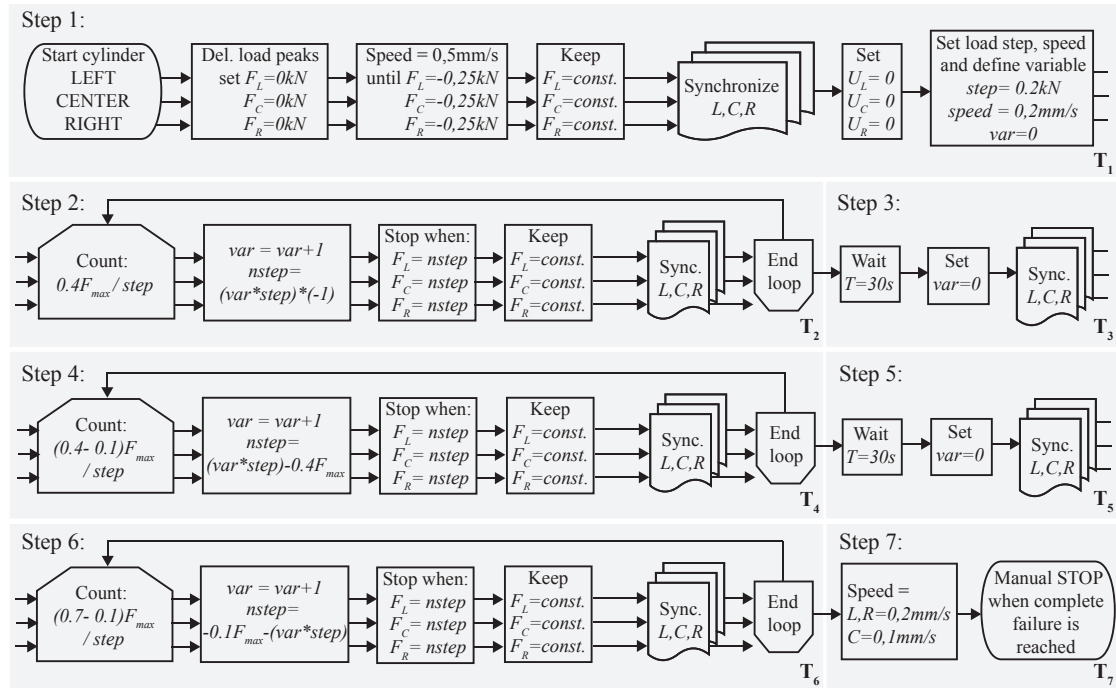


Figure 3.16 – Test loading process, separated according to the defined seven loading steps.

experimental replicates. The results show that the highest structural stiffness is achieved when using adhesive joints, 55% higher than MTSJ open slot and 26% higher than MTSJ closed slot structure elastic range stiffness (see Table 3.5). For all three structure types the results suggest that serviceability limit state (SLS) would be the one to govern the design of timber folded surface structures. For a span of 2.9m the SLS maximal allowed displacement, equal to 9.66mm ($L/300$ according to [27]), stays well within the elastic stage for all tested structures (Fig. 3.17b). The influence of the joint semi-rigidity on the displacements distribution and corresponding maximum value position is clearly visible in Fig. 3.18. For the least rigid connections, i.e. open slot MTSJ, the maximum values of displacements occur at the edge (Fig. 3.18b). As the rigidity of the joint increases for closed slot MTSJ, the distribution of displacements changes, locating the maximum value in the center of the two mid plates, around the loading ring (Fig. 3.18c). The most rigid case of adhesively joined structures retains the same position of the maximum displacement value as closed slot MTSJ, however, the distribution demonstrates higher concentration around the loading ring (Fig. 3.18a). The ratio of plate center over mid edge displacements at points marked **x** for adhesively joined, MTSJ open and closed slot structures is equal to 1.22, 0.97 and 1.07, respectively. Furthermore, even though the adhesively joined structures exhibited higher stiffness when compared to MTSJ closed slot structures, their characteristic total load at elastic limit point as well as mean maximum strength values are lower, respectively 14.5% and 21.26% lower than for MTSJ closed

3.5. Results

	Adhesively joined	MTSJ open slot	MTSJ closed slot
Characteristic linear region stiffness [kN/mm]	3.67	1.65	2.69
Characteristic total load when reaching SLS [kN]	35.44	15.97	25.99
Characteristic total load at elastic limit point [kN]	58.51	38.46	68.44
Mean maximum achieved strength [kN]	79.45	61.86	100.91

Table 3.5 – Comparison of results of three different large scale structure types.

slot (see Table 3.5). All three structure types failed as a result of connection failure, however, the failure mode and its progression were distinct for each type and are therefore explained in the following text (see Figs. 3.19, 3.20 and 3.21).

In adhesively joined structures, the first crack appears when the tensile stresses at the edge interface surpass the adhesives yield strength in tension (see point **A** in Fig. 3.19). Opening of subsequent cracks and widening of existing ones follows shortly after, causing progressive reduction in stiffness (see point **B**). For replicates 2 and 3, after reaching its maximum load-bearing potential, point (C) marks the sudden load drop associated with brittle connection failure along the full edge length simultaneously. Subsequently, as folded surface structures form statically indeterminate systems, a redistribution of forces within the system follows. Finally, when the alternative load paths become overloaded, multiple edges fail simultaneously in tension, (see point **D**). Unlike replicates 2 and 3, replicate 1 shows higher initial stiffness and maximum achieved load, but consecutive brittle failure at points (C) and (D) follow with almost no force redistribution in-between. For all three replicates after point (D) complete collapse follows in form of loss of structural integrity. It can be seen that failure happens due to tension entirely within the glued interface, where timber plates experience no structural damage (Fig. 3.22).

For three replicates of structures with MTSJ open slots (see Fig. 3.20), (A) marks a point after which reduction in the slope of the graph occurs, i.e. end of linear region, the gap caused by the slip of the joints at that moment is shown at the respective photograph. However, due to joint geometry defining the inclination of the tabs and slots side faces, the increase of the gap between the respective edges stops at a certain moment, i.e. when the gap size reached about 1/3 of the plate thickness, and does not lead to complete edge separation. Instead, as the load increases most of tabs and slots side faces lock in contact and disable the further gap growth, the further transfer of bending moments is then enabled through compression of

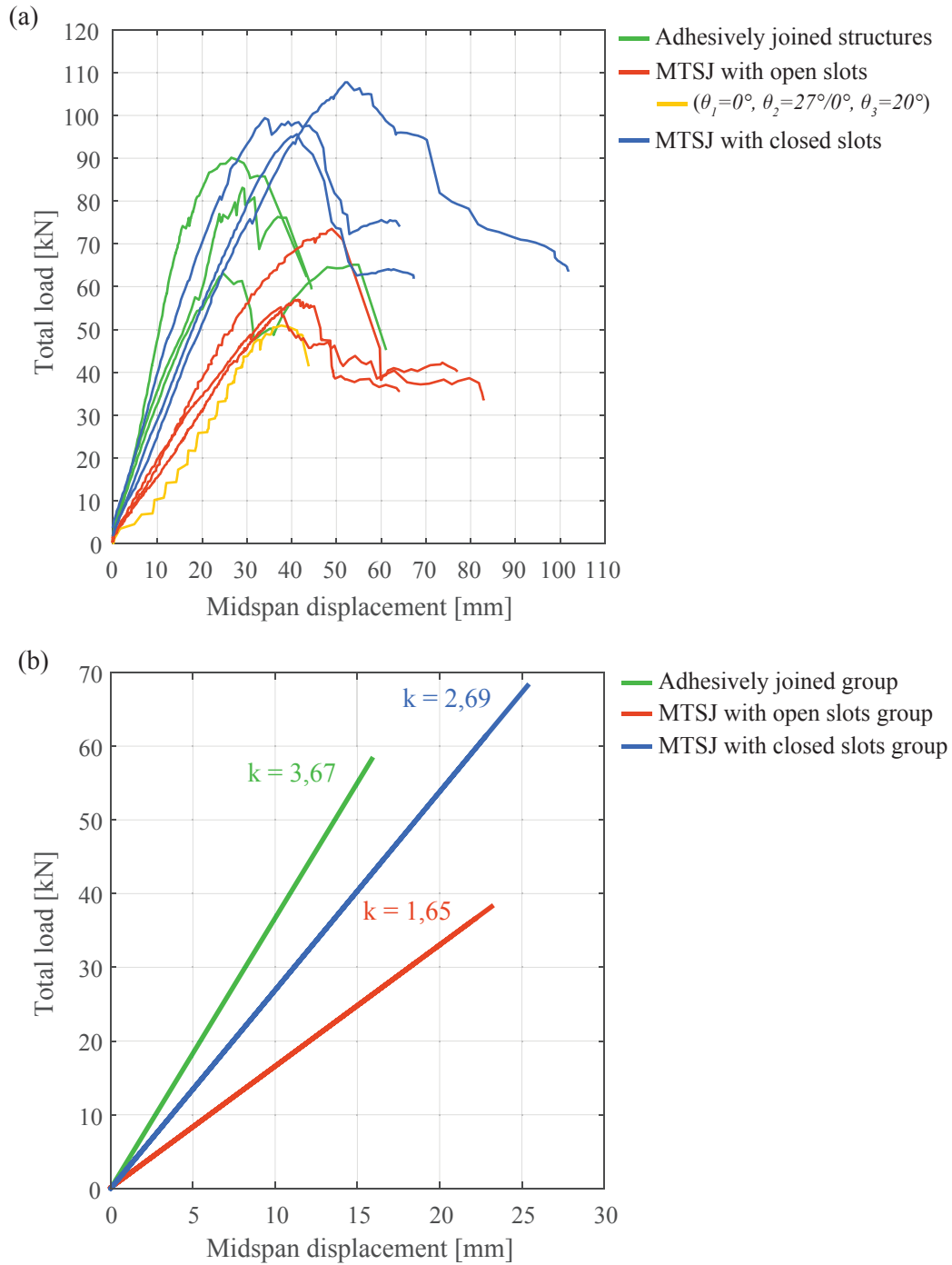


Figure 3.17 – (a) Total load vs. midspan displacement. Triplets of curves of identical connection type are marked with the same color. The part of the curves corresponding to the unloading of the specimens according to the established loading protocol are omitted for clarity; (b) Characteristic elastic region and stiffness, k , for each respective group. The coefficient k was determined by fitting a linear regression model to each of the 3 groups containing 3 replicates. The upper bound of the elastic region for each replicate was determined by imposing $R^2 > 0.99$, which corresponded to approximately $0.6F_{max}$ for all replicates.

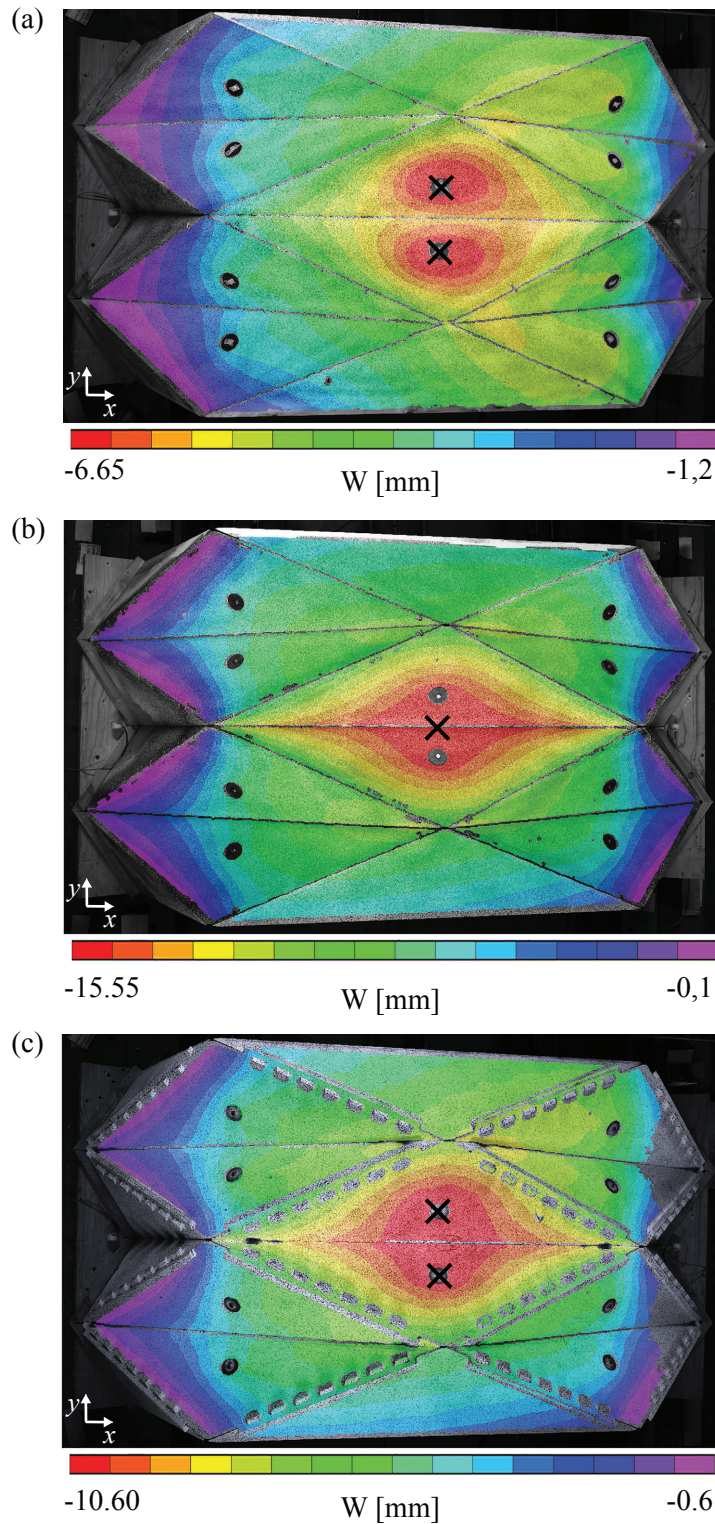


Figure 3.18 – Displacement fields of each of the tested structure type unfavorable replicate, shown at the moment when the total load on the structure amounted to 25 kN ; (a) Adhesively joined structure, replicate 3; (b) MTSJ with open slots, replicate 3; (c) MTSJ with closed slots, replicate 3. Points at which the displacement data was extracted for each type are marked with **x**, in case of (a) and (c) as the maximum displacement found around the loading ring.

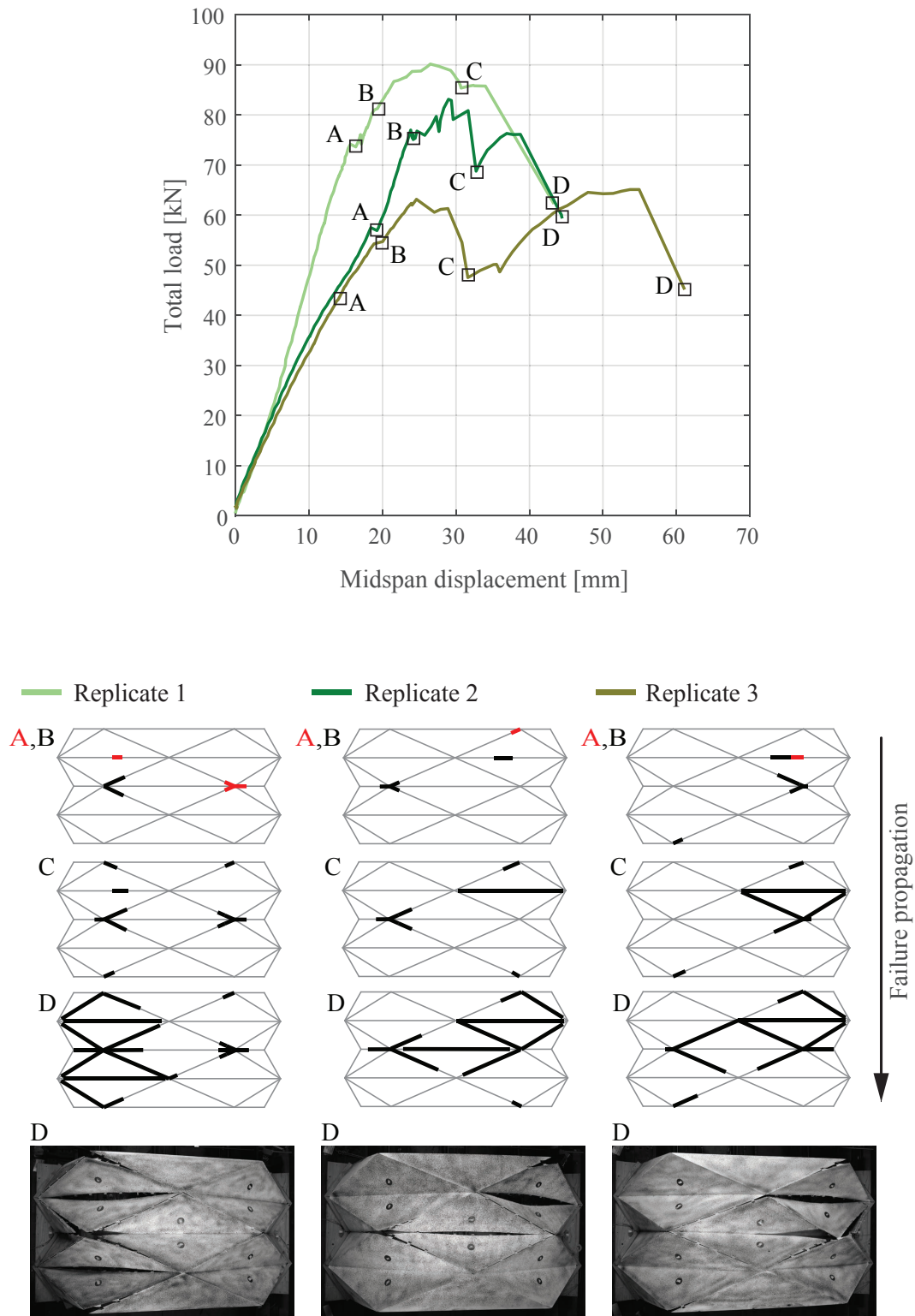


Figure 3.19 – Total load vs. midspan displacement graph and failure propagation for adhesively joined structure type.

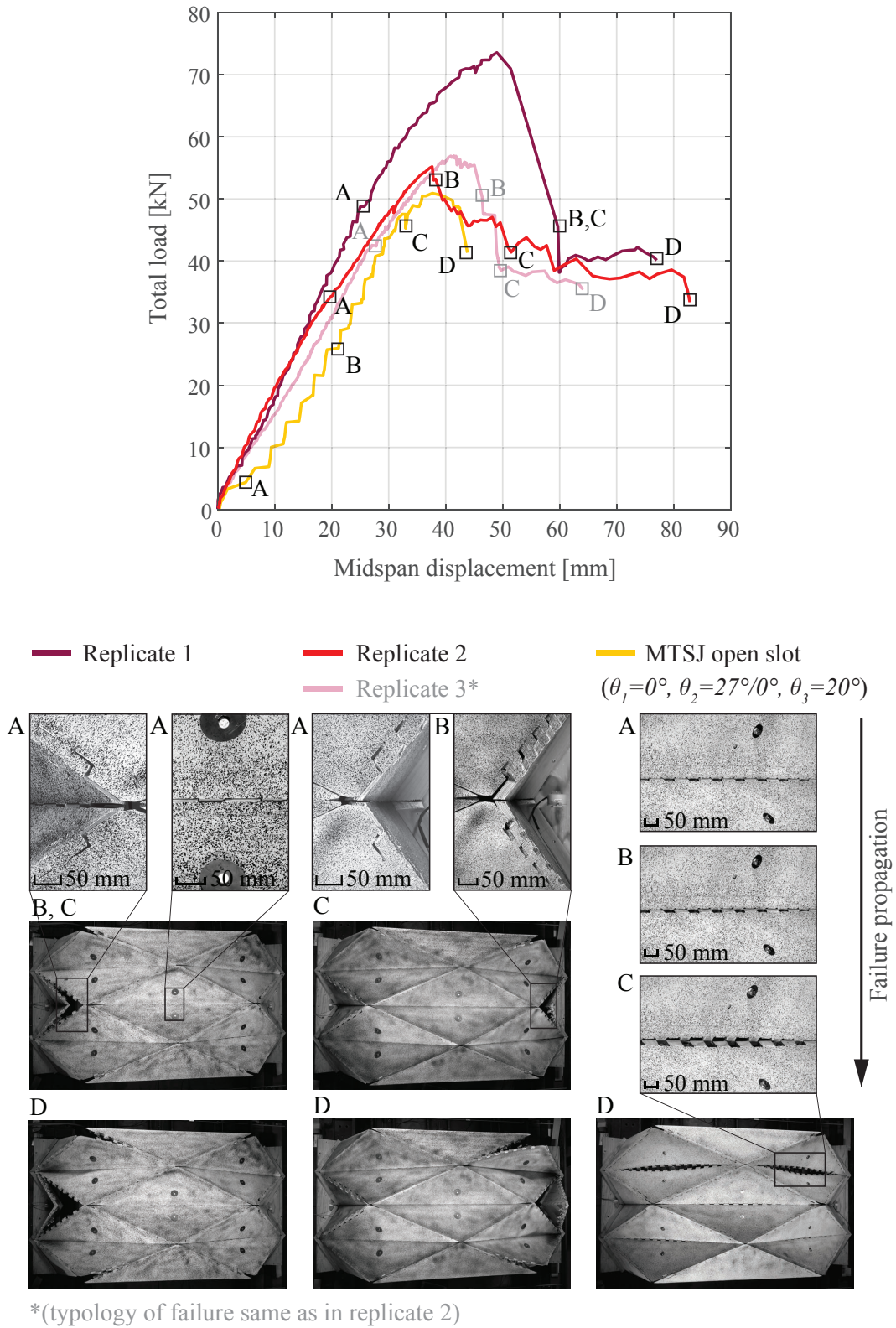


Figure 3.20 – Total load vs. midspan displacement graph and failure propagation for open slot MTSJ structure type.

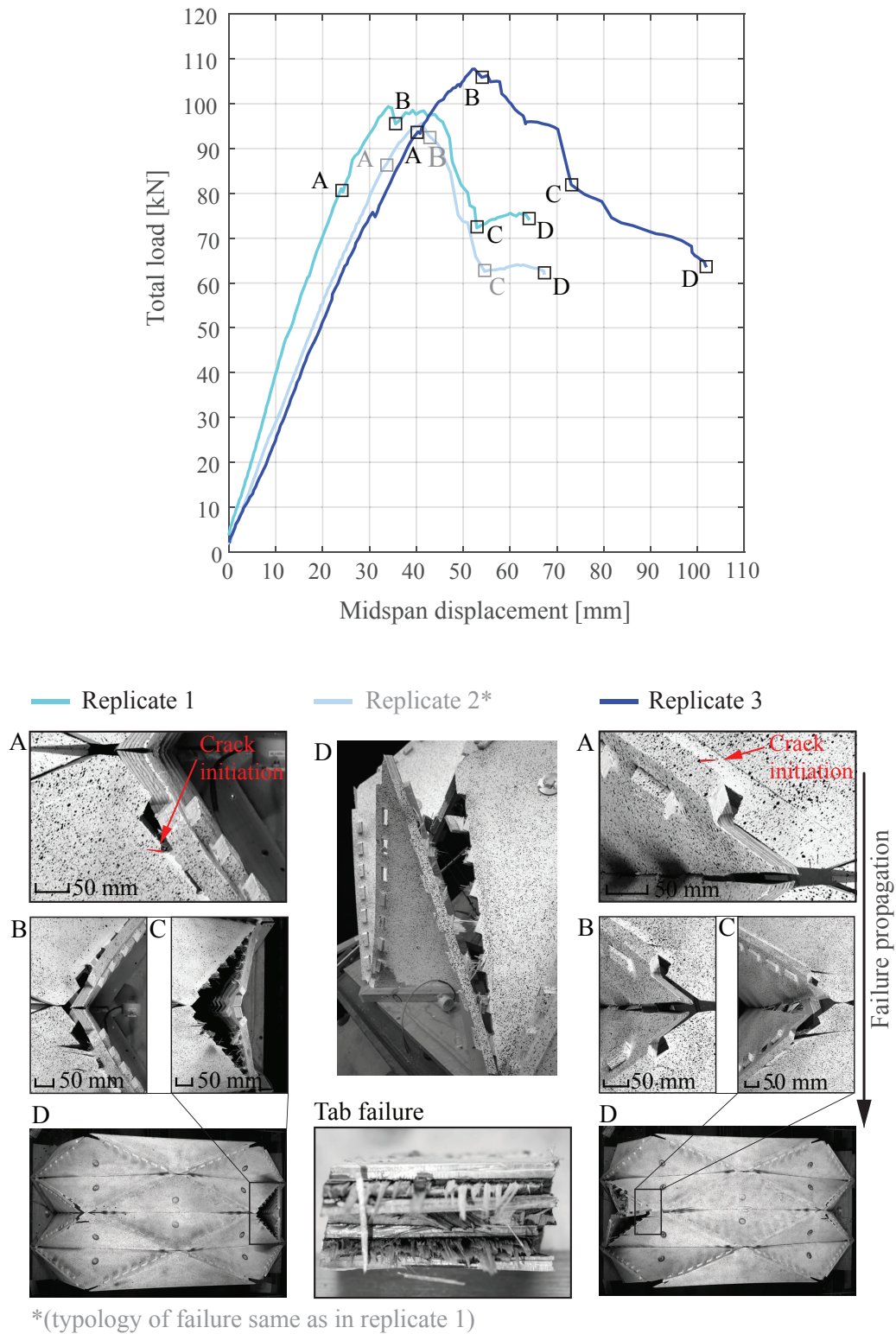


Figure 3.21 – Total load vs. midspan displacement graph and failure propagation for closed slot MTSJ structure type.

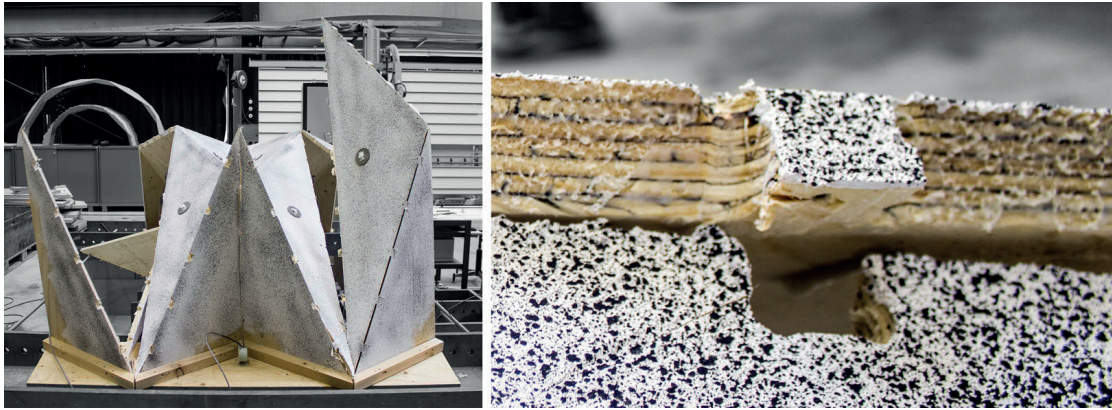


Figure 3.22 – Loss of structural integrity in adhesively joined structures after point (D) (left) and detail of edge after failure (right). Replicate 3 is shown as a representative of all three tested replicates since they exhibited same type of final collapse.

the side faces surfaces, therefore providing additional load bearing capacity to the structure. This further causes tension perpendicular to the plate plane and finally material failure by delamination (Fig. 3.23a), resulting in full loss of contact along one entire edge (see point **B** in Fig. 3.20). The second critical edge of the two half-sized side plates fails at point (C). In replicate 1 these two events happen simultaneously, characterized by a significant sudden load drop. At this point the two respective plates are no longer part of the load bearing system and their failure causes a rotation of the near-by side support (shown on the example of MTSJ closed slots replicate 3 in Fig. 3.24). This then results in failure propagation to other edges. Due to large displacements, where maximum piston stroke was exceeded, the tests were stopped at point (D). However, the structural integrity of main load-bearing elements was still preserved at this point. This suggests that the replicates would continue to sustain load as far as the connections between the main loaded plates would facilitate it.

In addition to the chosen MTSJ open slot theta angle combination, an example is also shown of a structure where all joint insertion vectors were chosen to be parallel to the $-y$ axis. This resulted in two different sets of angles, $\theta_1 = 0^\circ$, $\theta_2 = 27^\circ$, $\theta_3 = 20^\circ$ for the skewed edges, and $\theta_1 = 0^\circ$, $\theta_2 = 0^\circ$, $\theta_3 = 20^\circ$ for edges parallel to $-x$ axis. In fact, this was the initial set of angles intended for MTSJ open slot structures. However, after the structure with this set of angles showed deficiencies in mechanical behaviour within the global assembly, the final choice was modified. Significant edge opening was already observed at point (A) at a very low total load of 4.7 kN, when the first slip between adjacent tab and slots occurred (see MTSJ open slot ($\theta_1 = 0^\circ$, $\theta_2 = 27^\circ / 0^\circ$, $\theta_3 = 20^\circ$) in Fig. 3.20). With increasing load, such behaviour continues and can be clearly seen in the sawtooth behaviour of the total load vs. mid-span displacement curve of the respective sample. 50% of contact surface between mid-edge tab and slots is lost

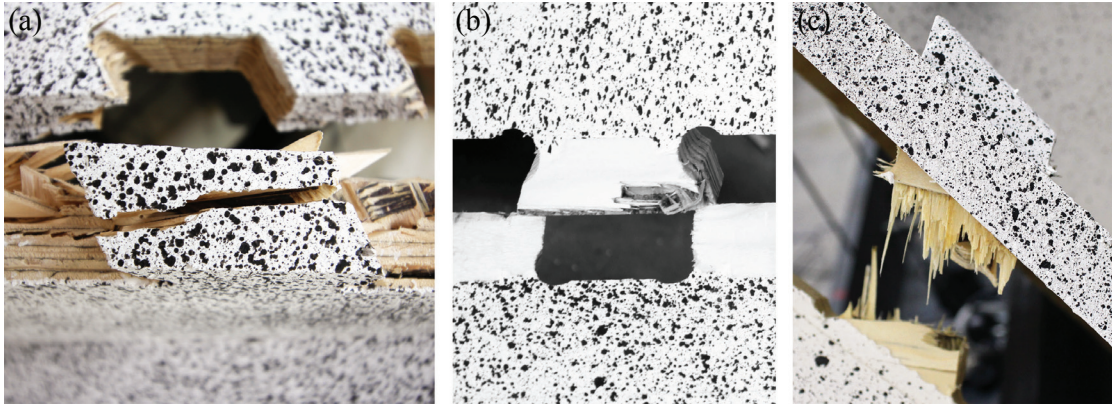


Figure 3.23 – MTSJ failure modes; (a) open slot; (b) open slot ($\theta_1 = 0^\circ$, $\theta_2 = 27^\circ / 0^\circ$, $\theta_3 = 20^\circ$); (c) closed slot.

when reaching the point marked **(B)**, while the complete loss of contact happens at point **(C)**. No structural damage was observed on the edges after failure (Fig. 3.23b). They simply disassembled as a result of the acting force being in the same direction as the joint insertion direction. This demonstrated a very important correlation between the joint geometry and acting forces direction and its influence on the load bearing performance of the structure. Accordingly, the final choice of Bryant angles for the MTSJ open slot structures was taken so that the long edges insertion directions divert from the structure's $-y$ axis (Fig. 3.4). Therefore, the joint geometry of skewed edges, for which parameters were constrained by simultaneous assembly, was used for all joints within the structure.

As expected, MTSJ closed slot structures showed a much steeper initial slope of the graphs in comparison to the ones with open slots, indicating a higher stiffness. This constant slope is followed by a kink, corresponding to the initiation of first crack visible at the top surface which appears at the point marked as **(A)**. It can be seen that this localized event hardly influences the global structure stiffness. Structural failure occurs and softening begins when material capacity in tension perpendicular to the plate main grain orientation is exhausted at the connection level (Fig. 3.23c). At that point, the first tab closest to the crack fails, **(B)**, characterized by the abrupt increase in the respective support rotation (Fig. 3.24). This greatly contributes to further enhancement of the tensile forces occurring at the long skewed edges of the half-sized plates. With continuation of imposing displacements, support rotation continues and failure progresses to the next tab and so on, until the end of the edge is met at the supports **(C)**. Same as in MTSJ with open slots, the tests were stopped at point **(D)**. However, at this point cracks along the middle of loaded plates bottom face were observed (Fig. 3.25). They were caused by out-of-plane bending when material capacity in tension perpendicular to the plate grain orientation was exceeded, this time at panel level. Fracture at

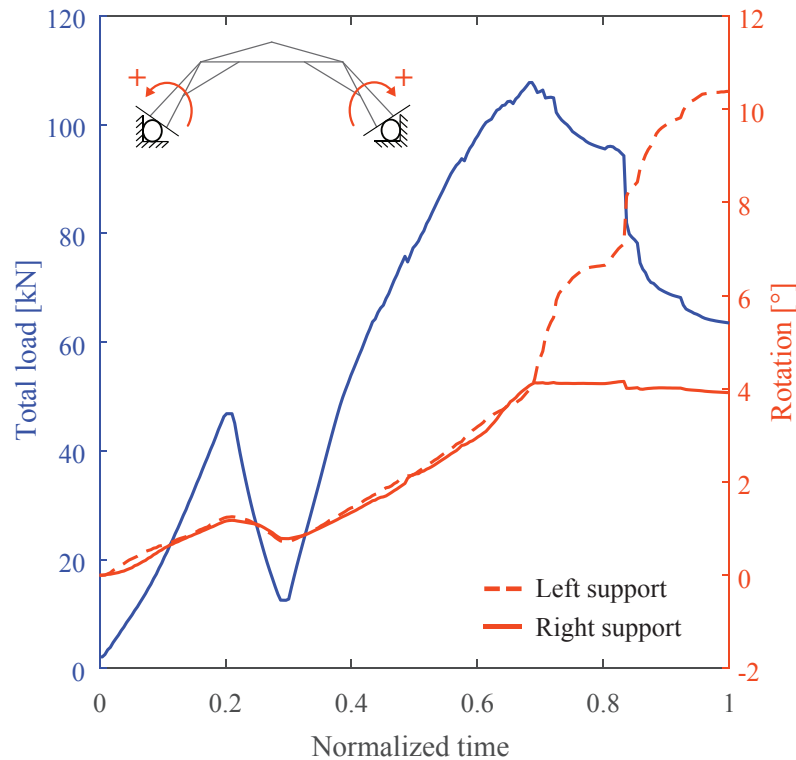


Figure 3.24 – Total load and rotation of supports vs. normalized time shown on the example of MTSJ open slot replicate 3. Sudden increase in rotation of left support occurs at the moment of MTSJ failure at the left side connection between half and full-sized plate. Both MTSJ open and closed slot structure replicates experienced the same reaction, where the support side with rotation increase varied depending on the failure side.

this level was observed only in MTSJ with closed slots, as opposed to other tested structure types, where it was always constrained to the level of connections.

3.6 Discussion

Comparing large scale to the preliminary detail test results, it is noted that the failure modes of connections within large scale structures are very similar to the ones observed in small scale samples under bending. They are altered mainly by additional tension forces which appear at the edges perpendicular to the panel main grain orientation, i.e. global structure – y axis direction. Certainly, due to complex geometry, where discrete plates lie in different planes, the failure modes in the connections of large scale replicates are additionally influenced by twisting moments and other edge forces, mainly shear, as well as joint edges not being parallel to the main plate grain orientation. However, the similarity still suggests that, together with tension perpendicular to grain which is a known weakness of timber, bending around the



Figure 3.25 – MTSJ with closed slots, replicate 3. Failure along the middle of the loaded plate bottom face.

edges is one of the most critical loading conditions when discussing timber folded surface structures. Furthermore, when looking at the initial slip of MTSJ open and closed preliminary detail test and comparing it to the respective MTSJ large scale tests, an important influence provided by interlocking is noticed. The initial slip effect in a multiple plate assembly is completely eliminated, mutual blocking of neighbouring edges is achieved as soon as the structure is put in position. This outcome is most visible in structures with MTSJ open slots.

MTSJ structures, both open and closed, experienced similar type of failure. For all six replicates it occurred at either the left or the right side at mid length of the structure, when the two half-sized plates edges failed in tension. As explained in Chapter 2 Section 2.4, structural behaviour of folded surface systems is defined by a mixture of extensional and flexural plate actions. Locally, at individual plate level the applied load is transferred to the plate edges by out-of-plane bending, where it is then resolved into components lying in planes of the adjoining plates. These are transferred between two adjacent edges by compression, when a pair of joint interfaces come into contact. In MTSJ with open slots there are three shared joint faces that can facilitate this transfer in compression, $i j_{1,2,3}$ (Fig. 3.26a). Faces i_4 and i_5 remain "open" and have no contact pair, resistance to the movement in their direction is achieved only through inclination of faces $i j_1$ and $i j_3$ when adequate Bryant angles are used (friction between the contact pair faces is not taken into consideration here). The mentioned faces lack of contact pair causes slipping when partial or complete loss of contact in compression occurs due to bending around the edges. Contact loss is additionally enhanced by inevitable fabrication tolerances and possible imperfections. On the other hand, in MTSJ with closed slots four pairs of contact faces exist, $i j_{1,2,3,4}$ (Fig. 3.26b), increasing its load-bearing potential. In this case, slip is only possible in the direction of insertion vector, so its influence is greatly reduced. The above explained difference between the MTSJ open and closed slot is indicated

by the smoothness of their total load vs. midspan displacement curves (see Fig. 3.17).

Additionally, MTSJ open slot structures exhibited relatively large edge openings quite early in their elastic stage, at 4.7 kN load. At this moment the gap between the two mid plates amounted to 8.75 mm which is equal to 41% of plates' thickness. Also, abrupt slipping between edges occurred during testing, even after correcting the initial set of Bryant angles intended for these structures. This indicates that they cannot be considered reliable for providing efficient load transfer between plates in large assemblies. In such structures plates and their edges lie in different planes, and even though this is what contributes to such joints mutual interlocking ability, it also implies forces acting in various directions. Accordingly, in order to avoid the undesirable behaviour mentioned above, the set of Bryant angles describing the joint geometry would have to be determined for each edge separately, depending on the respective load direction. Even so, there would be no way of ensuring they could retain their capacity for changing load conditions.

With respect to adhesively bonded structures, the semi-rigid behaviour of MTSJ with closed slots connections provides additional contribution to the system ductility. In such structures the cause of ductility after yielding as well as failure is twofold. Firstly, plastic behaviour after the yield point is enabled by the ductility of the connections. Even though timber is generally considered to be a brittle material, especially in tension, it does provide a substantial level of ductility in compression. This is very effectively utilized by MTSJ with closed slots as they transfer all edge occurring forces through compression between their adjoining faces. Such semi-rigid behaviour of connections is considered to be beneficial for increasing the reliability of the global system. [51, 11, 48]. Secondly, global structural ductility is achieved through redundancy of load paths. Due to their topology, folded surface structures form statically indeterminate systems, where the redistribution of forces between elements follows after their individual failure. However, the latter is also true for the tested adhesively bonded structures. But in their case, as the connections are very rigid and fail along the entire edge length simultaneously in a brittle manner, the soon following system failure is brittle as well. So in this case, it is the topology alone that provides the redistribution of forces and avoidance of complete structural failure immediately after the adhesive ultimate strength is achieved.

Although adhesively bonded connections generally provided the highest stiffness of the structure, they have multiple disadvantages for building scale applications. In-situ gluing of structural joints is not recommended and it is usually preformed off-site where constant curing conditions can be maintained. This implies preassembly and the loss of flat packing advantage of folded surface systems made of multiple discrete elements. When using adhesives, the moisture content of the components must be controlled and adequate pressure without rela-

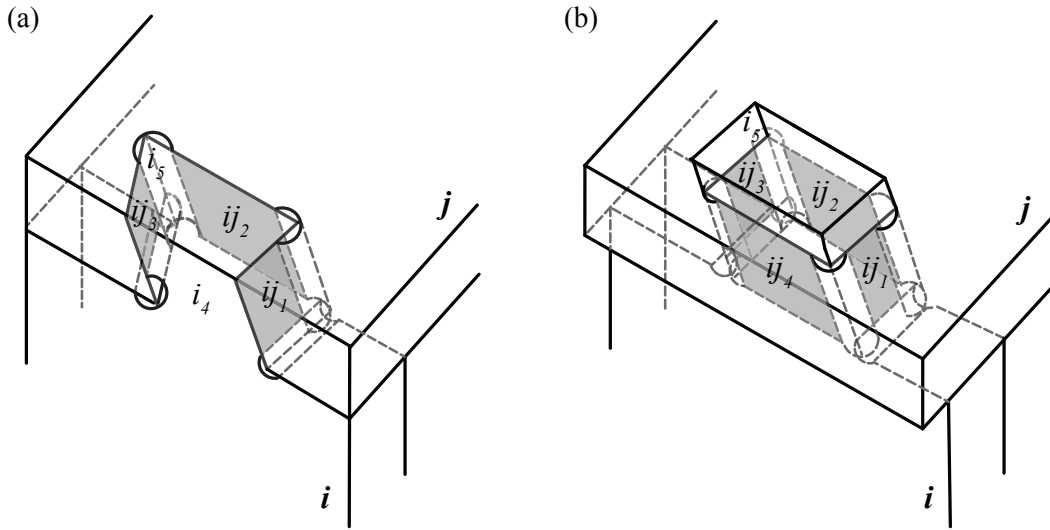


Figure 3.26 – MTSJ contact faces pairs; (a) open slot; (b) closed slot.

tive movement has to be assured. This has proved to be difficult even in controlled laboratory conditions. The aligning of the plate edges was aided by introducing one-faced finger joints, however, they could not ensure a precise dihedral angle positioning. The build-up of the so caused small inaccuracies in individual assembly, later caused gaps when positioning the structure on supports. In the presented case the gaps were small enough (max 25mm) to be closed by the timber slats used for fixing the structure on supports. However in larger structures, inaccuracies of such scale could cause more significant problems.

Considering the feasibility of tested structures types for building scale, they are further compared in terms of fabrication time and assembly (Table 3.6). Global and connection geometry generation for each structure was very fast and easy with the use of the developed tool (Appendix A). The tool also enabled the direct output of the CNC G-code used for fabrication. The fabrication time depends on the contour length and number of vertices, i.e. corner points, of each plate. It is a function of the CNC machine type, its maximum speed and number of used axis. In the presented case, 5-axis MAKHA MM7S CNC machine was used with a target cutting speed of 5000mm/min. The total fabrication time shown in Table 3.6 consists of preparation time needed to position and remove the cut panels from the machine as well as machining time itself. Machining includes: pre-drilling of holes for screws used for fixing the panels, drilling the holes at loaded plates geometrical center for fixing the pulleys, engraving plate numbers for later assembly, planarizing panel surface for achieving constant thickness and finally, cutting of the plate edges with integrated connectors. Plate edges were cut in 2 passes of the milling tool. All except the final machining step took equal amount of time for all three structure types, ~ 120min. The biggest difference was noted in the assembly time, where

	Adhesively joined	MTSJ open slot	MTSJ closed slot
Contour length / No. of vertices	134,44 m / 2408	171,15 m / 3834	224,46 m / 4398
Total fabrication time (ca.)	3:00h	3:30h	3:50h
Assembly time (ca.) / No. of people	3h / 3	1h / 2	1h / 2

Table 3.6 – Fabrication and assembly time for each of the tested large scale structure type.

adhesively joined structures proved to be quite time consuming. Two people were needed for holding the adjacent plates in position while the third one was necessary for spreading glue along the edges and inserting screws for applying pressure. The MTSJ structures, on the other hand, were very easy to assemble and only 2 people were required. Within the time noted in Table 3.6, the time for curing of the adhesive is not included, as well as the time required after the curing before further processing of the replicates [20]. It is important to note that all of the above mentioned times reflect the laboratory resources and conditions in which the replicates were produced.

3.7 Conclusions

In this Chapter, structural behaviour of timber folded surface structures was observed under continuous load and the influence of three different connection types was studied. Thereby, not only the global load-displacement behaviour was analysed, but also the occurring failure modes, based on detailed photo documentation of failure propagation obtained from the DIC system. Based on the obtained results and observations, the conclusions are as follows:

- When reaching the the maximal SLS prescribed displacement, all three tested structure types stay well within their elastic stage, exhibiting high reserve of load bearing capacity. However, the presented large variation in the elastic range stiffness of structures with different connection details, demonstrates the importance of taking the MTSJ semi-rigid behaviour into consideration in future evaluations of timber folded surface systems for structural application;
- All tested structures failed by exceeding the connection detail load bearing capacity. In addition to tension perpendicular to grain as the main cause of failure, the similarity between large scale and preliminary detail bending test failure modes indicates that bending is also one of the crucial loading cases when considering integrally attached timber folded surface structures;

- MTSJ open slot structures large scale test results indicate that such structures cannot be considered reliable for providing efficient load transfer between plates in large assemblies;
- Although, adhesively bonded connections provide higher stiffness when compared to MTSJ structures, due to multiple disadvantages considering the use of adhesives, their application for building scale timber folded structures suggests to be unfeasible;
- MTSJ with closed slots structures demonstrated the highest load-bearing potential leading to a structural efficiency of 158.3, i.e. strength-to-weight ratio. 21% and 38% higher than the characteristic structural efficiency of adhesively joined and open slot MTSJ structure respectively;
- The MTSJ with closed slot connection semi-rigidity provides additional ductility to the system, making such connections highly beneficial concerning the ultimate load-bearing capacity as well as the stiffness of the structures in the elastic range. In this manner robust structural systems with residual resistance are obtained, where localised failure does not endanger global structure integrity.

4 Numerical Modelling

This chapter is based on: A. Stitic, A.C. Nguyen and Y. Weinand, Numerical Modelling of Semi-Rigidity of Timber Folded Surface Structures with Multiple Tab and Slot Joints, manuscript submitted for publication.

4.1 Introduction

Timber folded surface structures assembled using integral mechanical attachments, specifically multiple tab and slot joints (MTSJ), have shown to form feasible structural systems with high load bearing potential. However, for efficiently realising such structures in building scale it is essential to provide a pertinent method for their structural analysis. The large scale tests presented in Chapter 3 provided insight into timber folded structures behaviour, but only for a certain loading condition and a specific geometry, i.e. vertical loading and anti-prismatic geometry. For different forms as well as varying load combinations, the load paths and load resisting mechanisms will not necessarily be the same. Therefore, developing a pertinent model for prediction of their structural behaviour is crucial for the efficient use of timber folded surface structures in building scale.

For structural analysis of complex folded surface structures, the commonly used theory for mathematical model definition is the theory of plates and shells. However, due to the complexities in the geometry, boundary conditions, heterogeneous material properties of timber etc., obtaining an analytical solution for such mathematical model is very difficult (generally impossible) [65, 93]. For these reasons the solution is usually obtained using numerical modelling, mainly based on finite element methods (FEM). Previously developed numerical

models for timber folded surface structures have shown that joint semi-rigidity representation has an important influence on the global structural behaviour [57, 18, 72]. The joints were either modelled as completely rigid or as hinges, leading to highly inaccurate estimations of structure displacements. The values of occurring plate strains were not addressed. Furthermore, experimental work performed on MTSJ connections [75, 21] as well as the one presented in the previous Chapter, also demonstrated the importance of including semi-rigidity in the numerical models. However, defining the MTSJ connections semi-rigidity by modelling their complete complex geometry has proved to be too cumbersome and computationally expensive to be used on larger scale models with multiple panels [59]. Examples of simplified numerical models of connection semi-rigidity were found in [12] where joint strips of different stiffness parameters were used for connection representation in glass plate shell structures, and in [47] and [55] where springs were used for modelling finger joints in a segmental plate shell structure. Therefore, two simplified models for MTSJ connection simulation within timber folded surface structures are studied within this Chapter: 1) strip element model; and 2) spring model. The test results used for validating the ABAQUS-based FE model are taken from large scale timber folded surface structures tests, presented in Chapter 3.

The Chapter is structured as follows:

- Section 4.2 presents additional remarks and results from large scale tests performed on MTSJ closed slot LVL folded surface structures, considered relevant for numerical model validation;
- Section 4.3 presents the description of the numerical models and two proposed simplifications for the connection detail modelling, as well as the obtained results;
- Section 4.4 includes the comparison of FEM results with the ones obtained from experimental testing as well as discussion on the found differences;
- Section 4.5 summarizes the main conclusions.

4.2 Experimental Investigations Revisited

Within the scope of interest of the numerical study, essential information, regarding the experimental tests performed on large scale folded surface structures with MTSJ closed slot connections, is repeated and additional results are presented hereafter. Material used was Kerto-Q structural grade Laminated Veneer Lumber (LVL) panels of 21 mm thickness. Fig. 4.1 presents the global geometry of the structures and MTSJ closed slot detail parameters are shown in Fig. 4.2. Load application was done in a quasi-static rate and boundary conditions

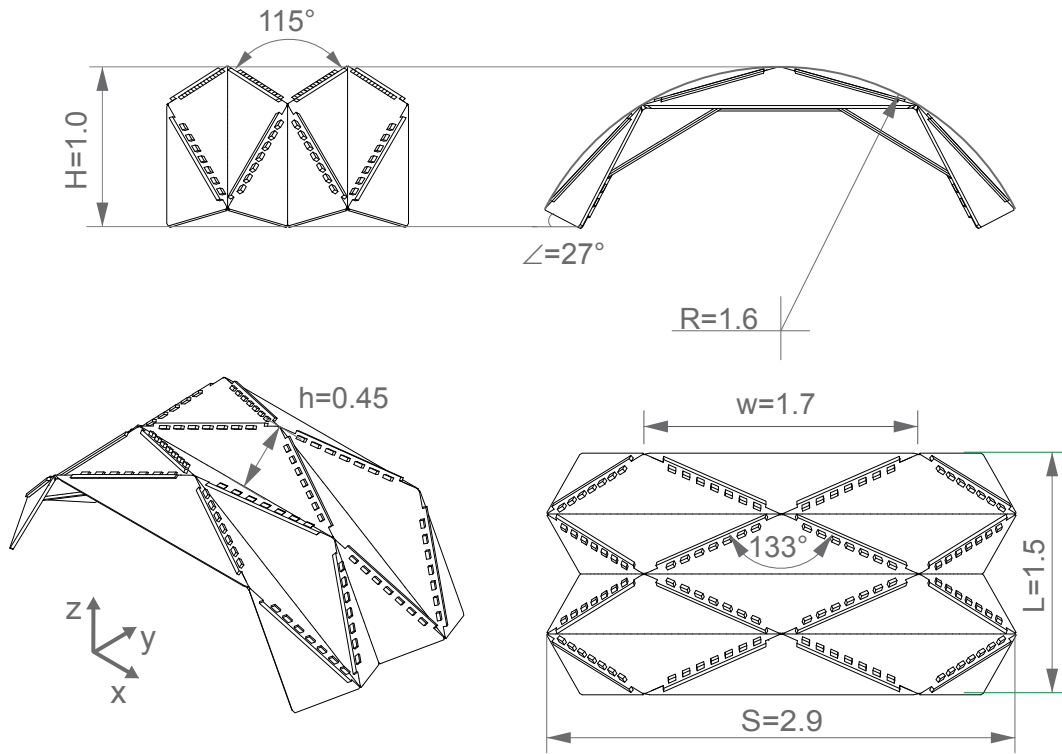


Figure 4.1 – MTSJ closed slot large scale structure geometry parameters.

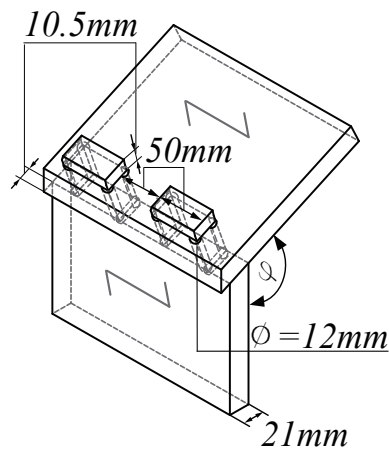


Figure 4.2 – MTSJ closed slot connection details parameters. Length of both tabs and slots was fixed to 50mm .

that allow rotation about $-y$ axis were used along the two supporting sides. In addition to force transducers, LVDT's and inclinometers, placed as shown in Fig. 3.11, a three-dimensional digital image correlation (DIC) system was used for obtaining strain and displacement fields of the entire structure. The DIC system was calibrated for each test individually in order to ensure the accuracy of measured values. Due to the sensitivity of the DIC measurements to the light source and random speckle pattern quality, as well as difficulties related to obtaining reliable results near the boundaries and sharp edges, strain gauges were used for validating the DIC results at selected points. Data acquired from the tests was analysed using both VIC 3DTM provided by Correlated Solutions, and custom algorithms developed within Matlab®.

4.2.1 Results

The relevant MTSJ closed slot structure total load vs. midspan deflection curves are shown in Fig. 4.3a. A group of three experimental replicates was produced and each replicate was fitted with single curve. The results suggest that when considering the proposed timber folded surface structures for building scale, the governing limit state in their design will be the serviceability one (SLS). The results further show that for a span of $2.9m$ the SLS maximal allowed displacement, equal to $9.66mm$ ($L/300$ according to [27]), stays well within the elastic stage for all tested structures. For this reason, only linear elastic material behaviour is considered here and in further presented numerical models. The representative structure stiffness in the elastic domain, k , was determined by fitting a linear regression model to the 3 replicates within the elastic region of their load-displacement curves (see Fig. 4.3b). The upper bound of the elastic region of each replicate was determined by imposing $R^2 > 0.99$, where R^2 is the coefficient of determination of the linear regression. The values of displacements in Fig. 4.3 were extracted from the DIC measurements at the point marked with **x** (see Fig. 4.4), as the maximum deflection found around the loading ring.

Fig. 4.4a shows the displacement field of the entire structure obtained from the DIC system, with respect to the structure global coordinate system (see Fig. 3.2). Strain fields are shown for one selected central plate only, as the global system coordinates need to be transformed into local plate coordinates to obtain correct values of strain for each individual plate (see Fig. 4.4b). The replicate chosen for representing the results of an entire group is the one with most unfavorable results in terms of stiffness. Validation of DIC obtained results was performed by using strain gauges for measuring strain at selected points. Low elastic strain gauges of LFLA-10-11 type and $10mm$ length, were used as recommended for wood based materials [8]. The position of strain gauges is shown in Fig. 4.4b. The strain data obtained from DIC measurements was examined at the same positions and directions as those of respective strain

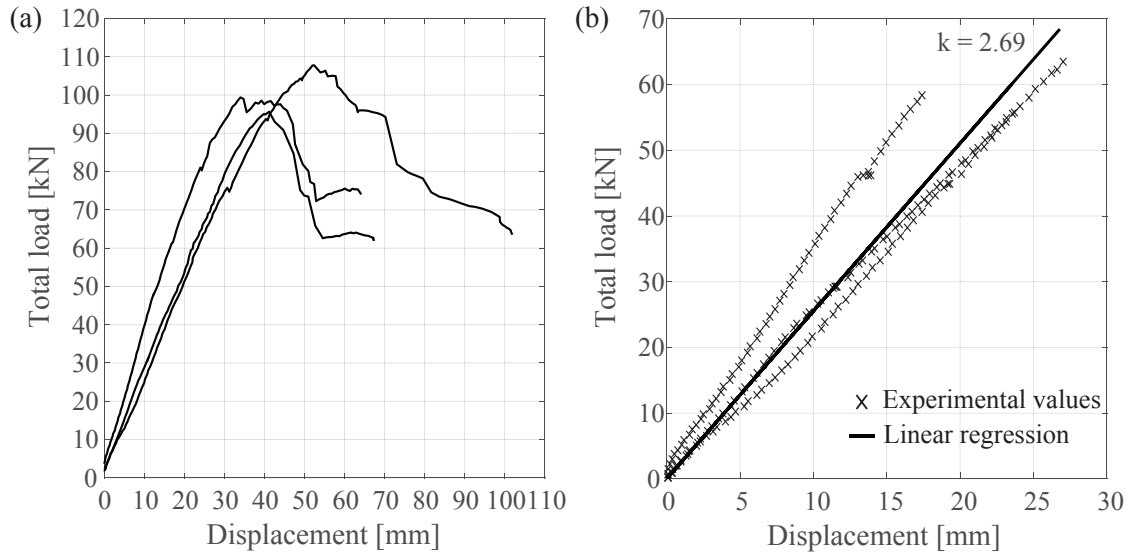


Figure 4.3 – (a) Total load vs. midspan deflection of the 3 replicate; (b) Elastic part and stiffness, k , representing the entire group.

gauges. Within Vic-3D™ software, the image matching was performed on a subset size of 23×23 pixels with the correlation analysis performing at every 5th pixel within the area of interest (step size = 5). With respect to the set step size the filter size was set to 9 data points, in order to represent a virtual gauge with a physical smoothing length of ~ 10 mm. Furthermore, the strain values were calculated with respect to the local plate coordinate system, with $-z$ axis corresponding to the plate normal direction. For validating the DIC results by comparing them to the strain gauges data, a noise reduction algorithm using moving average filter was applied for reducing the noise influence and enabling a more straightforward comparison [81]. The strain gauge and DIC obtained results showed good agreement, (see Fig. 4.5), where DIC strain noise levels were within the typical prescribed resolution of ± 100 microstrain [9].

4.3 Numerical Modelling

In order to create a pertinent numerical model for analysing the structural behaviour of timber folded surface structures, first, a correct mathematical model describing the physical structure needs to be chosen. Such a mathematical model consists of three fundamental parts: 1) the geometrical description of the structure; 2) specification of material properties; and 3) mathematical expressions of the basic physical laws which govern the structural behaviour.

The geometrical description of the structure form is given by means of its geometrical components, consisting of points, lines and surfaces, all connected within a logical structure for constructing the global form. The geometry is identical to the one used in laboratory tests and

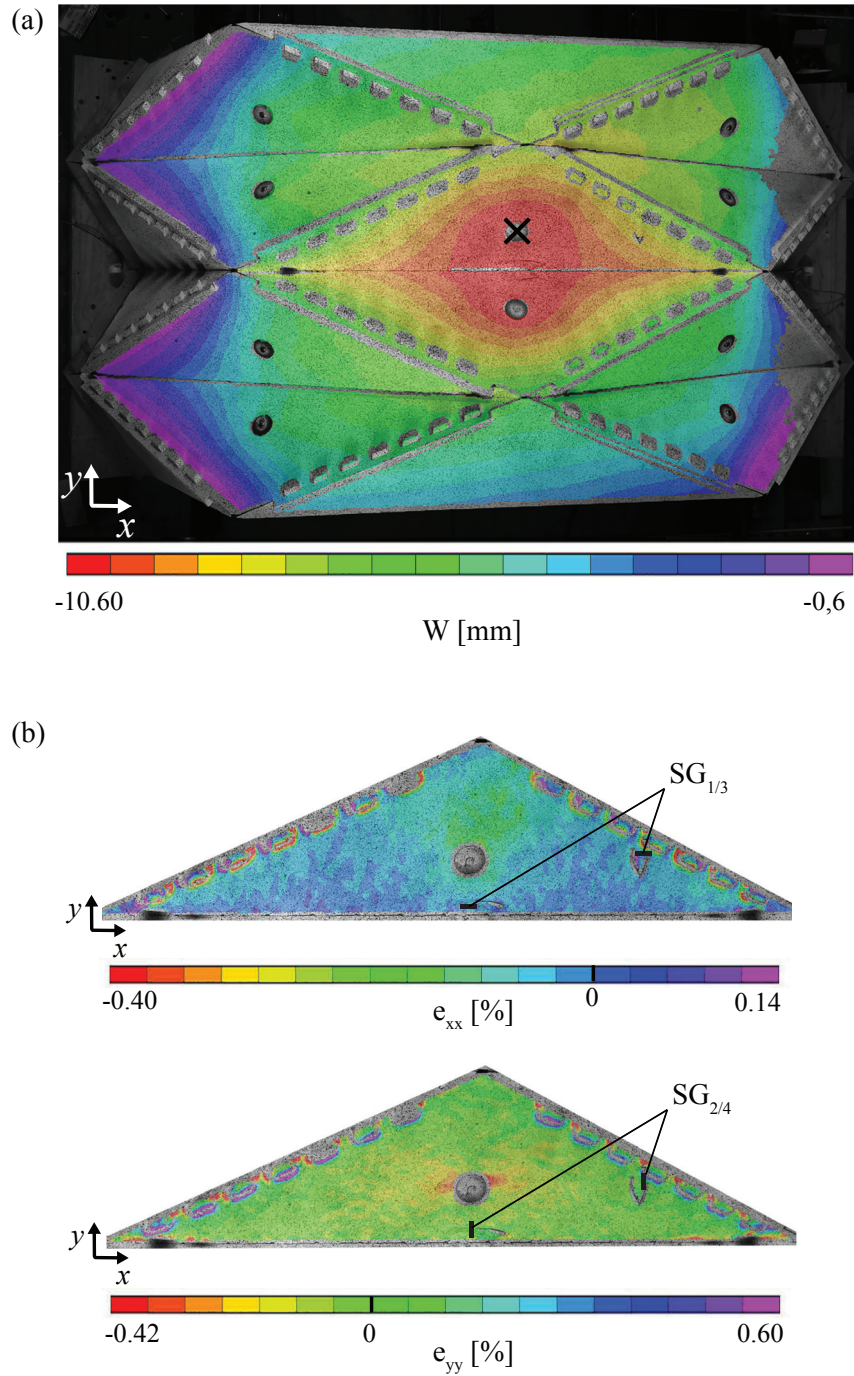


Figure 4.4 – MTSJ open slot structure, displacement field (a) and strain field of a single mid-fold plate (b) are shown at the moment when the total load on the structure amounted to 25 kN , which approximately corresponds to the occurrence of SLS maximal allowed displacements. Positions of strain gauges used for validating the DIC obtained strains in $-x$ and $-y$ direction are shown on individual plate respective strain fields.

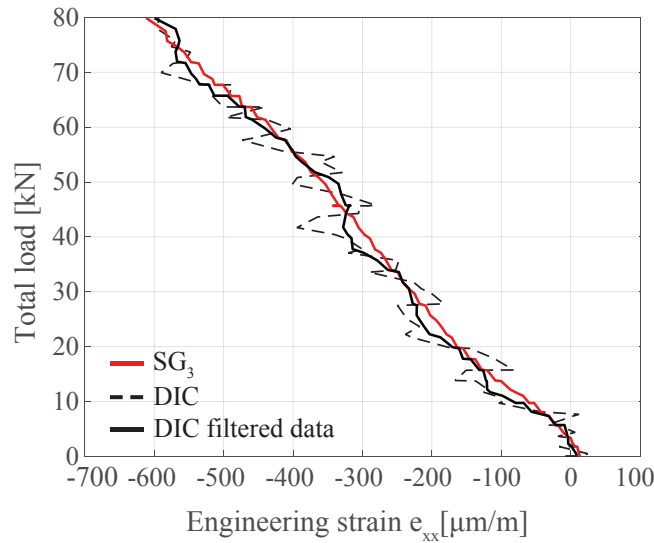


Figure 4.5 – Comparison between strain gauge SG_3 e_{xx} data with the DIC strain measurements at the same point. Applying a smoothing function for removing DIC noise, a good agreement is found between the two, with DIC strain noise levels being within the typical prescribed resolution of ± 100 microstrain.

was directly imported into the numerical analysis software from the CAD software used for its initial generation.

When modelling the material, it has to be noted that implementing the exact properties of structural LVL timber panels in the FE model, would be unrealistically cumbersome. Therefore, a simpler orthotropic model is proposed, which provides sufficiently accurate representation of the material behaviour. As previously mentioned, panel material was chosen as 21 mm thick Kerto-Q structural grade LVL. Such panels consist of seven 3 mm thick spruce peeled-veneer laminates from which one fifth is glued crosswise in a lay-up $|-||| -|$ (Fig. 4.6). This kind of structure improves the lateral bending strength and stiffness of the panel. More importantly, in this way very homogenous and mechanically strong panels are obtained which can be assumed as having orthotropic material properties [94]. The used characteristic values of elastic properties for Kerto-Q LVL material principal directions are shown in Table 4.1. These moduli further define the elastic compliance matrix according to Eq. 4.1.

The regarded timber folded surface structures are composed of discrete planar elements of continuous nature, where the plate thickness dimension is considerably smaller compared to its other dimensions. Therefore the plates can be considered as "thin" (thickness/average side ratio: $t/L \leq 0.05$ [65]). For this reason, appropriate "thin" plate theories are used for the mathematical model definition. The applied theory choice further defines the element type used in FE numerical solution procedures. For the presented problem ABAQUS provides an

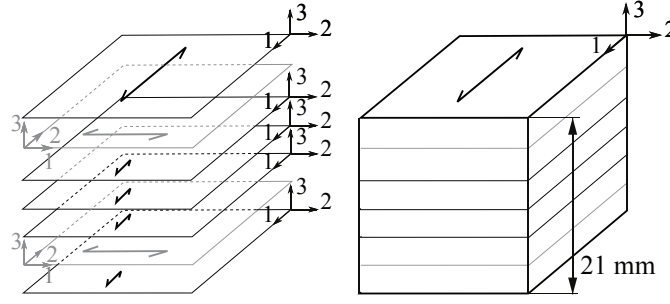


Figure 4.6 – Material orientation of LVL panels. Individual spruce veneer laminate layers (left) and the composed panel (right).

element type called *conventional shell element*, where the element geometry is specified at the reference surface which is coincident with the shell's mid surface. The desired thickness of the panels is defined by section property. In this case a three-dimensional continuum is approximated with a two-dimensional theory. This reduction in dimensionality is achieved by using the fact that the element thickness is considered small when compared with its other characteristic dimensions [6].

4.3.1 Finite Element Type Study

A study of both thin conventional shell element types and general-purpose elements, which are considered relevant to the modelled structure, is presented hereafter.

$$\begin{pmatrix} \varepsilon_{11} \\ \varepsilon_{22} \\ \varepsilon_{33} \\ 2\varepsilon_{12} \\ 2\varepsilon_{13} \\ 2\varepsilon_{23} \end{pmatrix} = \begin{pmatrix} \frac{1}{E_{11}} & -\frac{\nu_{21}}{E_{22}} & -\frac{\nu_{31}}{E_{33}} & 0 & 0 & 0 \\ \frac{\nu_{12}}{E_{11}} & \frac{1}{E_{22}} & -\frac{\nu_{32}}{E_{33}} & 0 & 0 & 0 \\ -\frac{\nu_{13}}{E_{11}} & -\frac{\nu_{23}}{E_{22}} & \frac{1}{E_{33}} & 0 & 0 & 0 \\ 0 & 0 & 0 & \frac{1}{G_{12}} & 0 & 0 \\ 0 & 0 & 0 & 0 & \frac{1}{G_{13}} & 0 \\ 0 & 0 & 0 & 0 & 0 & \frac{1}{G_{23}} \end{pmatrix} \begin{pmatrix} \sigma_{11} \\ \sigma_{22} \\ \sigma_{33} \\ \sigma_{12} \\ \sigma_{13} \\ \sigma_{23} \end{pmatrix} \quad (4.1)$$

$$\text{where } \frac{\nu_{ij}}{E_{ii}} = \frac{\nu_{ji}}{E_{jj}} \quad \text{for } 1 \leq i, j \leq 3, \quad i \neq j$$

As the plate thickness dimension is considerably smaller compared to its other dimensions and the structures are studied within their elastic range, firstly, thin conventional shell elements were used, which allow for large rotations but only small strains. In such elements, transverse

Property	Symbol	Value	Unit
Elastic modulus 11	E_{11}	10000	N/mm^2
Elastic modulus 22	E_{22}	2400	N/mm^2
Elastic modulus 33	E_{33}	130	N/mm^2
Shear modulus 12	G_{12}	600	N/mm^2
Shear modulus 13	G_{13}	60	N/mm^2
Shear modulus 23	G_{23}	22	N/mm^2
Poisson's ratio 12	ν_{12}	0.09	
Poisson's ratio 13	ν_{13}	0.85	
Poisson's ratio 23	ν_{23}	0.68	
Density	ρ	510	kg/m^3

Table 4.1 – Elastic properties used for orthotropic material model of Kerto-Q 21 mm panels [94].

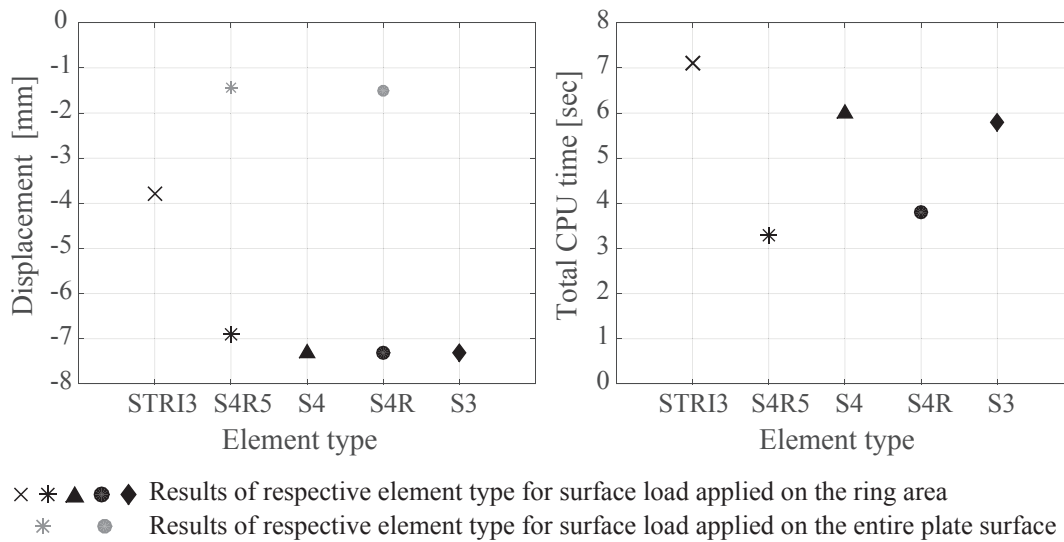


Figure 4.7 – Element type vertical displacement results for one isolated triangular plate under 5kN/surface area load and clamped boundary conditions (left). Total computation time needed for the analysis (right).

shear flexibility is negligible and the Kirchhoff constraint is satisfied accurately, i.e. the shell normal remains orthogonal to the shell reference surface [6].

Two types of thin shell elements were tested: 1) STRI3, a 3 node element with 6 degrees of freedom, where the thin shell theory is solved by satisfying the Kirchhoff constraint analytically; and, 2) S4R5, 4 node elements with 5 d.o.f. which converge to thin shell theory as the thickness decreases and the Kirchhoff constraint is satisfied numerically. Comparing to the experimentally obtained results STRI3 elements have shown to be overly stiff, where the strain values were significantly over estimated and the displacements under estimated. S4R5 element results seemed to be more in agreement with the experimental results as well as being much less computationally expensive.

Next, general-purpose conventional shell elements with finite strains formulations were studied: 1) S4, 6 d.o.f. quadrilateral element with full integration; 2) S4R, 6 d.o.f. quadrilateral element with reduced integration; and 3) S3, a 6 d.o.f. 3 node triangular element. Such elements normally use thick shell, Reissner–Mindlin plate theory, however, as the shell thickness decreases and the transverse shear deformation becomes very small they converge to classical thin shell theory. The elements become discrete Kirchhoff thin shell elements, where transverse shear strains are neglected while all features of the Reissner–Mindlin C^0 continuous formulation are kept [65]. All three element types results did not differ significantly, even when reduced (lower-order) integration was used (see Fig. 4.7left). However the S4R element did show superior performance with respect to total computation time (Fig. 4.7right), which is why it was chosen as the most favourable among the three.

When comparing the thin shell elements results with the general-purpose ones, better agreement with the experimental results was found when general-purpose elements were used. In order to better understand the reason of this finding, one triangular plate element was extracted and examined under load with fixed boundary conditions around its edges for representing the surrounding plates. It was found that results of both element types, general purpose S4R and thin element S4R5, converge when loading is applied on the entire plate surface instead of being concentrated to the ring area (see Fig. 4.7left). This suggested that the local element displacements around the ring boundary require a C^0 continuous formulation of the displacement field in order to be modeled accurately. Additionally, when springs or strips are added along the edges, the difference in results becomes even more evident, as this also contributes to the appearance of significant discrepancies between the displacements of elements within the boundary area.

Finally, the plates were formulated using quadrilateral 4-node, 6 degrees of freedom, large-strain shell elements of type S4R with reduced integration. This is a robust, general-purpose quadrilateral element that is suitable for a wide range of applications [6]. Both linear and geometric nonlinear analysis were performed, i.e. material nonlinearity is not considered.

A geometrically nonlinear, updated Lagrangian shell formulation was employed for reviewing the influence of rigid body rotations and translations as well as to account for coupling between axial and bending action within the plates.

4.3.2 Mesh Convergence Study

A mesh density study was performed to ensure that reliable results are obtained. The mesh was refined in steps of $0.0025m$ seed size, until the two consecutive solutions were found to be in good agreement and the results were converging. The total computation time was also taken into consideration. The study was performed on one isolated triangular plate under $5kN/ring$ surface area load and clamped boundary conditions. A good agreement between a fine and a coarse mesh, with respect to relative deflection error of its consecutive refinement (Eq. 4.2) and computation time efficiency, was found in the case of using a mesh density corresponding to $0.0075m$ seed size (Fig. 4.8). For reference to full plate assembly analysis, a $0.0025m$ seed size mesh within the spring element model took five and a half hours to compute while $0.0075m$ seed size took only 4 minutes.

$$\frac{Y_{i+1} - Y_i}{Y_i} < 5\% \quad (4.2)$$

As strains are concentrated along the edges of the panels, a meshing strategy using fine elements in these regions and coarser elements away from them was also tested. Similar results were obtained for vertical displacements and strains using a uniform mesh of $0.0075m$ and a mesh where more fine elements were used along the edges. However the computation time was significantly reduced when using uniform "coarser" elements of $0.0075m$. Therefore, a mesh density corresponding to a seed size of $0.0075m$ was found to be sufficiently refined and was used in all further presented models. For reference, the computer used for all FE analysis was a Lenovo Intel®Core™ i7-4800MQ CPU @ 2.7GHz with 16 GB of RAM.

4.3.3 Connection Detail Modeling

Considering that the plates were modelled as shell elements, the overall behaviour of the joint needs to be modelled on a two-dimensional level as well. In this regard, two different possibilities for detail modelling are explored hereafter:

- Introducing a connecting strip element between the panels with characteristics which represent the stiffness of the connection detail (Fig. 4.9b).
- Assigning a set of springs along the adjacent edges with appropriate stiffness parameters (Fig. 4.9a).

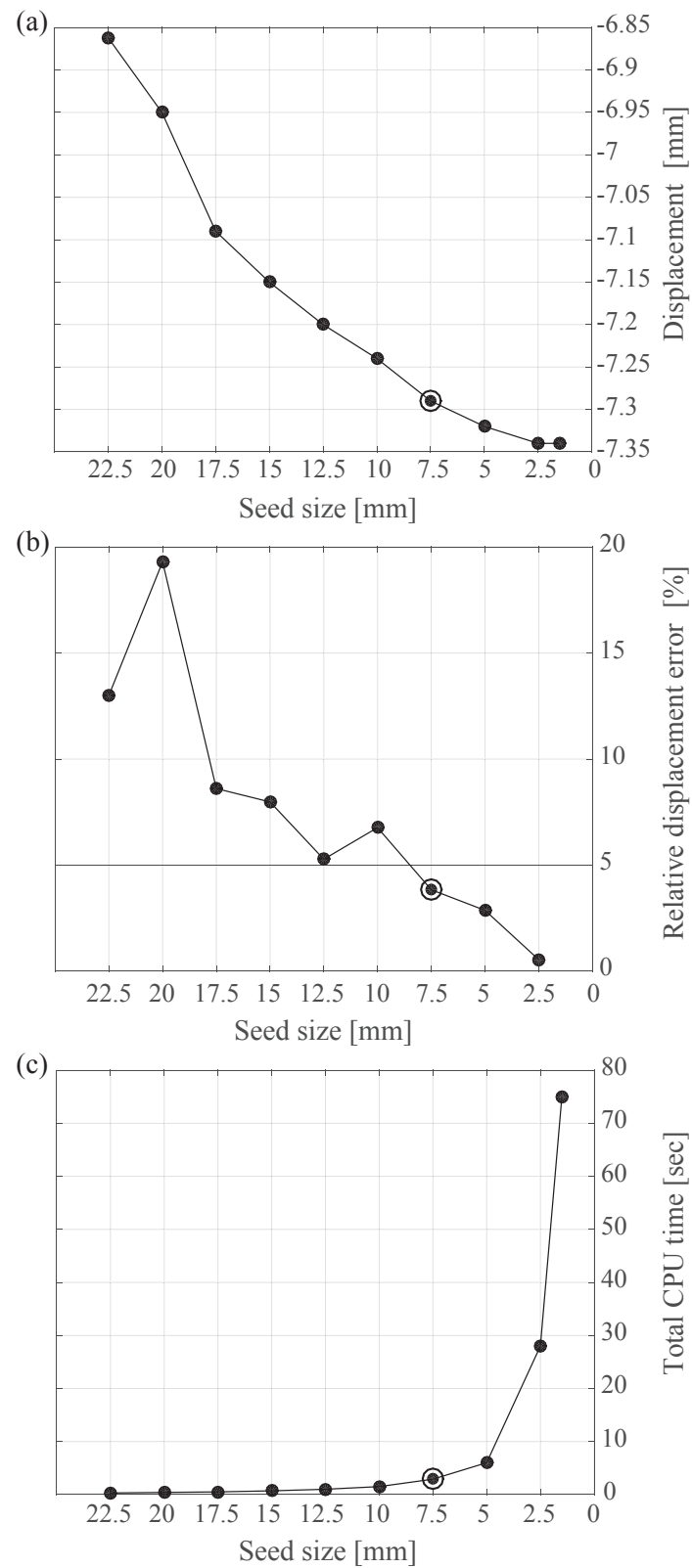


Figure 4.8 – (a) Mesh seed size convergence with respect to displacement results; (b) Relative displacement error of the consecutive refinement; (c) Total computation time needed for the analysis. Chosen seed size is marked with a circle.

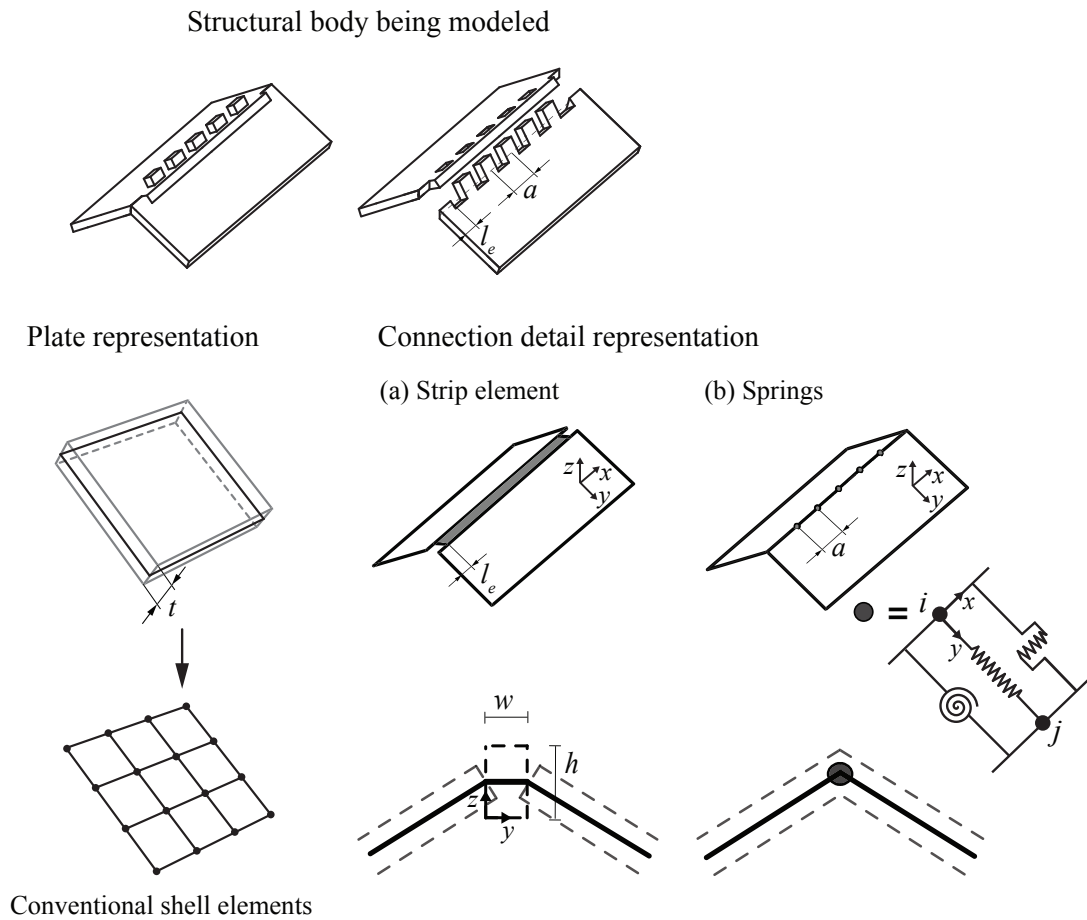


Figure 4.9 – Schematic of numerical modelling of timber plates and MTSJ details. In the spring model shown here, one MTSJ tab is shown to be represented by only one set of three spring types.

Detailed experimental work performed on MTSJ connections [75, 21] provided valuable input of bending and shear stiffness, used for the simplified numerical modelling of the connections within the scope of this thesis.

For realizing adequate boundary conditions within the experimental setup, heavy steel and LVL plates were used for fixing the structure ($\sim 33\text{ kg}$ at each support side, for comparison the total structure weight was $\sim 65\text{ kg}$) (see Fig. 4.10). As the supports were positioned under an angle of 27° in order to follow the curvature of the structure, their center of mass was not in line with the center of rotation of the steel rollers (see Fig. 4.11a). This resulted in nonlinear secondary moment effects which needed to be taken into account in the FE model. In Fig. 4.12 the order of magnitude of support weight influence on rotations is explained on a simple example of an equivalent size singly curved shell with same support conditions as in the used models. Finally, the supports were represented with equivalent single plate

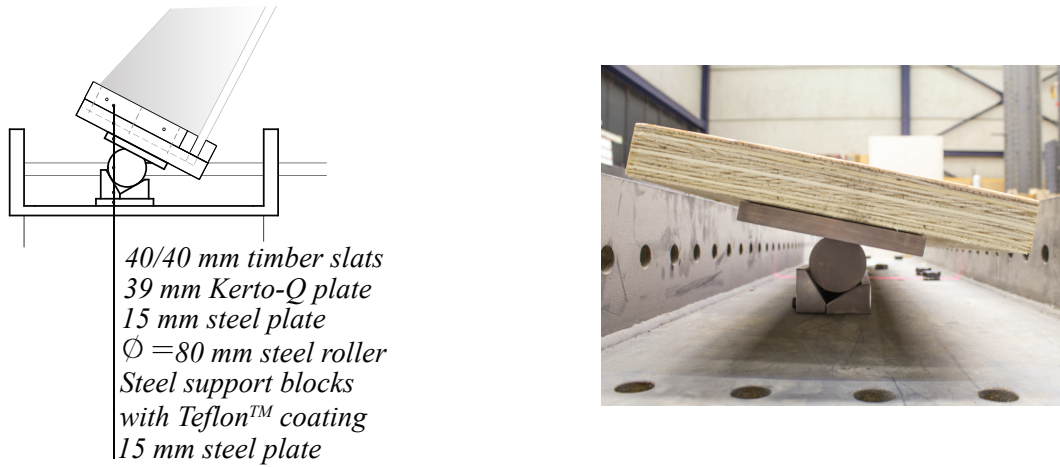


Figure 4.10 – Experimental setup side support detail.

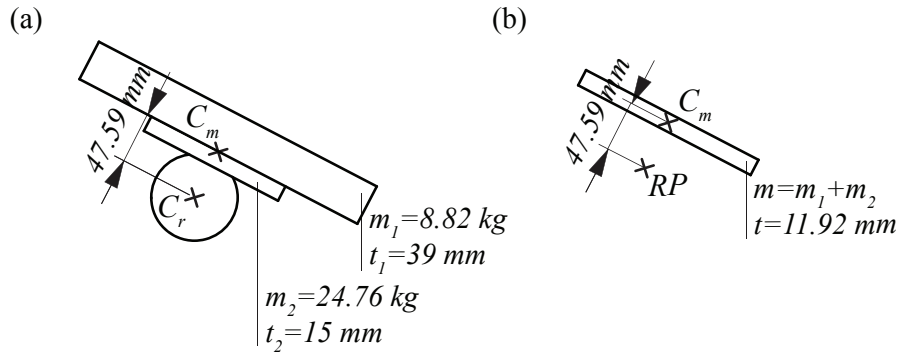


Figure 4.11 – Addressing the influence of secondary moments introduced by heavy supports; (a) experimental setup supports with marked weight and thickness of the plates as well as center of mass, C_m , and center of rotation, C_r ; (b) FE model with corresponding weight and equal distance to the center of rotation, defined as a reference point, RP .

of the same weight and the center of rotation determined with respect to the actual setup (Fig. 4.11b). The modelled support plates were defined as *rigid bodies*, where only rigid body motion is allowed. Their rotation was constrained to the center of rotation, RP . The boundary conditions allowing rotation about the structure $-y$ axis were prescribed at the center of rotations at the reference points RP_1 and RP_2 , for left and right support side respectively. Furthermore, the degrees of freedom of the nodes along the plate edges fixed to the supports, were constrained by using *Multi-point constraint* (MPC) definition within ABAQUS. As the local coordinate system of each plate differs from the globally defined one, the rotation of the above mentioned edges and their constituting nodes, needed to be set in a global coordinate system to properly simulate the experiment conditions. Therefore, MPC type BEAM was used to provide a rigid beam between the edge nodes and the respective reference point. In this way the nodal displacements and rotations were constrained to the ones of the reference point,

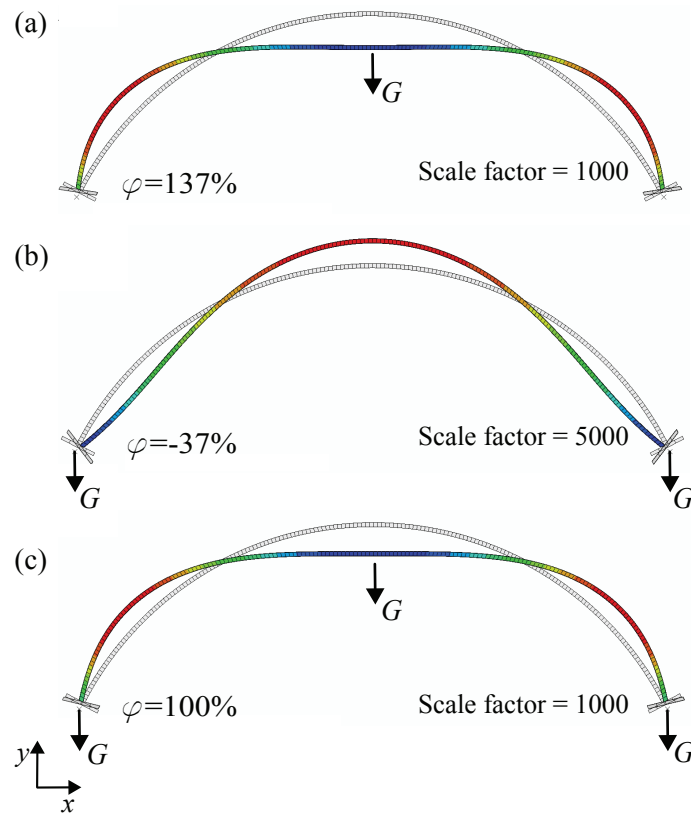


Figure 4.12 – Influence of gravity load on the rotations of the simplified curved shell structure; (a) Gravity load is imposed only on the shell structure, causing outward rotation of the supports; (b) Gravity load is imposed only on the supports, resulting in an opposite direction rotation; (c) Gravity is imposed on the entire model, resulting in the final outward rotation; The rotations and displacements of the structure are scaled for clarity.

corresponding to the presence of a rigid beam in-between [6]. In the FE model the load was applied in the same manner as in the actual test setup. In the first step the gravity load was imposed on the entire model. In the second step, the $70mm$ diameter circular surfaces in the plates geometrical center, obtained by partitioning the plates, were loaded by surface traction, same as loading rings in the tested structures (see Fig. 4.13).

It is noteworthy to mention that due to complex geometry and large number of plate elements the entire model generation was done automatically using Python programming language and Abaqus Scripting Interface. This allowed for fast changes in element type, mesh size as well as spring and strip properties, for exploring different modelling techniques while avoiding tedious manual work.

Strip Element Model

In the first approach for modelling the connection details, a small gap of $17mm$ was introduced between the connecting plate elements in order to represent the existing joints. The overall dimensions of the structure were kept the same, but the size of individual plate elements was reduced by 5%, with the origin point set at the geometrical center of each scaled plate respectively. The gap was then filled by adding a strip element for representing the connection between the neighbouring faces (Fig. 4.13). The thickness and material characteristics of the connecting strip were assigned according to the stiffness of the actual connection detail used. This way of modelling joint details was used as in [12], where isotropic joint strips of different stiffness parameters were used for connection representation in glass plate shell structures and have shown satisfying results. Secondly, the $70mm$ diameter circular surfaces in the plates geometrical center, obtained by partitioning the plates, were loaded by surface traction same as loading rings in the tested structures (see Fig. 4.13).

In the presented FEM, rotational, axial and shear stiffness were used for defining the strip material behaviour. The MTSJ connections representing strips were modelled as linear elastic and orthotropic. As opposed to [12] where the joint material was modelled as isotropic, in the presented model the orthotropy needed to be introduced due to large over estimations of shear modulus parameters when isotropic material stiffness matrix was used. The values for rotational and shear stiffness per strip unit length, k_m and $k_{v,12}$, were taken based on small scale test results presented in Chapter 3, Section 3.3 and [21] respectively. As MTSJ connection details are in fact an integral part of the plates themselves, the representing shear stiffness in the remaining two directions, $k_{v,13}$ and $k_{v,23}$, as well as axial stiffness, k_n , were calculated using the generalized Hooke's law with the use of LVL material elastic properties (see Table 4.1). Concerning the axial stiffness, k_n , since the strips' and the plates' local coordinate systems do

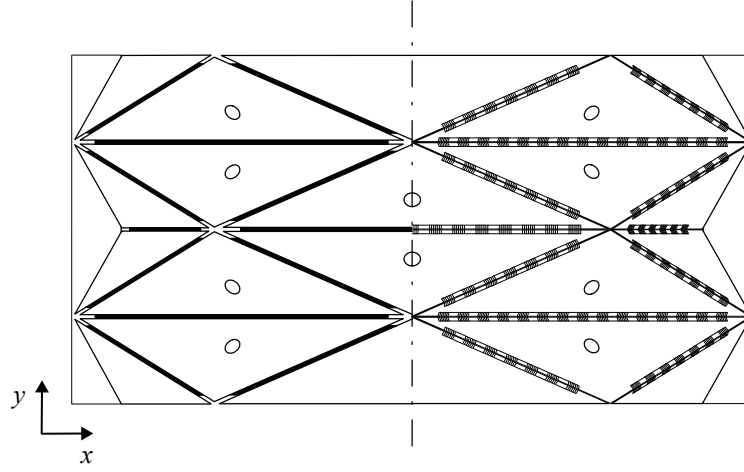


Figure 4.13 – Strip model (left) and spring model (right) geometry representation within ABAQUS. Partitioned circular surfaces for applying load are also shown. In the spring model presented here, each MTSJ tab is represented by groups containing seven sets made of three different spring types, uniformly distributed along the tab length.

not coincide (see Fig. 4.9a), the known plate elastic properties had to be rotated from the plate local coordinate system, where the $-z$ axis corresponds to the panel normal, to the strip local coordinate system, where the $-z$ axis corresponds to the respective strip normal orientation. The latter was performed by using Hankinson's equation, Eq. 4.3 [16], where θ was equal to 32.5° .

$$E_\theta = \frac{E_{22}E_{33}}{E_{22}\sin^2\theta + E_{33}\cos^2\theta} \quad (4.3)$$

The rotational, axial and shear stiffnesses for determining the strip material properties are derived hereafter, by assuming plane stress distribution and zero value for the Poisson ratio [12], according to the strip models presented in Figs. 4.14, 4.15 and 4.16, where the strip is considered to have a rectangular cross section of width, w , height, h , and unit length, l .

- The bending stiffness, k_m , is defined as follows:

$$k_m = \frac{M}{\varphi} \quad (4.4)$$

where M is the bending moment and φ is the rotation of the strip section.

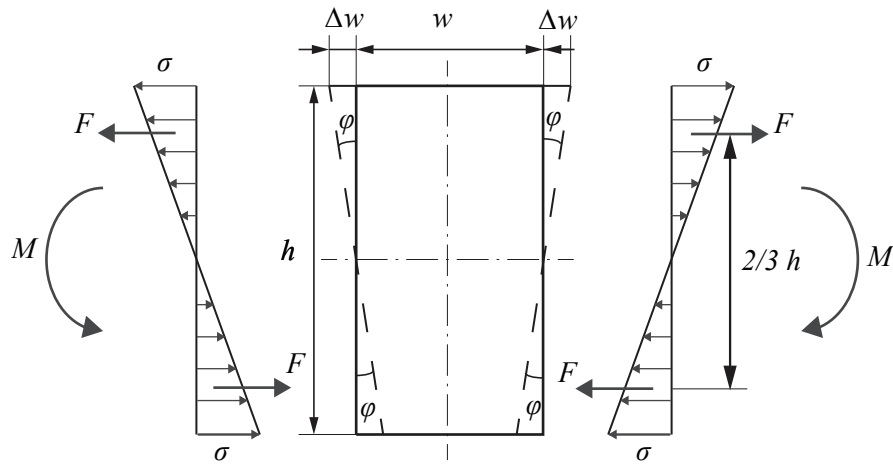


Figure 4.14 – Strip element model for the derivation of the bending stiffness, k_m .

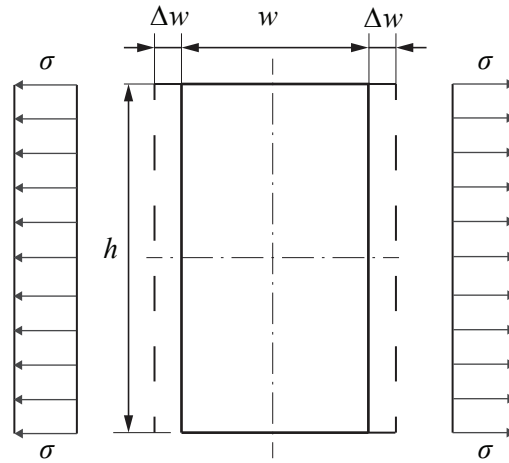


Figure 4.15 – Strip element model for the derivation of the axial stiffness, k_n .

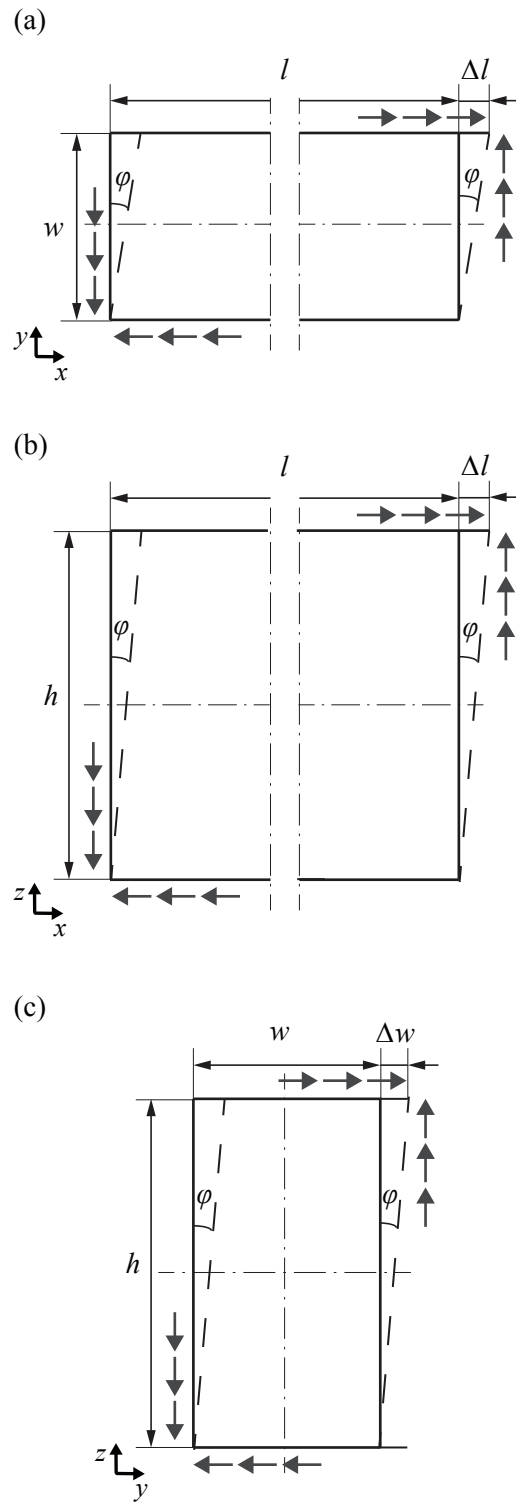


Figure 4.16 – Strip element model for the derivation of: (a) shear stiffness, $k_{v,12}$; (b) shear stiffness, $k_{v,13}$; and (c) shear stiffness, $k_{v,23}$

With reference to Fig. 4.14 the bending moment, M , can be defined as:

$$M = F \frac{2}{3} h \quad (4.5)$$

where:

$$F = \frac{1}{2} \frac{1}{2} h \sigma, \quad \text{with} \quad \sigma = E \varepsilon = E \frac{\Delta w}{1/2 w} \quad \text{and} \quad \Delta w = \tan \varphi \frac{1}{2} h \quad (4.6)$$

Substituting the variables from Eq. 4.5 with those from Eq. 4.6:

$$M = \frac{1}{6} \frac{h^3}{w} E \tan \varphi \quad (4.7)$$

By using Eq. 4.7 in Eq. 4.4 and assuming small rotations, where $\tan \varphi \approx \varphi$, the final expression of the bending stiffness is derived:

$$k_m = \frac{1}{6} \frac{h^3}{w} E \quad (4.8)$$

- The axial stiffness, k_n , is defined as follows:

$$k_n = \frac{N}{\Delta w} \quad (4.9)$$

where N is the force acting in the strip $-y$ axis direction and Δw is the deformation of the strip section in the same direction.

With reference to Fig. 4.15 the force, N , can be defined as:

$$N = t \sigma \quad (4.10)$$

where:

$$\sigma = E \varepsilon = E \frac{\Delta w}{1/2 w} \quad (4.11)$$

Substituting the variables from Eq. 4.10 with those from Eq. 4.11:

$$N = 2 \frac{\Delta w t}{w} E \quad (4.12)$$

By using Eq. 4.12 in Eq. 4.9 the final expression of the axial stiffness is derived as:

$$k_n = \frac{N}{\Delta w} = \frac{2h}{w} E \quad (4.13)$$

- The shear stiffnesses, k_{ij} , are defined as follows:

$$k_{v,ij} = \begin{cases} \frac{F_{ij}}{\Delta l} & \text{for } i, j \in \{1, 2\} \cup \{1, 3\}, \quad i \neq j \\ \frac{F_{ij}}{\Delta w} & \text{for } i, j \in \{2, 3\}, \quad i \neq j \end{cases} \quad (4.14)$$

where F is the shear force and Δ is the resulting deformation of the strip section.

With reference to Fig. 4.16 the shear force, F , can be defined as:

$$F_{ij} = \begin{cases} \frac{\tau_{ij}}{h} & \text{for } i, j \in \{1, 2\}, \quad i \neq j \\ \frac{\tau_{ij}}{w} & \text{for } i, j \in \{1, 3\} \cup \{2, 3\}, \quad i \neq j \end{cases} \quad (4.15)$$

where:

$$\tau_{ij} = G_{ij} \gamma_{ij}, \quad \text{with } \gamma_{ij} = \tan \varphi \quad (4.16)$$

Substituting the variables from Eq. 4.15 with those from Eq. 4.16:

$$F_{ij} = \begin{cases} G_{ij} h \tan \varphi & \text{for } i, j \in \{1, 2\}, \quad i \neq j \\ G_{ij} w \tan \varphi & \text{for } i, j \in \{1, 3\} \cup \{2, 3\}, \quad i \neq j \end{cases} \quad (4.17)$$

By using Eq. 4.17 in Eq. 4.14 the final expression of the axial stiffness is derived as:

$$k_{v,ij} = \begin{cases} \frac{h}{w} G_{ij} & \text{for } i, j \in \{1, 2\}, \quad i \neq j \\ \frac{w}{h} G_{ij} & \text{for } i, j \in \{1, 3\} \cup \{2, 3\}, \quad i \neq j \end{cases} \quad (4.18)$$

Having a predefined strip width, $w=17mm$, and according to 4.8, 4.13 and 4.18, the height, Young and shear modulus parameters for the orthotropic material strip are given by Eq. 4.19, Eq. 4.20 and Eq. 4.21 respectively.

$$h = \sqrt{12 \frac{k_m}{k_n}} \quad (4.19)$$

$$E = k_m \frac{6w}{h^3} \quad (4.20)$$

Property	Symbol	Value	Unit
Rotational stiffness	k_m	1684	N
Axial stiffness	k_n	126.5	N/mm^2
Strip width	w	17	mm
Strip thickness	h	12.64	mm
Elastic modulus	E	85.13	N/mm^2
Shear stiffness 12	$k_{v,12}$	31.35	N/mm^2
Shear stiffness 13	$k_{v,13}$	108.76	N/mm^2
Shear stiffness 23	$k_{v,23}$	39.88	N/mm^2
Shear modulus 12	G_{12}	42.17	N/mm^2
Shear modulus 13	G_{13}	80.85	N/mm^2
Shear modulus 23	G_{23}	29.65	N/mm^2

Table 4.2 – Strip element model, estimated stiffness parameters per strip unit length.

$$G_{ij} = \begin{cases} k_{v,ij} \frac{w}{h} & \text{for } i, j \in \{1, 2\}, \quad i \neq j \\ k_{v,ij} \frac{h}{w} & \text{for } i, j \in \{1, 3\} \vee \{2, 3\}, \quad i \neq j \end{cases} \quad (4.21)$$

The complete set of parameters used for modelling the strips are given in Table 4.2. The strip offset from the edge ends, marked as l_e in Fig. 4.9a, was equal to the offset of the first tab, where the connection between the two plates is established. Within the MTSJ connections design process, the length of this unconnected edge part was limited to a maximum 10% of the total edge length. Accordingly, the strip dimensions were modeled to correspond to the realized plate connection length.

Spring Modelⁱ

In the second approach, the semi-rigidity of the joints is introduced by means of springs along adjacent edges. Similar to the strip model, each plate surface was reduced by 1%, introducing a small gap ($\sim 3mm$) between the plates. This was needed in order to be able to define the direction in which they act. Each tab of the MTSJ was modelled by a group of sets containing

ⁱThe spring model was developed in collaboration with the publication co-author, A.C. Nguyen.

Property	Symbol	Value	Unit
Rotational stiffness	k_m	168449.52	Nmm
Axial stiffness	k_n	12656.63	N/mm
Shear stiffness 12	$k_{v,12}$	3135	N/mm

Table 4.3 – Spring model, estimated stiffness parameters per tab of the MTSJ closed slot connection. The stated values are further divided by the number of spring connectors of each spring type used within one group.

three spring types, representing the rotational, axial and shear stiffness of the connection (Fig. 4.9b). Appropriate springs stiffness values were determined according to the mechanical and material properties of the actual MTSJ, same as in the strip model. However, their values were taken as such and divided only by the number of spring connectors of the respective spring type within each individual group (see Table 4.3). It is important to note that in the presented model, all springs were considered as being uncoupled. Furthermore, assigning multiple sets within one group used for modelling the behaviour of each MTSJ tab, was assessed for obtaining improved results. First, a group with one set of spring connectors was examined. The obtained results showed that such modelling generates an overly flexible system leading to overestimated vertical displacements. A higher number of sets consisting of three types of spring connectors, with their respective stiffness reduced according to the total number of sets used within a group, provided more accurate results. As shown in Fig. 4.17, increasing the number of spring sets, causes the obtained results to converge. A good agreement was found in using 7 sets per group for representing each individual tab of MTSJ (see Fig. 4.13).

4.4 Results and Discussion

In order to compare the numerical and experimental results, the numerically obtained data needed to be corrected for the values caused by the gravity load imposed in the first loading step. This was necessary because the measurement of the total load in the performed experiments was done by force sensors placed under the plates, therefore the gravity load was not a part of the measured force. Additionally, all the measurements started to be recorded from the time when the structure was already put in position, meaning that all the initial effects of gravity load were also disregarded in the experimental results. On the other hand, in the experiments, both the displacement and the strain field were captured from above the structure with the DIC system, meaning that in the subsequent loading steps there existed a propagated influence of gravity on the resulting deflections and strains. For this reason, in

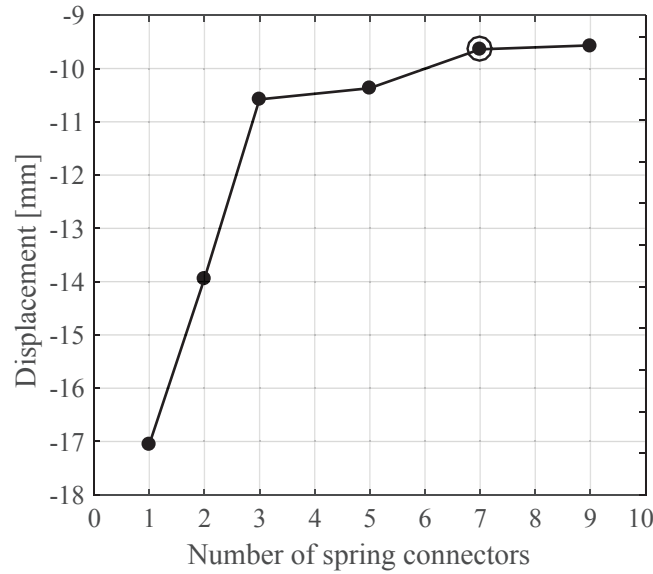


Figure 4.17 – Maximum vertical displacement of a spring model, obtained under $25kN$ by using 1, 2, 3, 5, 7 and 9 sets of three spring connector types per group representing individual tabs of MTSJ.

the numerical model the first loading step including gravity could not be simply excluded, as gravity propagated influence in the subsequent steps needed to be simulated. Therefore, for correcting the results of the numerical model, the values obtained at each step were reduced for the initial gravity load influence of the first loading step but the propagation of gravity load in subsequent steps was kept intact.

The elastic part of the total load vs. midspan deflection curve of the tested structures is compared to the numerically obtained results in Fig. 4.18. Both strip and spring model linear analysis results show very good agreement with the linear approximation of the three tested samples. On the other hand, the results of models where geometric nonlinearity was included seem to capture with better accuracy the slight tendency of experimental results to deviate from the linear approximation with increasing loads. In both types of analysis, the strip shows slightly less stiff behaviour compared to the spring model. This is attributed to its possibility to introduce additional properties for modelling the connections behaviour, such as shear stiffness in the remaining two directions, $k_{v,13}$ and $k_{v,23}$. When examining the displacement profile along two lines, as shown in Fig. 4.19, the error of the spring model is more pronounced. Both strip linear and nonlinear analysis models represent with more accuracy the experimental curve. The maximum absolute error with respect to the experimentally obtained results, amounted to 6.6% for the spring and 2.2% for the strip model with linear analysis, 4.8% for the spring and 3% for the strip model with geometrically nonlinear analysis.

Furthermore, a comparison of the strain results shows that not taking into consideration

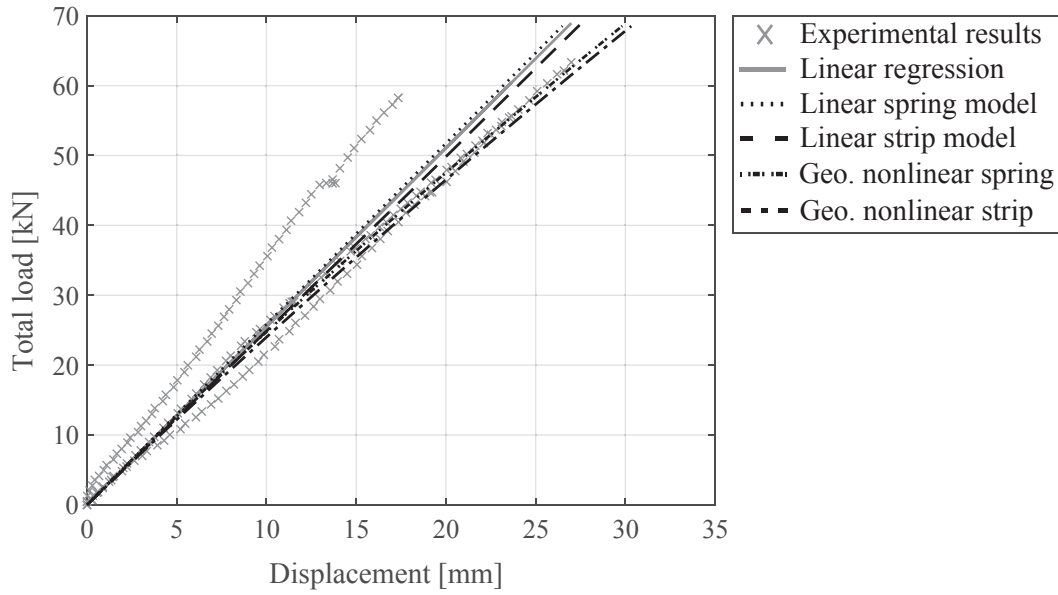


Figure 4.18 – Comparison of experimental and numerically obtained results. Total load vs. maximum vertical displacement.

geometric nonlinearities gives highly erroneous values of strain, especially in some cases (see SG_1 in Fig. 4.20). The stiffness matrix which is formulated for the undeformed geometry at the beginning of the linear analysis is not updated after each loading increment, as is in the case with geometrically nonlinear analysis, and cannot capture the change in strain values as the system deforms. Generally, the results show that the strains in the plates are fairly low in magnitude even for high total loads but have a strong nonlinear dependence on the load at certain positions, SG_1 and SG_4 (see Fig. 4.20). However, even though the limit state design is governed by the values of displacements, for modelling accurate strain magnitude, including geometric nonlinearity seems to be essential. When comparing the strain results of strip and spring models it can be seen that higher discrepancies are found along the skewed edges of the plates, strain gauges SG_3 and SG_4 . This is due to the fact that the forces which appear at the straight edge connections are acting very much in the same directions as the defined bending, axial and shear springs within the spring model. However, on the skewed edges, where shear forces are more dominant, twisting of the mutually connected panels and shear which occurs in the other two in-plane directions, 13 and 23, are not taken into account with the assigned springs. This seems to be the main shortcoming of the spring model. As the plates are modeled as shells, represented by their mid surface, the springs can only be assigned to connect nodes on those mid surface planes, meaning that only one direction of shear in that specific plane can be represented. The numerically obtained results of the linear and geometrically nonlinear analysis show that the plates themselves undergo what

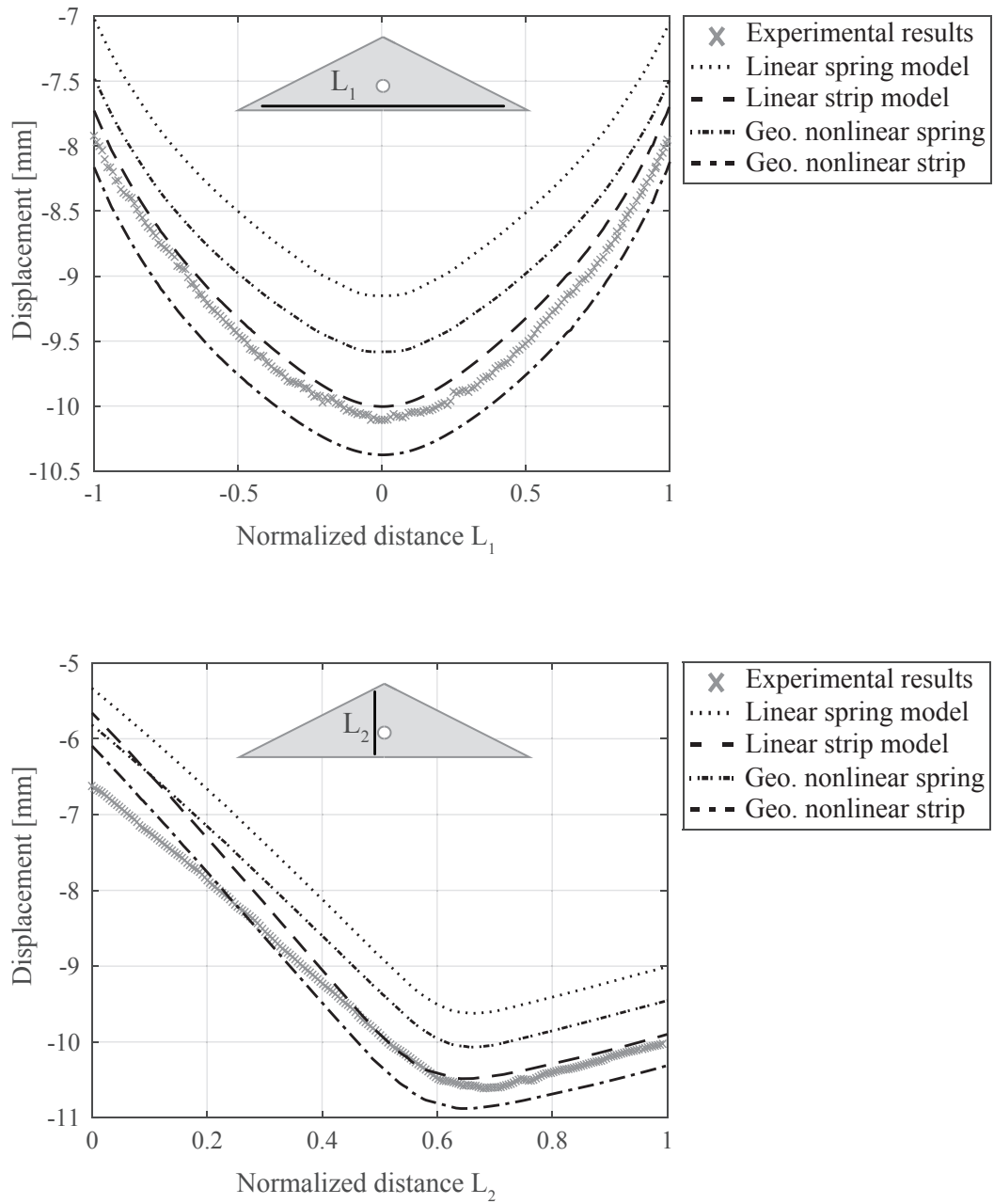


Figure 4.19 – Comparison of experimental and numerically obtained results for 25kN total load, which approximately corresponds to the occurrence of SLS maximal allowed displacements. Vertical displacements profile along the length of the marked lines L_1 and L_2 .

can be considered small strain and deformations, i.e. the values of resulting engineering and logarithmic strains are equal, indicating that an important part of the structures displacements are in fact plate rigid motions as well as system rotations due to semi-rigid connections.

4.4.1 Comparison to the rigid connection model

For examining the level of the MTSJ semi rigidity, a structure with completely rigid connections was modelled using high rigidity springs within the spring model (see Fig. 4.21). At the load of 25 kN , when MTSJ structures reached the SLS maximal allowed displacement of 9.66 mm , the displacement of the rigid jointed structure show to be 5.7 mm , only 60% of the maximal allowed value. The 9.66 mm displacement for the rigid model correspond to the load of 42 kN , 68% higher load then in the case of MTSJ structures, which clearly indicates that the semi rigidity indeed plays a decisive role in the structural behaviour of systems using closed slot MTSJ. Additionally the rigid model results are compared to the experimentally obtained ones form adhesively joined structures, shown in Chapter 3 Section 3.5, with the aim to inspect the quality of the experimentally achieved adhesive connection. The numerical model stiffness equals to 4.37 kN/mm , 19% higher with respect to the characteristic stiffness of the adhesively joined structures group (see Fig. 4.21). The results suggest that the adhesively joined edgewise connections realized in the experimental tests cannot be considered rigid, as is typically the case in simplified structural analysis with other types of adhesively joined connections. This can be attributed to the problems related to gluing as explained in Chapter 3 Section 3.6, as well as difficulties in achieving full rigid potential of adhesives when gluing along the faces of a butt or miter joined edges, especially in thin plates meeting end-grain to end-grain in certain layers [32]. It is also important to note that the bond quality depends on many factors, such as bonded surface roughness and moisture content, thus the presented results relate only to the specified adhesive type and bond quality achieved in the presented experimental tests.

4.5 Conclusions

In this Chapter, two simplified methods for modelling the semi-rigid behaviour of timber folded surface structures with MTSJ connections were examined. Based on the obtained results and observations, the conclusions are as follows:

- Compared to the spring, the strip element model presents more accurate results with respect to the experimentally obtained values. It is inferred that the main advantage of using strips is due to their possibility to include more connection properties into the model, such as shear stiffness $k_{v,13}$ and $k_{v,23}$. Respectively, the inability to do so was

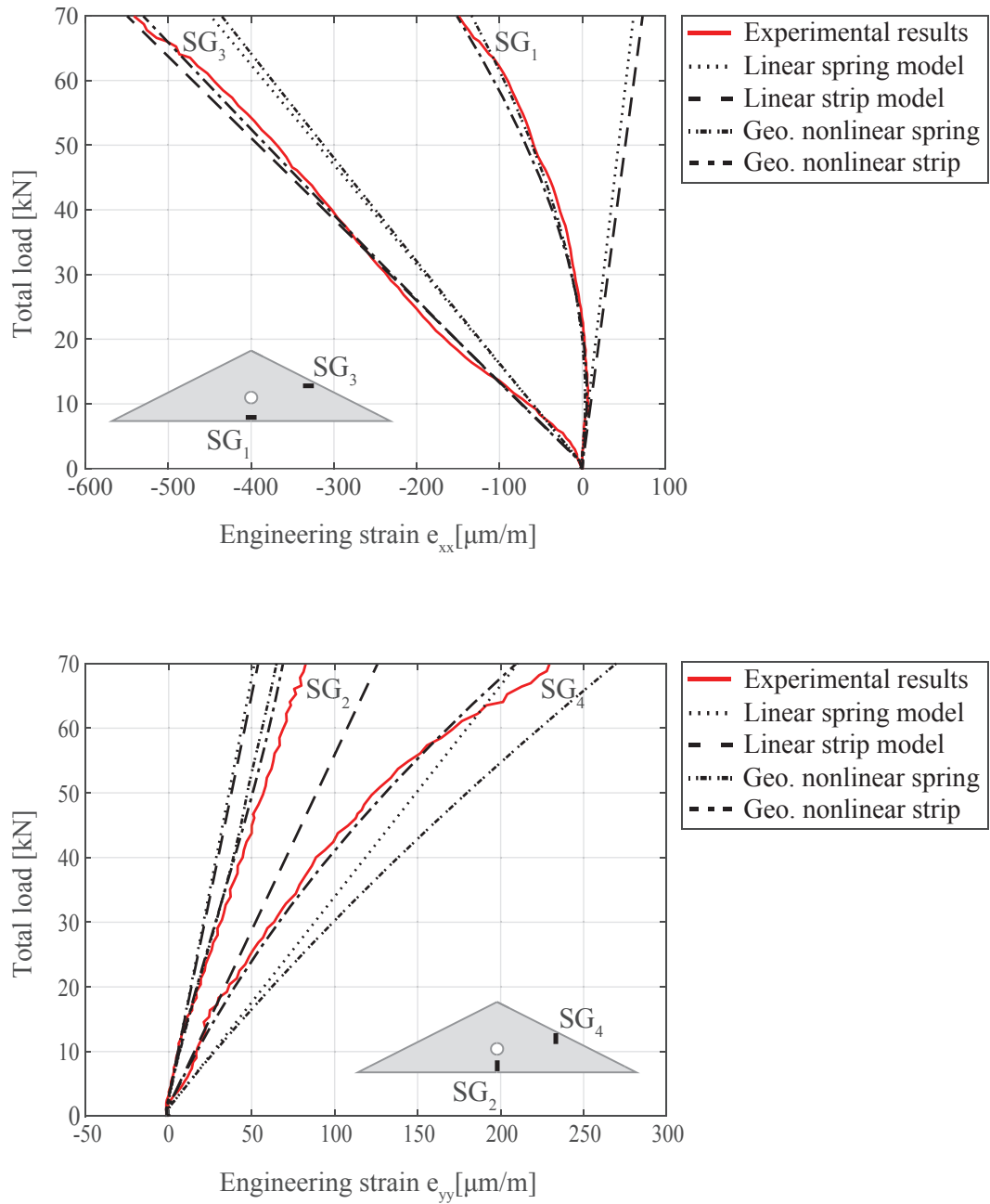


Figure 4.20 – Comparison of experimental and numerically obtained strain results. Engineering strain is used as it is the output obtained from strain gauge measurements. Also, as the plates themselves undergo only small deformations, in the numerical results the engineering strains were found to be equal to the logarithmic strain values.

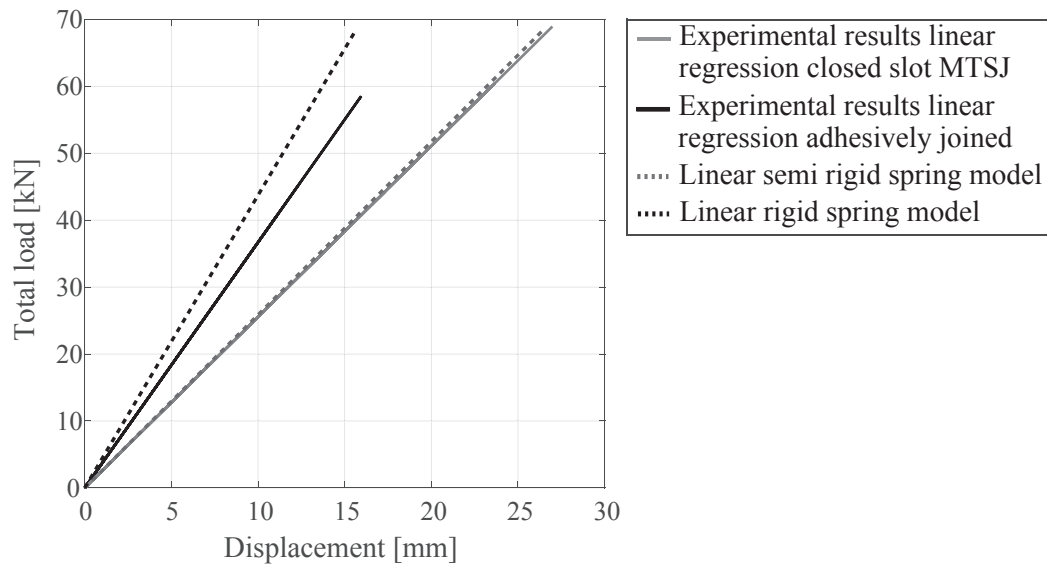


Figure 4.21 – Comparison of semi-rigid and rigid spring model results with experimental tests. Total load vs. maximum vertical displacement.

found to be the main shortcoming of the spring element model;

- The results show that using the strip element seems to be a feasible way for modelling the MTSJ semi-rigid behaviour within a folded plate system in its linear part. Both linear and nonlinear analysis could be used for this purpose as the displacements are a key parameter for modelling such structures. However, including geometric nonlinearities in the analysis showed to be essential for accurate modeling of occurring strains as well as for displacements when considering higher load levels;
- On the other hand, the potential advantages of using the spring element model could be found in their slightly more fast and straightforward generation. Total time needed for the automatic generation of the spring model takes only 2 minutes of total CPU time, while the strip element definition takes 4 minutes. This time includes geometry input, material and sections definition, assembly, step generation, defining the springs/strips and their local coordinate systems as well as specifying loads and boundary conditions (i.e. final analysis computation time was found to be approximately equal). When considering more complex geometries with possibly varying MTSJ geometrical parameters, for which the computation time would increase exponentially, using the spring elements could prove to be more efficient. Additionally, using spring elements would be more appropriate for geometry cases with nonparallel adjoining plate edges, as using strips would result in their inconsistent widths along a single edge (for example timber plate-shell geometries as shown in [69]).

In conclusion, when comparing MTSJ structures to those with completely rigid connections, the presented results demonstrate that the MTSJ details have a significant influence on the structural behaviour of the global system. Therefore, it is suggested that rigorous models including the connection semi-rigidity are necessary for appropriately analysing the structural response of timber folded surface structures with closed slot MTSJ.

5 Foldability of the Form with Respect to Structural Performance

5.1 Introduction

Achieving larger spans in timber folded surface structures precipitated the need for forms with multiple elements along the width of the structure. Due to difficulties related to the realization of pertinent thin timber panel edgewise connections using state-of-the-art techniques, a search was initiated for finding new ways of increasing structural rigidity for providing efficient load bearing systems. For now, this search has mainly focused on developing more suitable connections which would be able to provide sufficient load bearing capacity, where recently a very promising outcome was presented by the one-degree-of-freedom MTSJ, also used within this thesis. However, a complementary approach could be found in exploring the influence of form on the structural behaviour of the folded systems as well as requirements concerning its connection details, and understanding how additional stiffness can be provided by modifying the structure's geometry. In this regard, this Chapter focuses on form deployability, that is, its inherent kinematics determined by its topology.

It is noticed that even though the connection detail requirements for kinematic and static structures are completely opposite, the forms used for both structure types seem to be very similar. As stated by K. Miura in [62], for the forms used in origami, i.e. deployable structures, the transformations from the initial state to the folded one occur with relatively little energy (and therefore unexpectedly), meaning that the phenomenon can be dangerous when it occurs. Furthermore, in his review of folded structures [56], A. Lebee notes that as folding is continuously transforming a flat surface in the 3D space, a folded shape is not a structure, it is a mechanism, and the key for turning a folded surface into a structure consists in closing that mechanism. Therefore, since for static folded structures foldability of the form is not a requirement and seeing that it can be potentially disadvantageous, it seems beneficial to use

forms for which folding capacity is minimised. In this regard, by examining the deployability of a certain form, this Chapter aims to demonstrate its relation to the structural capacity under load when such a form is used within a static system. It is further shown how the form's deployability directly relates to the plate elements strength requirements and even more so to the connection details, which are considered a key structural component in these systems. The performed study concentrates on forms of built examples by analysing their structural behaviour within the framework of MTSJ timber folded surface structures.

The Chapter is structured as follows:

- Section 5.2 presents the concepts of foldability and foldability range, as well as their use within this study. Also, the explored structure forms are presented and their transformation paths are explained and compared;
- Section 5.3 includes the FE structural analysis of the observed forms, used within a static system, as well as discussion on the found differences;
- Section 5.4 examines the analogy between the presented numerical results and the respective form foldability range;
- Section 5.5 summarizes the main conclusions.

5.2 Rigid Foldability

Foldability of a form is a term most commonly used within the area of deployable structures. With their main characteristic being the ability to transform from a closed compact configuration to a predetermined expanded form, in which they are blocked from further movement for achieving stability and carrying load. This transformation path from the closed state to the final one is called *deployment* or *unfolding*, while the reverse transformation is called *retraction* or *folding* [22]. Depending on the type of structural members used, such systems can be made as surface structures consisting of plate elements or strut structures consisting of bar elements. These elements may further be stiff plates and struts or flexible membranes and cables [35]. The choice of structural system as well as the material further defines their load bearing behaviour. To draw an analogy with static folded surface structures examined within this thesis, further text refers only to deployable structures made from stiff plates.

To explore the kinematic potential of static folded plate structures form, their initial state, i_0 , is considered to be somewhere in between the two extreme states: 1) developed state, i_d , which corresponds to the state where all faces are coplanar, lying in the same plane, and

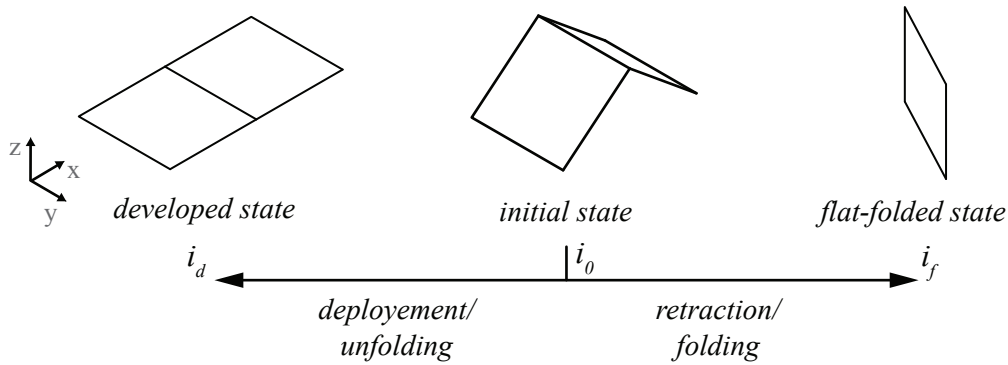


Figure 5.1 – Foldability and the transformation paths of a simple form including one fold unit consisting of two quadrilateral plate elements.

no overlapping exists; and 2) flat-folded state, i_f , which corresponds to the state where all faces are coplanar and overlapping (see Fig. 5.1). Therefore, from the initial state, i_0 , the structure can either be deployed or retracted. The two terms no longer indicate the same path of opposite direction but two distinct paths starting from the initial, static, form. In this Chapter the term foldability will be used to describe the complete transformation path range, including both folding and unfolding of the form.

While observing the foldability of a rigid form an important mathematical concept that needs to be followed is rigid foldability. This concept focuses on the folding process and it requires that during folding the form only bends at the fold lines, i.e. edges, which are kept straight while all faces are kept planar. In this case the faces can be considered as rigid panels mutually connected with perfect hinges [85, 95, 77]. This enables a purely geometrical mechanism to be developed which does not rely on the elasticity of the material. The length of this *continuous* path between the initial and final states represents the foldability potential of the form itself. It is important to note that within this study the thickness of the plates is neglected, as the interest is put on the form's folding range and not the actual compactness of the ultimate retracted state.

5.2.1 Foldability range

For defining the foldability range of a certain structure form, a method for the description of rigid foldable mechanisms folding motion proposed by F. Gioia et al. [36] is used. In this method, possible variations of the folding angles during the folding or unfolding operation are described by using a global descriptor G_Ω , for a specific state of the corrugated surface, Ω :

$$G_\Omega = \frac{1}{q} \sum_{ij} \frac{a_{ij}}{\pi} \quad (5.1)$$

where q is the number of folding angles, a_{ij} , between the plates adjacent faces, i and j . Since $0 \leq a_{ij} \leq \pi$, one gets $0 \leq G_\Omega \leq 1$, where $G_\Omega = 0$ corresponds to all faces coplanar with no occurring overlaps (developed state) and $G_\Omega = 1$ corresponds to all faces overlapping (flat-folded state). For a more detail geometrical description of the used method, its considered surface orientations and folding angles the reader is referred to [36]. Hereafter, the global descriptor, G_Ω , is used as an intrinsic characteristic of the folded state configurations for describing the initial as well as extreme unfolded and folded state.

Depending on their foldability range, folded surface forms can be divided into three groups. First group includes forms most often used in deployable structures where full developability and/or flat-foldability is required, where G_Ω extreme state values equal to 0 and/or 1 respectively. Second group contains forms with no available kinematic modes, i.e. self-locking corrugation patterns. For such cases total foldability range is equal to zero. A very interesting study concerning such self-stabilizing geometrical forms for application in truss and plate shell structures is given by T. Wester in [96]. However, for forms applicable to folded surface structures, it is impossible to achieve a complete global self-locking mechanism when large number of faces are considered. Typically, locally there always exist certain edges within the form, arranged so that they achieve compatibility in rotation mechanism when actuated by a force of specific direction. Accordingly, such forms fall into the third group, together with other forms which behave like a mechanism up to a certain point when self-blocking of the panels occurs and there are no more soft kinematic modes available. This types of forms have extreme values of global descriptor equal to: $G_\Omega > 0$ for the extreme developed state, i_d , and $G_\Omega < 1$ for the extreme flat-folded state, i_f .

Foldability of five forms intended for static timber folded surface structures is further examined. Naturally for this purpose their boundary conditions are considered to be free, with movements and rotations possible in all directions. First two examined forms are taken from realized timber folded plate structures, *St. Loup Chapel* and *Thannhausen Music Rehearsal Hall* (see Fig. 5.2 and 5.3, state i_0). Both structures have similar overall dimensions, however,

a very significant difference in the used surface folding technique is the main reason for the interest in their comparison. In *St. Loup Chapel* a reverse folding technique is used, where looking at the folds along the span ($-x$ axis of the structure), it can be observed that the roof mountain folds turn into valley folds in the walls, and vice versa. In geometrical terms this is achieved by reflecting the fold about a reflection plane which is perpendicular to the interior angle bisector of the main crease edges [18]. On the other hand, in *Thannhausen Music Rehearsal Hall* form, the folds along the span do not change their direction in space and mountain folds are followed by mountain folds and valley by valley folds. To demonstrate more clearly the mentioned difference, a form is designed with exactly the same dimensions and number of parallel folds as the original *Thannhausen Music Rehearsal Hall*, but using the reverse folding technique (see Fig. 5.4). For brevity, in further text the original *Thannhausen Music Rehearsal Hall* form will be noted as *TO* and its modified reverse fold version as *TR*.

The third examined form is a regular anti-prism based folded form, also known as *Yoshimura* pattern, used throughout this thesis (see Fig. 5.5a). The foldability of its modified version is analysed as well (see Fig. 5.5b). In this case, the modification of the form was not as straightforward as in the *TO* form example, where reverse folding technique was used. Herein, dynamic relaxation (DR) method is proposed for the modification of the *Yoshimura* form.

The benefits of using the DR method are twofold: 1) an algorithm with imposed geometrical restrictions can be defined so that a controlled final form is obtained, with same topology (same connectivity pattern, number of edges and vertices) but different geometry (dimensions and geometry of plate elements, folding angles and positions of vertices); and 2) the obtained form is always in equilibrium to the applied loads, resulting in a stable solution.

Basic methodology of DR is shortly explained in the following text, for a more detailed description please refer to [10, 50, 92, 26]. DR method is a numerical procedure that traces the motion of a structure through time under applied loading. The structural form is discretized into a particle-spring system, built of translational spring elements connecting the particles. These particles are represented by nodes in which the mass of the spring elements is lumped. The load is then applied to the nodes which causes the system to oscillate around its equilibrium position. These oscillations are damped until the final form is obtained, by using either viscous or kinetic damping. For the presented application viscous damping is used, as it is easy to incorporate in the basic equations that update the nodal geometry and is sufficient for the presented problem. Viscous damping is mathematically modelled so that it is proportional to the nodal velocity while acting in the opposite direction, therefore slowing the movement.

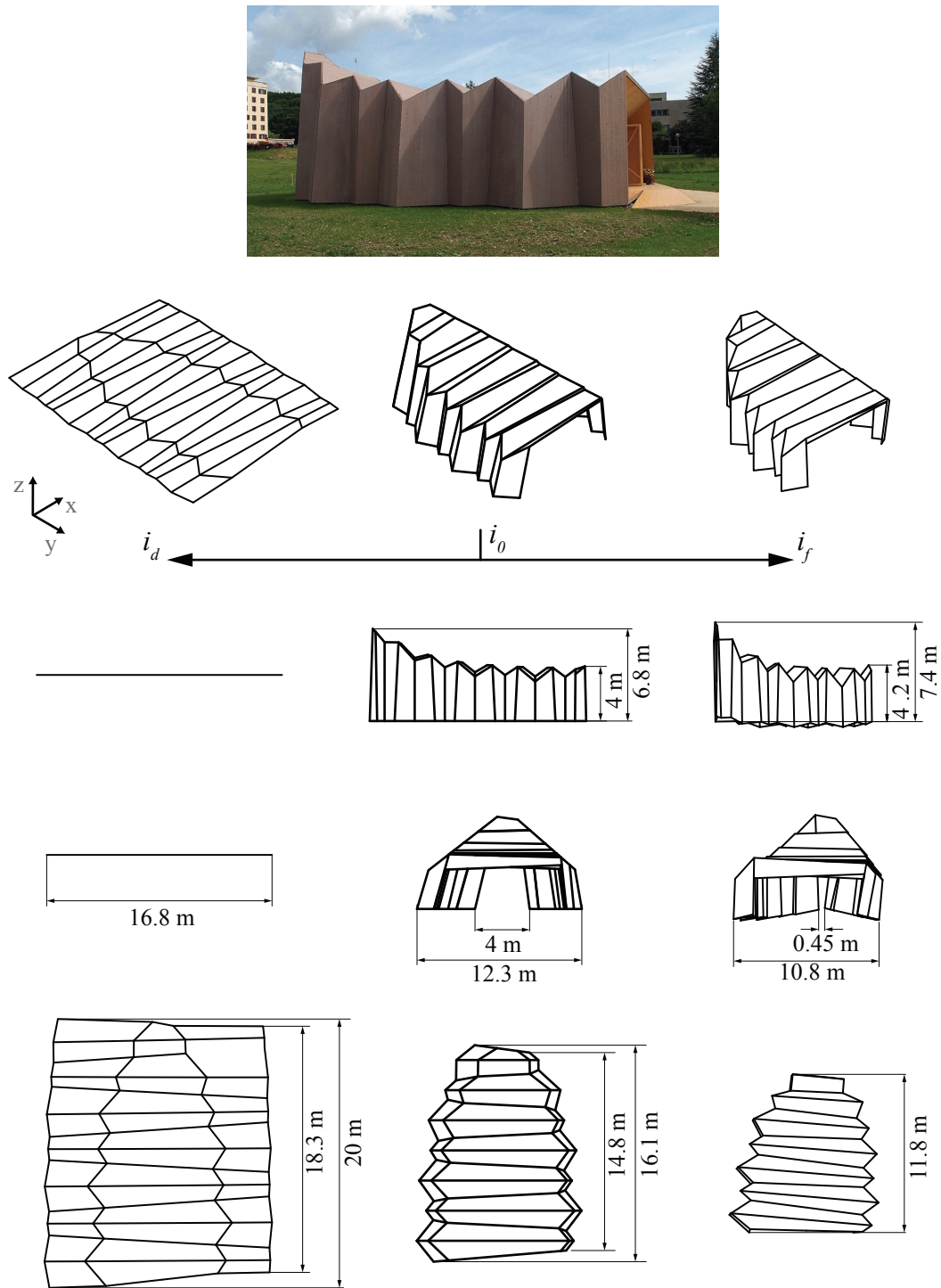


Figure 5.2 – Foldability range of the St. Loup Chapel form. Initial state of the structural form, i_0 , and the two extreme states obtained by its deploying, i_d , and retracting, i_f .

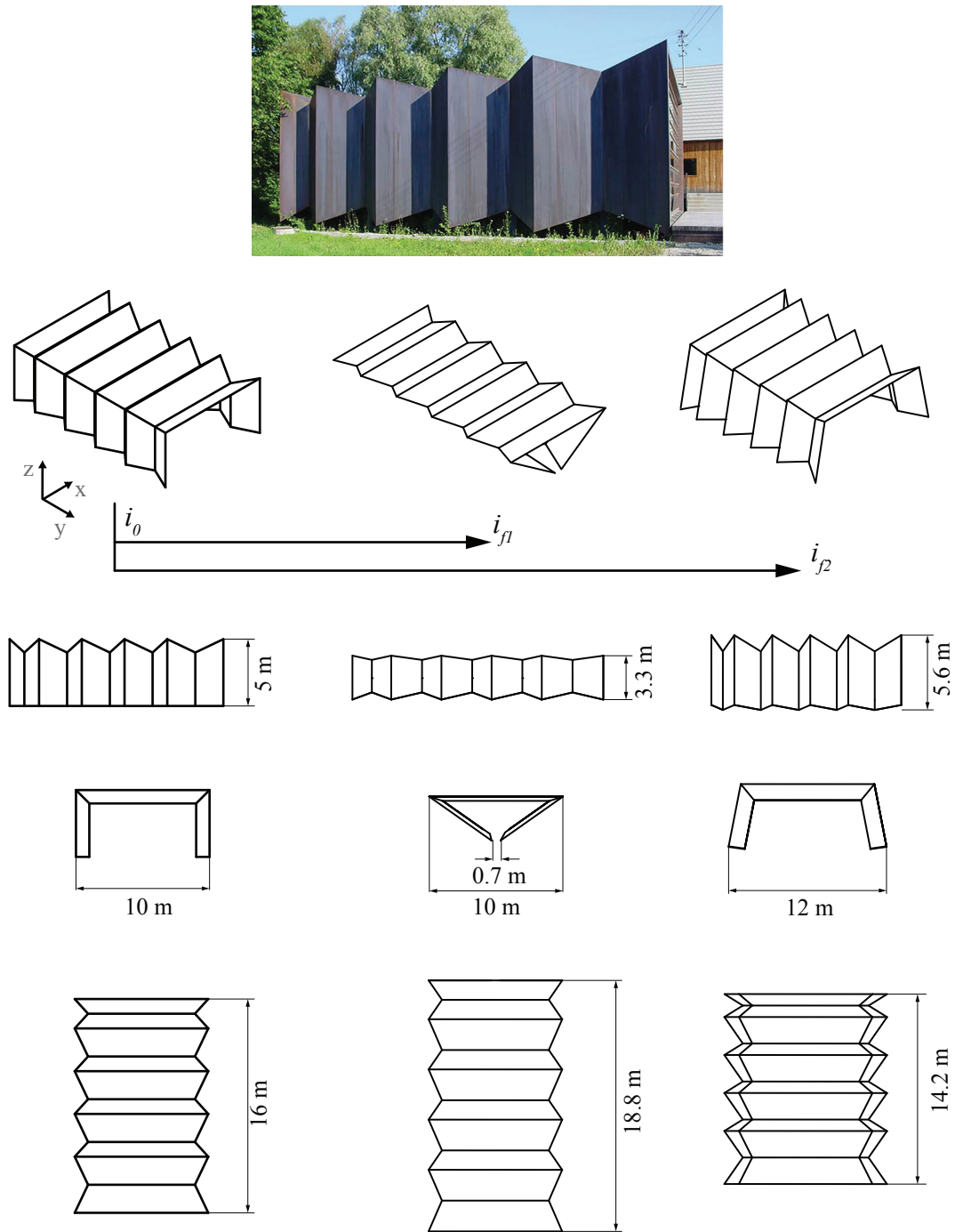


Figure 5.3 – Foldability range of the Thannhausen Music Rehearsal Hall form. Initial state of the structural form, i_0 , and its two extreme states, both obtained by retracting the initial state, i_{f1} and i_{f2} .

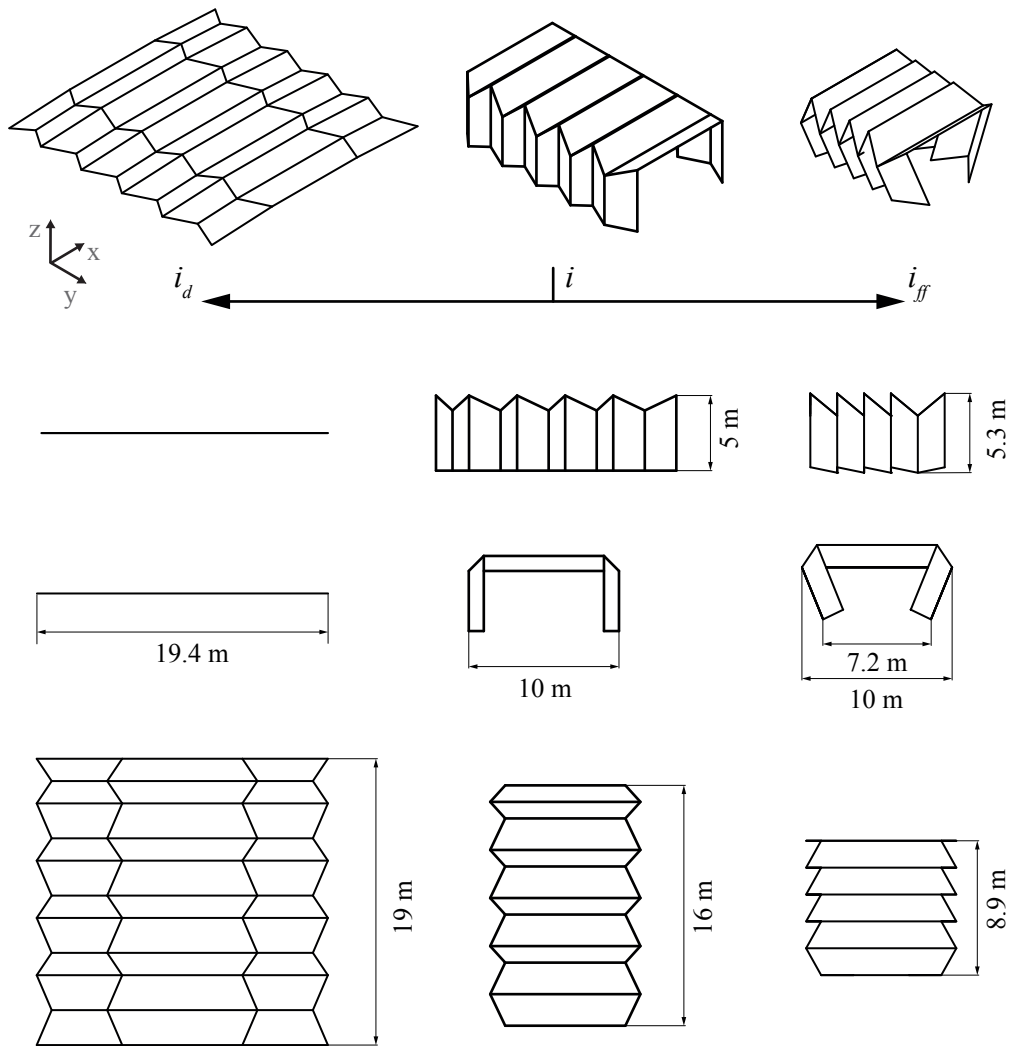


Figure 5.4 – Foldability range of the Thannhausen Music Rehearsal Hall modified form. Initial state of the structural form, i_0 , and the two extreme states obtained by its deploying, i_d , and retracting, i_f .

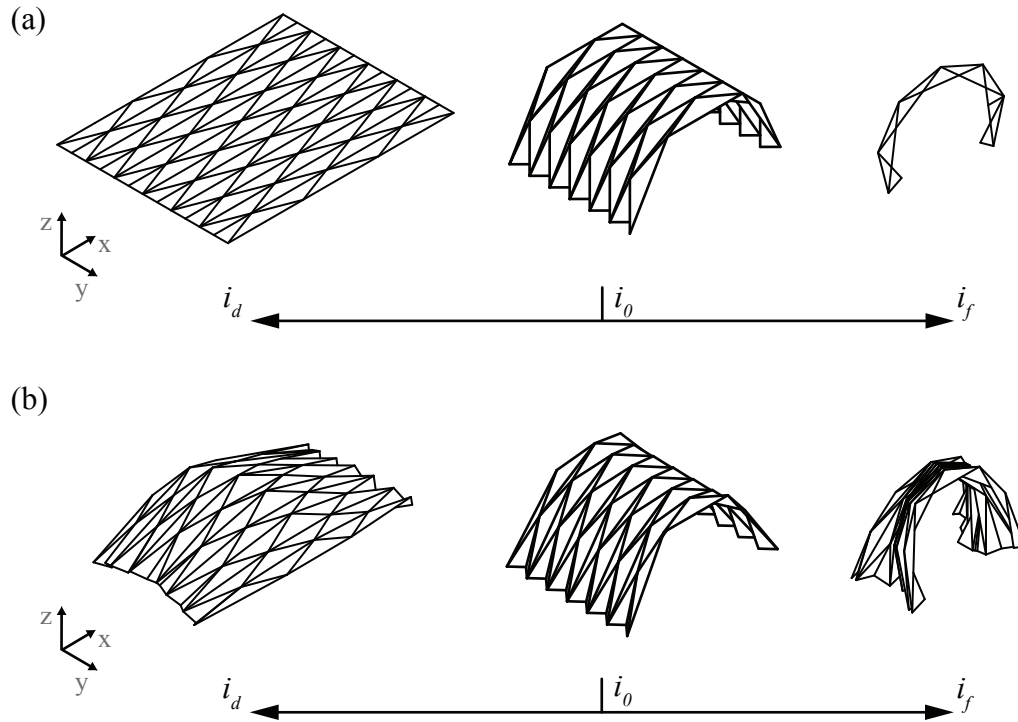


Figure 5.5 – Foldability range of the Yoshimura pattern folded form (a) and its modified version obtained by dynamic relaxation (b). Initial state of the structural form, i_0 , and the two extreme states obtained by its deploying, i_d , and retracting, i_f .

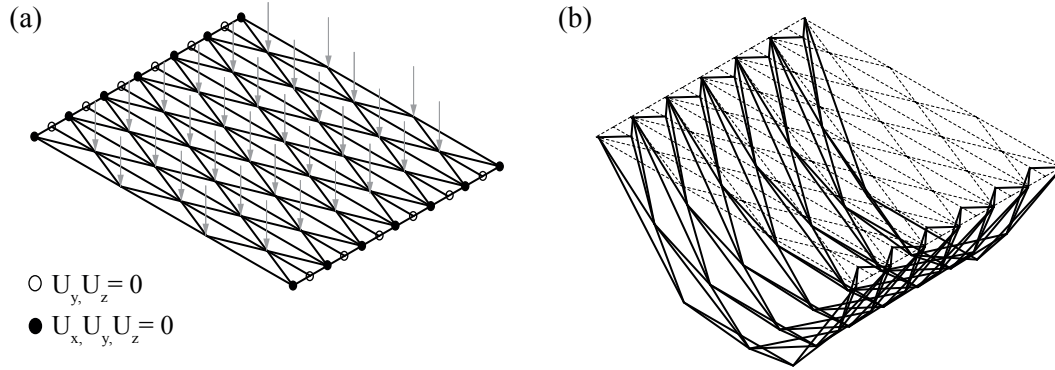


Figure 5.6 – Dynamic relaxation of the Yoshimura pattern connectivity (a), for obtaining the modified version of the Yoshimura pattern form (b).

The DR relaxation method explained above was used on the *Yoshimura* pattern formulated as a grid of nodes and links, where the nodes represent the vertices and links between them represent the pattern edges. With regard to MTSJ timber folded surface structures feasible geometries, the imposed restrictions concern the maximal values of the dihedral angles, apex angles and maximal plate size (see Chapter 2, Section 2.3). Through a custom developed algorithm, using Rhinoceros 3d®, Grasshopper® and Kangaroo plugin [66], the above mentioned geometrical restrictions were imposed and the boundary conditions were applied on the edge nodes along the $-y$ axis of the generated grid. In order to obtain a folded form corresponding to the *Yoshimura* pattern form, the boundary conditions were set so that all the nodes at the edge vertices where valley folds meet are restrained from movement in $-y$ and $-z$ directions, while free to move in the $-x$ axis direction. All the remaining edge vertices were blocked from movement in all three directions (see Fig. 5.6). This enabled the achievement of a modified *Yoshimura* form with a slight second curvature in the $-y$ axis direction while covering the same surface area and having a constant span. It is important to note that the above presented method was not used for dynamic relaxation of a folded plate structure in itself, but rather the connectivity of the original *Yoshimura* pattern. Therefore, during the form-finding process the values of all numerical quantities, such as stiffness EA and load, were arbitrary since it is only their ratios that effect the final shape [26]. This ratio was chosen so that the final form of same span to rise ratio as the original *Yoshimura* form is obtained.

For finding the extreme configurations of the above presented folded forms it is necessary to explore their available continuous kinetic mechanisms under the constraints of rigid-foldability. For this purpose the *Freeform Origami* software written by T. Tachi was used [86]. This software enables the simulation of continuous transformation path of a given polyhedral surface under imposed geometric constraints. For ensuring rigid-foldability conditions, the imposed constraints during folding transformation were as follows: keep all faces of the

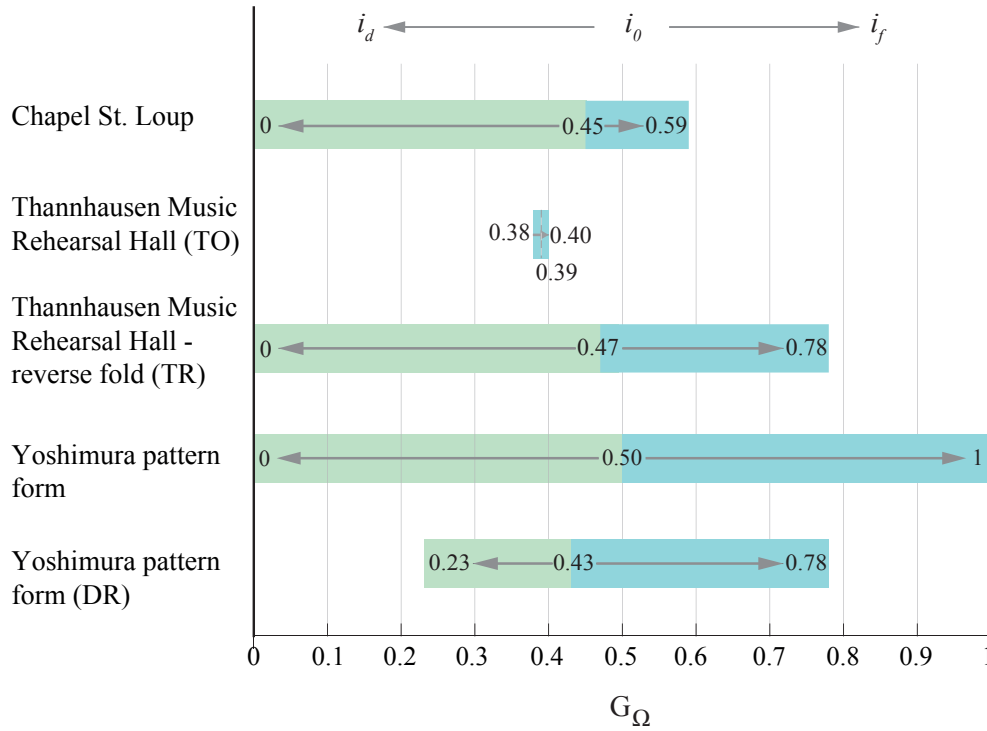


Figure 5.7 – Global descriptor G_Ω values for initial and two extreme states of the observed forms.

mesh planar, avoid local collision between faces sharing a vertex, strictly follow assigned mountain and valley folds (no flips allowed). In this way, the initial form's extreme unfolded and folded states 3d polygon meshes were obtained. The values of the global descriptor, G_Ω , for the extreme states were then determined by exporting the 3d meshes into a CAD software Rhinoceros 3d®. Together with the 3d mesh of the initial state, using a Grasshopper® algorithm, all the folding angles between adjacent faces, a_{ij} , and the number of common edges, q , were computed. From this, the finite rigid-foldability range of the examined forms was obtained and described with the values of G_Ω for their initial and extreme states (see Fig. 5.7).

When comparing the foldability range of the form used for the *St. Loup Chapel* and *Thannhausen Music Rehearsal Hall* as well as its modified version, a large influence of using reverse folding is noticed (see Fig. 5.7). In both of forms where reverse folding is used, it enables complete unfolding of the form, up to the state i_d where $G_\Omega = 0$. Comparing their flat-folded states, the influence of using oblique folds is seen in the *St. Loup Chapel* extreme state, i_f . Such folds allow sooner self-blocking of the faces due to their particular geometry. The parallel folds in *TR* modified version allow more movement and finally block at a state equal to $G_\Omega = 0.78$, displaying a wider foldability range. On the other hand, the original *TO* form shows a very

narrow foldability range and a completely different transformation path than its modified version. Compared to its initial state G_{Ω} , the global descriptor of the extreme states shows that the transformation is only possible towards the flat-foldable state. Unlike the previous two examples of *St. Loup Chapel* and *TR*, where there is a unique continuous path between the extreme states and the initial state, which belongs to a certain intermediate stage, the *TO* initial state is equal to the extreme developed state. From it, two distinct folding paths lead towards two separate extreme flat-folded states. Examining the foldability range of the two *Yoshimura* pattern forms, it can be seen that the original one achieves a developable state equal to $G_{\Omega} = 0$ and a flat-foldable state equal to $G_{\Omega} = 1$, achieving a full folding capacity. The DR significantly reduces the original folding range, due to variable plate geometries (analogous to the relation between *TR* and *St. Loup Chapel* form).

5.3 Structural Analysis

The substantial difference in the examined forms' foldability range and transformation paths suggests that when using such forms in static structures a potential difference in their load bearing mechanisms could be found as well. To verify this presumption, a comparative FE analysis of two of the reviewed structures is presented hereafter. The structural behaviour of *Thannhausen Music Rehearsal Hall (TO)* form is compared to its modified reverse fold version (*TR*). These two forms are chosen in order to be able to carry out a straightforward comparison, as they differ only in the folds arrangement while their global as well as individual plate dimensions remain the same.

To stay consistent with the main focus of this thesis, the structures are considered built with 21mm KERTO-Q panels with plates mutually connected using closed slot multiple tab-and-slot joints (MTSJ). In this way a realistic semi-rigidity of the connections is included in the analysis, as it has shown to have a big influence on the structural behaviour of the entire system (see Chapter 3 Section 3.5). Both of the examined structures are scaled down by a factor of 0.5 in order to remain realistic when using the plate thickness of 21mm and connection modelling properties as presented in Chapter 4, (see Fig. 5.8). Pinned boundary conditions were imposed on the wall naked plate edges along the $-y$ axis of the structures. The two roof plate naked edges at the open ends of the structures were blocked from movement in the $-z$ axis, while the corresponding end side wall naked edges were blocked in the $-x$ axis. This was done in order to avoid high deformations of the roof plates and buckling of the wall ones and the resulting influence on the global behaviour of the entire system, as they are of different lengths in the two compared structures. Surface load in the negative $-z$ axis direction was applied on the entire roof consisting of 10 individual plates. The middle portion of structures, which is

considered the area of interest for the presented comparison, is indicated in gray in Fig. 5.8. It consists of three wall plates (marked as 1,3 and 5) and three roof plates (marked as 2,4 and 6). Considered sections, A,B and C are shown as well in the same figure.

With respect to their 5m span, the maximal allowed displacement of the structures corresponding to the serviceability limit state (SLS), equals to 16.6mm ($L/300$ according to [27]). *TO* structure reaches this value at a total load of 50.11kN (1.22kN/mm^2) while the *TR* reaches it at a slightly lower load of 49.09kN (1.19kN/mm^2), suggesting a negligible difference in stiffness of 2%. However, more significant differences are observed in the two structures' internal moment and force distributions, shown in Figs. 5.9, 5.10, 5.11 and 5.12. The comparison of results presented in the mentioned figures is summarized in Fig. 5.13, as a percentage change relative to the *TO* structure: $\xi = (TR - TO/TO) \cdot 100$. The comparison between maximum values of in-plane forces, maximum twisting moments exerted on the connections as well as the difference in reaction forces is also shown in Fig. 5.13. All the presented results correspond to the above-mentioned SLS load values.

Fig. 5.9 shows insignificant difference between out-of-plane M_x bending moments occurring in the plate elements of the two structures ($\xi = 0.5\%$, see Fig. 5.13). In the same section, the *TR* structure shows notably higher maximal bending moments exerted on the connections ($\xi = 11.6\%$, see Fig. 5.13). When examining the section defined by plane B (see Fig. 5.10), M_y bending moments in the roof plate are slightly higher in the *TO* structure, while the wall plate bending moments are higher in *TR* ($\xi = -1.7\%$ and $\xi = 7.3\%$, respectively, see Fig. 5.13). Furthermore, in section C both roof and wall plate M_y bending moments are higher in the *TR* structure ($\xi = 11.3\%$ and $\xi = 23.8\%$, respectively, see Figs. 5.11 and 5.13). However, in both sections B and C, *TO* structure shows higher bending moments values exerted on the connection ($\xi = -8.0\%$ and $\xi = -22.6\%$, respectively, see Fig. 5.13). Maximal values of the plates' in-plane compression exerted on the connections, occurring at the structure corners, seem to be significantly higher in the *TO* structure ($\xi = -40.3\%$, see Figs. 5.12 and 5.13). Tension, on the other hand, shows considerably higher value in the *TR* structure ($\xi = 27.6\%$, see Figs. 5.12 and 5.13). Higher maximum in-plane shear forces develop in the *TO* structure ($\xi = -10.0\%$, see Fig.5.13). At the same time, in the *TR* structure maximal twisting moments as well as reaction forces in both x and y axis, show a considerable increase ($\xi = 54.4\%$ and $\xi = 16.0\%$, respectively, see Fig. 5.13).

To summarize, considering all three sections A,B and C, design governing critical values of bending moments within the panel as well as those exerted on the connections appear in section A and are higher in the *TR* structure. Furthermore, when comparing the developed in-plane tension forces to the compression ones, the former ones need to be regarded as

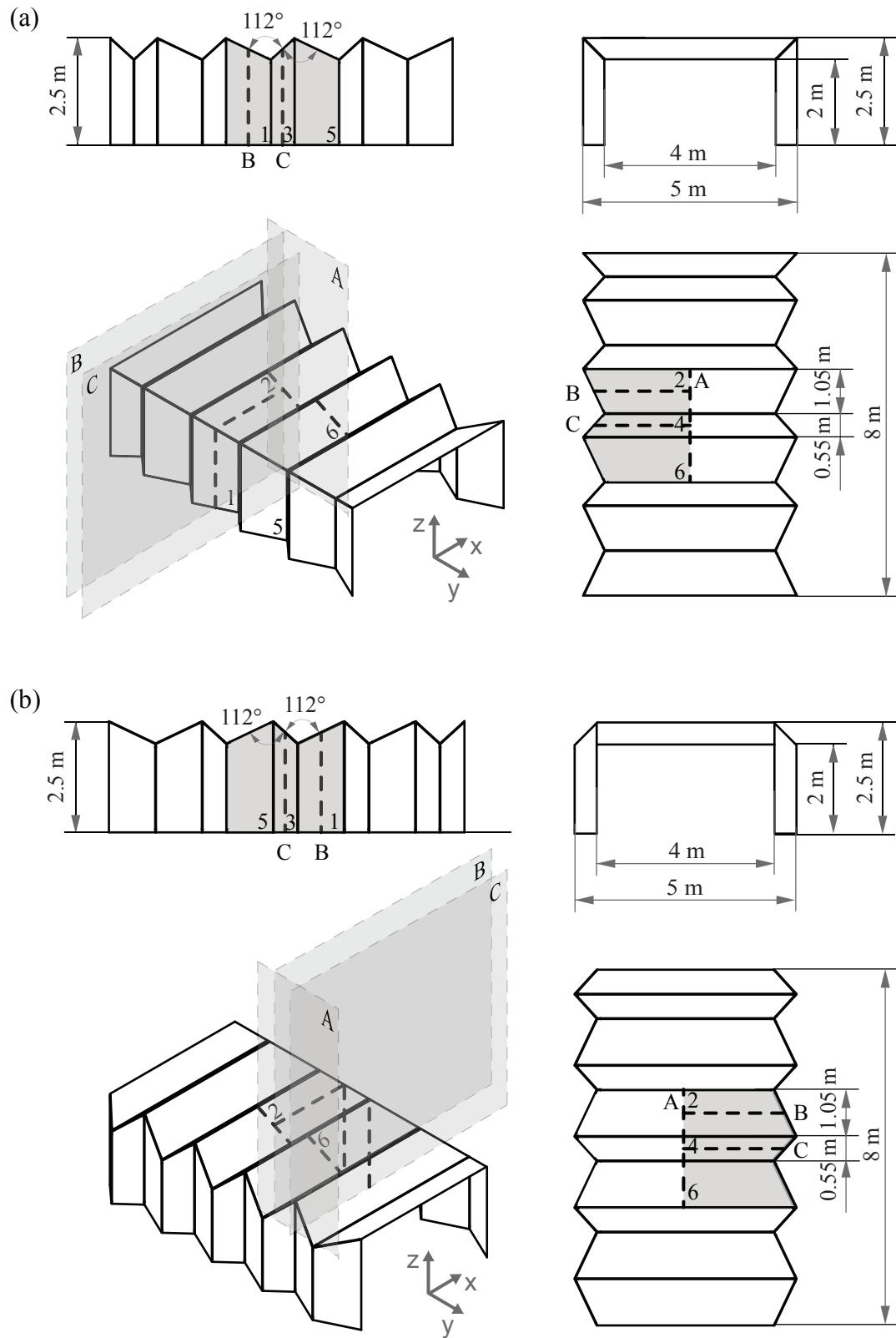


Figure 5.8 – Geometry of the FE model structures with marked section planes as well as the observed portion of the structure displayed in gray (area of interest).

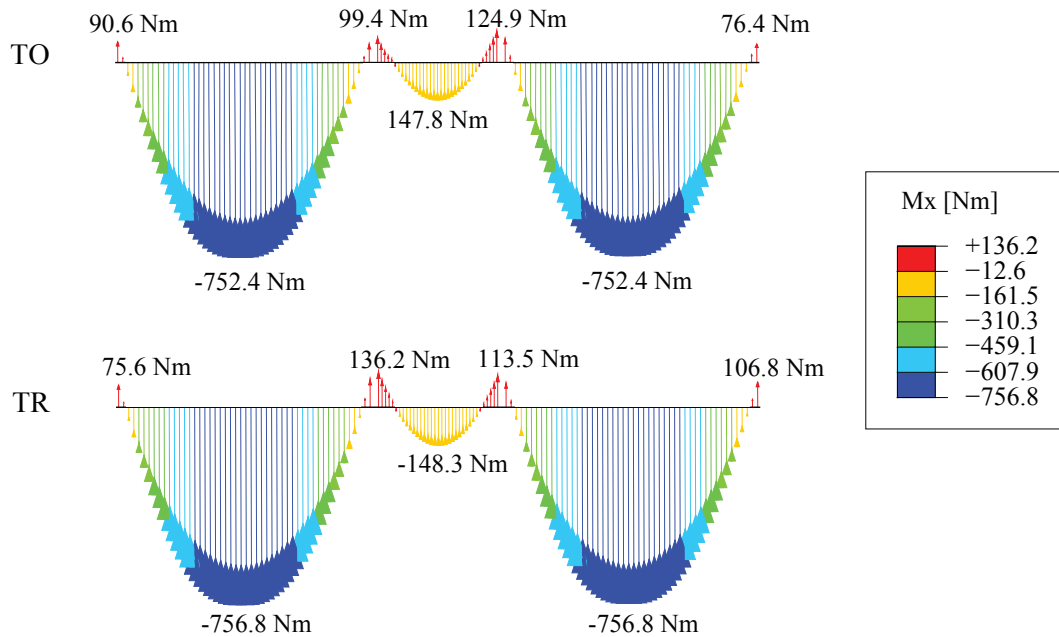


Figure 5.9 – Bending moment about local $-x$ axis of the plates, M_x , in the section defined by plane A, cutting through roof plates 2, 4 and 6 of the observed portion of the structure. TO bending moments are shown above and the TR structure bending moments below.

more relevant, even though the latter ones show to be of higher magnitude. This is given by the fact that the tensile strength of the KERTO-Q timber panel material is 33% lower than the compression one. Also, when looking at the experimental tests presented in Chapter 3, Section 3.5, it is noted that the failure of the MTSJ structures initiates from the equivalent corner position, due to tension exerted on the tabs of the MTSJ connection. Occurring twisting moments in the connections additionally enhance this effect, as moments of opposite sign develop on the connection edge opposite ends.

5.4 Correlating Foldability and Structural Behaviour

Examining the above presented results with regard to the corresponding form foldability and transformation path, a direct link can be established between the two. It is shown that the form transformation movement leads from the initial state, i , in which the structures were analysed, to the extreme states, either following a unique or multiple paths. However, when looking at the above presented foldability of the forms from a structural point of view, only one of their possible extreme states needs to be considered. Using a folded form in a static structure implies certain boundary conditions at the free edges, as well as specific load directions which can potentially actuate the transformation mechanism. The predominant load directions

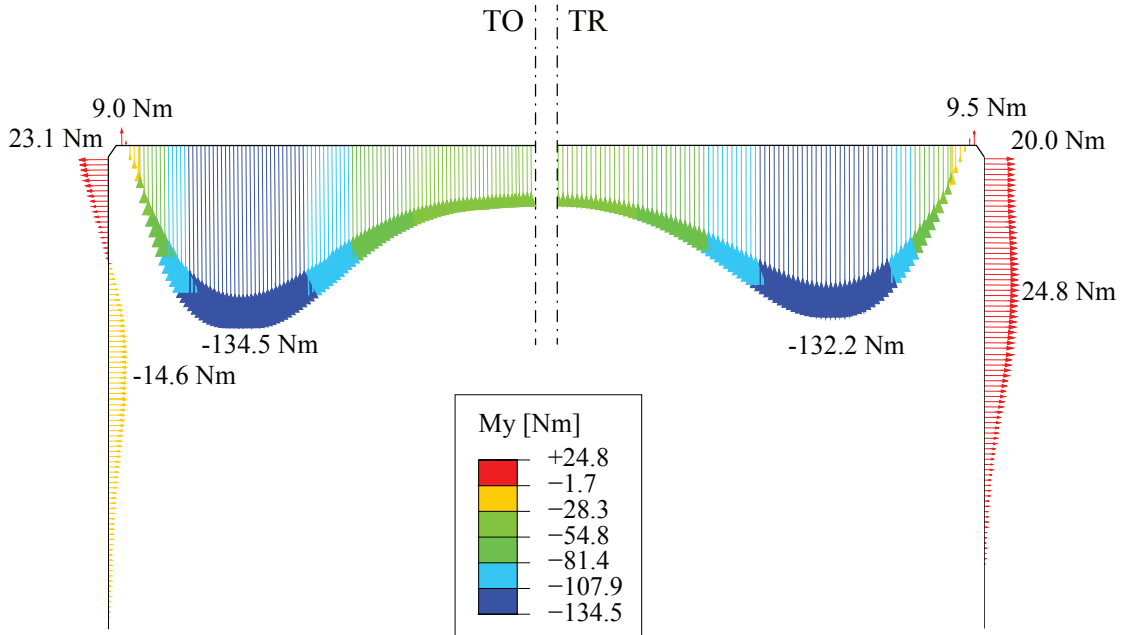


Figure 5.10 – Bending moment about local $-y$ axis of the plates, M_y , in the section defined by plane B, cutting through wall plate 1 and roof plate 2 of the observed portion of the structure. TO bending moments are shown on the left hand side and the TR structure bending moments are shown on the right hand side of the figure.

on civil structures are vertical and/or horizontal, which together with the supports in the presented structural forms allow only for the activation of a certain *folding* transformation. Thus, for examining the correlation between foldability and load bearing behaviour of the presented structural forms, the flat-folded states considered of relevance are: *TO*- state i_{f2} and *TR*- state i_f .

Both of the forms initial state transformation to the above mention states, occurs by rotation around the local $-x$ axis of the connections. During this rotation the more narrow roof and wall plates (number 3 and 4 within the area of interest, see Fig. 5.8) experience higher rotation. In *TO* structure the narrow plates rotate by 12° , while the more wide ones rotate by 6° , in *TR* structure these rotation amount to 48° and 14° , respectively. Such rotations in an unconstrained system cause simultaneous change in the position of vertices, enabling the transformation to the form's final flat-folded state. However, when in a constrained system such movement of wall plates is blocked by imposed boundary conditions, so instead of undergoing large displacements and rotations around its hinge edges, the imposed loads introduce stresses in the structure elements. At first, vertical surface loads acting on the roof plates cause out-of-plane bending. This is then transferred to the connections as bending around local $-x$ axis, as well as axial and shear forces, passing further onto the joining plates

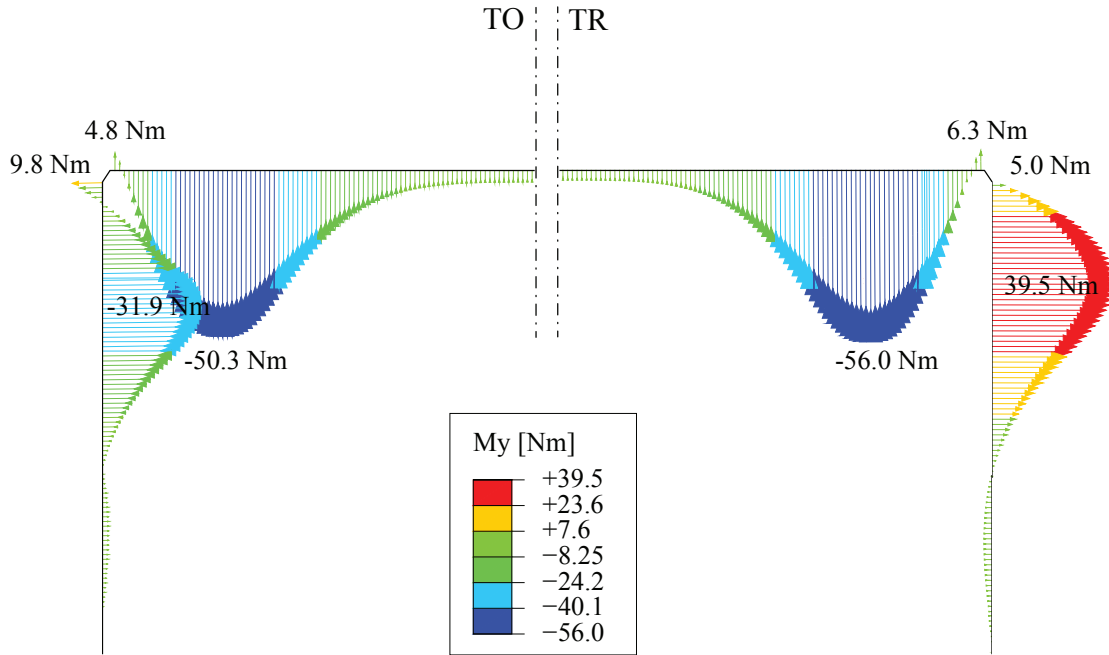


Figure 5.11 – Bending moment about local $-y$ axis of the plates, M_y , in the section defined by plane C, cutting through wall plate 3 and roof plate 4 of the observed portion of the structure. TO bending moments are shown on the left hand side and the TR structure bending moments are shown on the right hand side of the figure.

resolving into components lying in their respective planes.

Related to the previously mentioned difference in rotation of the structure's wide and narrow plates, when examining the sections defined by planes B and C, the same trend is also observed in the analysis results (see Fig. 5.13). Higher percentage change appears in section C which includes the larger rotation experiencing narrow plates, 3 and 4 (see Figs. 5.13 and 5.8).

Further comparing the results of all three sections, each form's distinct foldability range inherent kinematic mechanism clearly reflects on the static system structural behaviour, in the sense of distribution of its internal forces and percentage change shown in Fig. 5.13. Since the *TR* form folding transformation allows higher rotations around the connection local $-x$ axis, accordingly, higher M_x bending moments are exerted on the connections within a static system ($\xi = 11.6\%$, see Figs. 5.9 and 5.13). These are primarily caused by out-of-plane bending of the vertically loaded plates. Due to the compatibility in rotation mechanisms between the roof and wall plates, higher out-of-plane bending around the plate local $-y$ axis also appears in the *TR* structure. As a result of boundary conditions blocking the naked edges of wall plates, these higher M_y roof bending moment values further induce higher out-of-plane bending in the walls ($\xi = 7.3\%$ and $\xi = 23.8\%$, see Fig. 5.13), which therefore become more susceptible to buckling issues. Because such compatibility in rotation does not exist in the *TO* structure,

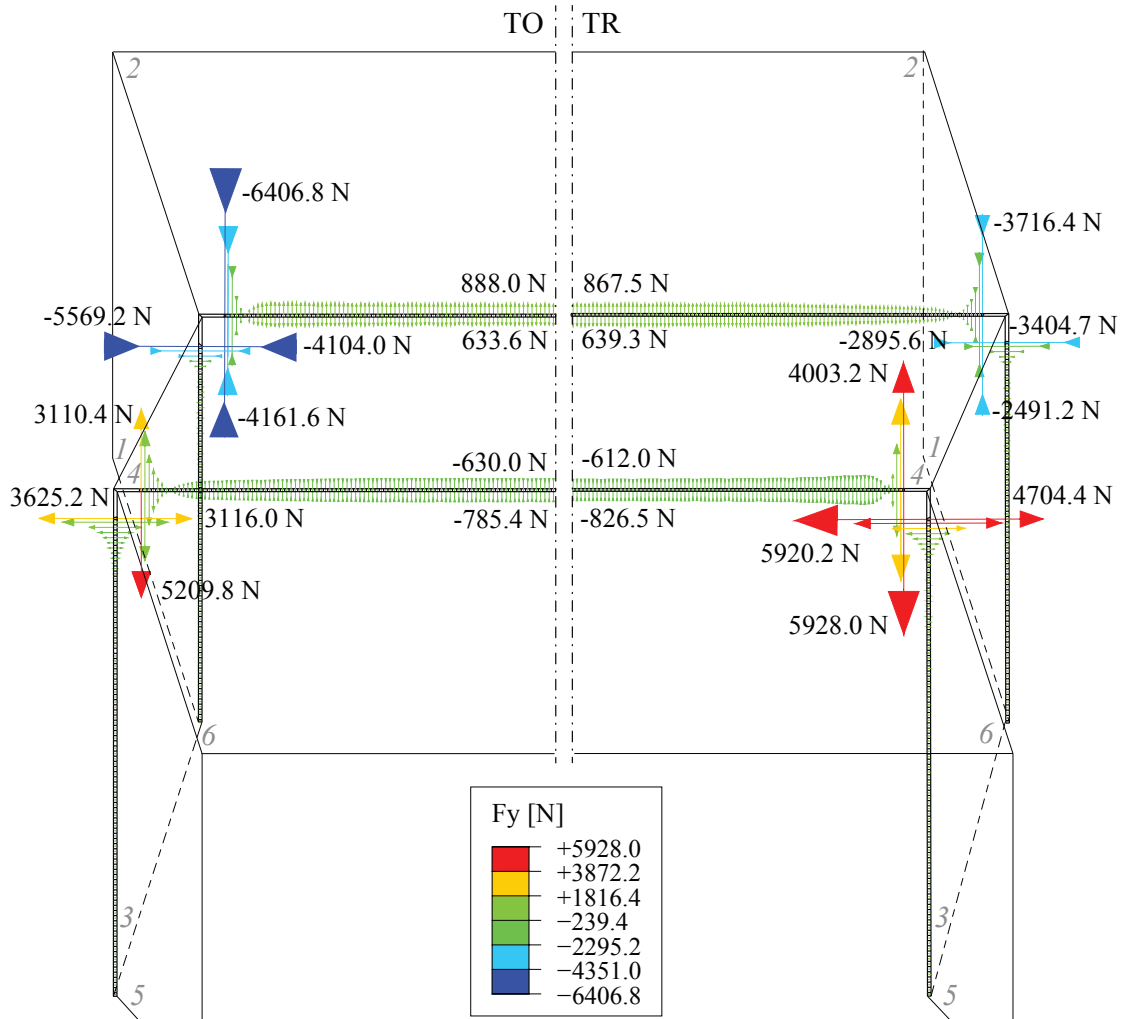


Figure 5.12 – In-plane compression (-) and tension (+) forces exerted on the connection representing strips, in local $-y$ axis of the plates. Strips are shown between wall plate pairs 1-3 and 3-5 as well as roof plate pairs 2-4 and 4-6. TO structure is shown on the left hand side and TR on the right hand side of the figure.

5.4. Correlating Foldability and Structural Behaviour

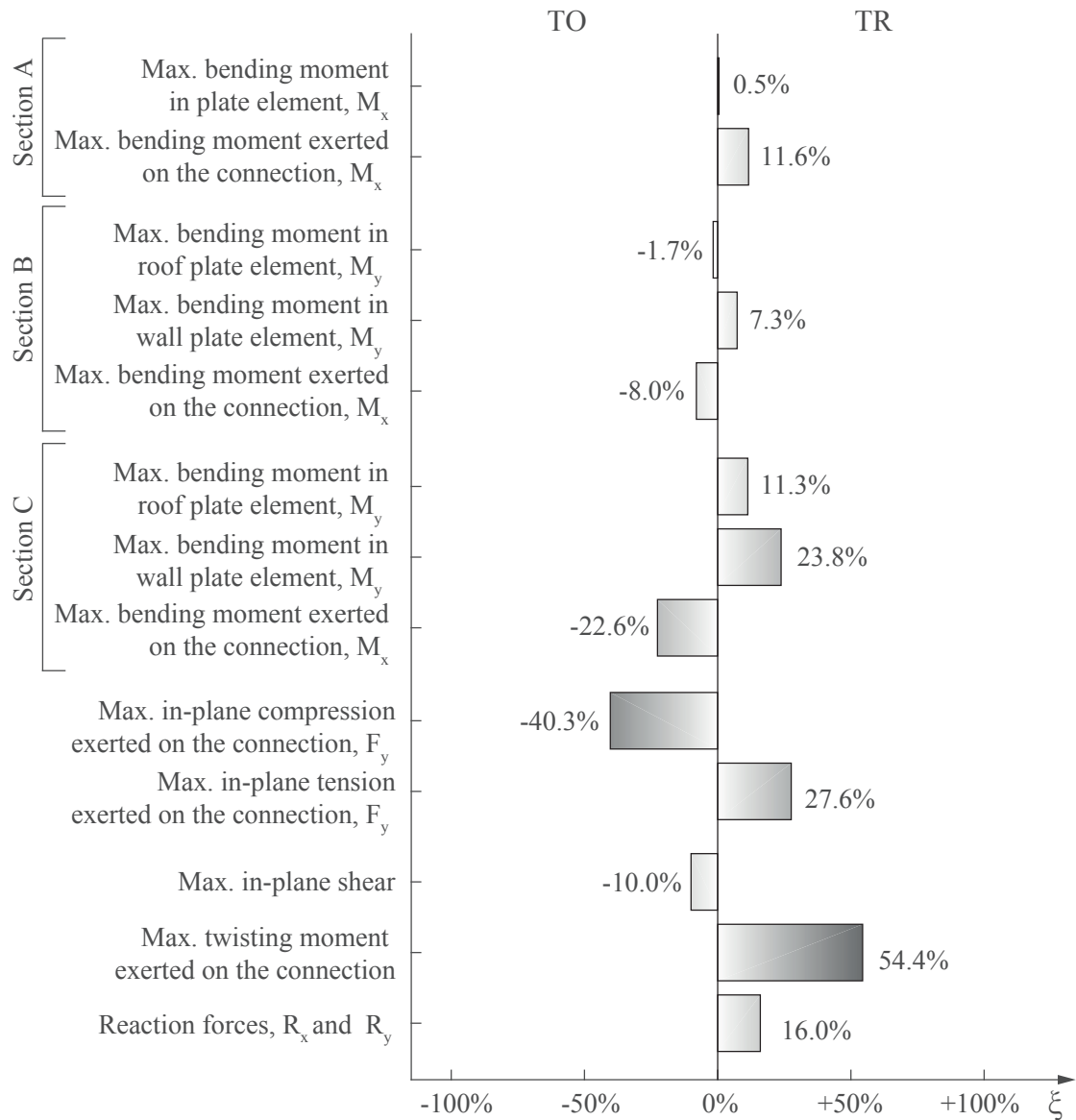


Figure 5.13 – Comparison of TO and TR structure results shown in Figs. 5.9, 5.10, 5.11 and 5.12, corresponding plane sections are marked on the left hand side. Percentage change is shown relative to the TO structure obtained values. In case of opposite sign bending moments in the corresponding elements of the two structures, absolute maximal values are considered for the comparison.

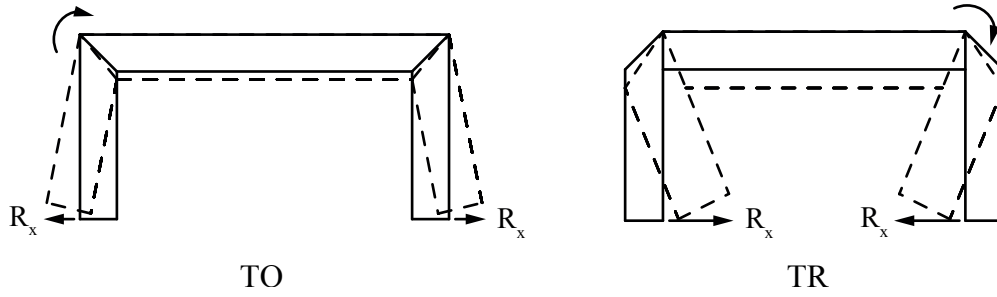


Figure 5.14 – TO and TR structure reaction force, R_x , pointing direction shown in respect of their flat-folded state form. The resulting rotation directions at the roof-wall interface regarding the corner details are also shown.

the occurring out-of-plane M_y bending of the plates exerts higher bending moments on the connections at the roof-wall interface ($\xi = -8\%$ and $\xi = -22.6\%$, see Figs. 5.10, 5.11 and 5.13). Additionally, as a consequence of the plates mutual blocking in the *TO* structure, the mentioned out-of-plane forces transfer to the neighbouring plates in a higher amount through in-plane shear ($\xi = -10.0\%$, see Fig. 5.13).

The final reaction forces directions clearly indicate the forms inclination towards its flat-folded state (see Fig. 5.14). They point inwards and are higher in the $-x$ as well as $-y$ axis for the *TR* structure ($\xi = 16.0\%$, see Fig. 5.13), while pointing outwards for the *TO* structure. The resulting rotation directions at the roof-wall interface are also shown in the same figure, causing the critical tension forces in the connections and the *opening* in the global $-y$ direction of the roof-mountain/wall-mountain corner in the *TR* structure, and *opening* in the global $-x$ and $-y$ direction of the roof-mountain/wall-valley corner in the *TR* structure (see Fig. 5.15). The opposite configuration of folds in both structures (roof-valley/wall-valley in *TO* and roof-valley/wall-mountain in *TR*) causes *closing* of all eight involved edges. This results in moments of opposite sign at the ends of roof-wall interface connections in the *TR* structure, causing the presented increase in twisting moments ($\xi = 54.4\%$, see Fig. 5.13).

Numerical FE analysis was also performed for the *Yoshimura* pattern form static structure as well as its DR modified version. The results obtained confirm the observations made regarding the comparison of *TO* and *TR* form structures. Most notably, higher M_x bending moments and in-plane tension exerted on the connections develop within the *Yoshimura* structure, $\xi = -34.0\%$ and $\xi = -62.5\%$, respectively. The values are shown corresponding to the previously presented analysis, as the percentage change relative to the *Yoshimura* structure. However, it is important to note that no direct correlation exists between the folding form range and structural behaviour of different types of structures. Therefore, it seems that the folding range capacity can only be used for comparison of structures which present variations

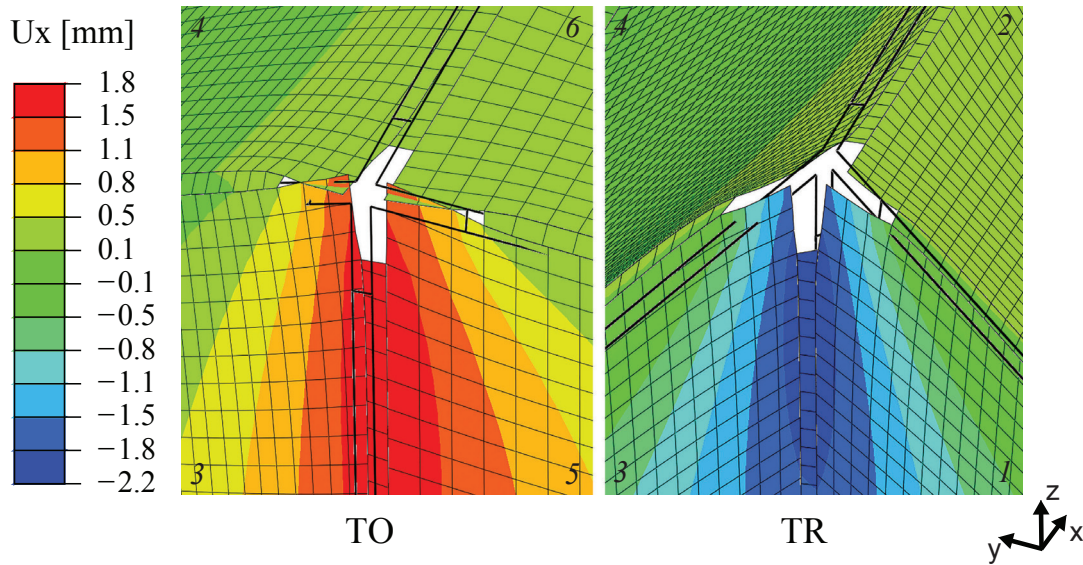


Figure 5.15 – Roof-wall plate interface detail displacement in the global $-x$ axis direction. TO structure roof-mountain/wall-mountain corner (left) and TR structure roof-mountain/wall-valley corner (right). Both structures displacement contour plot is scaled by an equal factor of 20 to enhance the occurring edge opening and closing.

of the same initial pattern, e.g. *St. Loup Chapel* versus *TO* versus *TR* form, or *Yoshimura* versus the *Yoshimura* DR form.

5.5 Conclusions

In this Chapter, the relation is established between the form foldability range and the load carrying behaviour of a static folded surface structure using that same form. Based on the performed FE analysis results and observations regarding folding transformation path of the five considered structure forms, the derived conclusions are as follows:

- When using folded forms within static folded surface systems only one of their flat-folded extreme states appears to be relevant. The unfolding transformation towards the developed state seems to have no consequence on the load bearing behaviour of the folded structure;
- The amount of internal forces occurring in the panels as well as those exerted on the connections of the structures with the same topological properties, correspond well to the folding transformation movement trend of the used form. In an unconstrained folded system, the positions where the plate rotations are high coincide with the positions of highest bending moments in a static constrained system. Moreover, higher in-plane

shear forces develop in constrained systems where the corresponding unconstrained system shows small plate rotations. Also, reactions which develop in the supports follow the direction of the relevant movement which occurs during folding;

- The results suggest that when designing timber folded surface structures, foldability of the form should be considered in addition to previously mentioned geometric conditions arising from material, fabrication and connection details requirements (presented in Chapter 2). This would allow for a more efficient use of extensional action of plate members, reducing the overall requirements imposed on connection details. With respect to the findings presented in Chapter 3, where three differently joined structure types (adhesively joined, MTSJ open and closed slot) were tested, the connection details strength properties indicate to have crucial importance in affecting the feasibility of the entire timber folded surface system;
- Using the dynamic relaxation (DR) for obtaining variations of regular bidirectional forms shows to be a viable method for reducing the foldability range, having further significant positive influence concerning the load bearing behaviour when such forms are applied in static folded systems;
- Even though fairly clear for simple forms, where changing from reverse to regular folding has an influence on the structural behaviour which is perhaps intuitive, for more complex forms consisting of a large number of plates, recognising the available global and/or local kinematic modes and relating them to structural behaviour under load is certainly not as straightforward. Therefore, examining the form foldability range and its transformation path toward the relevant flat-folded state in the structural design stage of folded surface structures, seems to be a feasible way to assess various design variations of a topologically consistent surface folded form. In this way more structurally efficient folded structures could be obtained with minimal form intervention.

6 Conclusion and Outlook

6.1 Conclusions

Within this thesis, several studies have been presented in relation to the main purpose of facilitating the realization of timber folded surface structures on a building scale. Undertaken investigations straddle both the architectural and structural engineering domain, in order to answer the questions regarding geometry, structural behaviour, modelling and optimization of multiple tab-and-slot connected timber folded systems.

In the first investigation, presented in Chapter 2, such interdisciplinary approach permitted to integrate the conditions of construction into the initial design, by formulating geometries directly applicable for the regarded structural use. Setting the relation between the structural form and constraints imposed by the material, feasible connection details as well as fabrication, allowed for their implementation into the design from the very start. This has been shown to be of high importance for the regarded structures as the mentioned constraints significantly limit the viable forms. Furthermore, the construction of the first MTSJ prototype structure provided valuable initial experience concerning the used fabrication methods and the assembly process. It demonstrated that folded surface structures in combination with structural advantages of timber panels are able to form very lightweight systems with high structural potential.

This finding was the motivation for instigating the next research stage, concerning experimental investigations of relevant scale timber folded surface structures, presented in Chapter 3. For this purpose an innovative test setup was devised for simulating uniformly distributed load onto surface active structures. The main novelty of the proposed pulley based setup consists of the possibility to apply simultaneous, continuous loading to discrete plates while compensating for their differential displacements. This further allowed for carrying out the first reliable, in-depth experimental analysis of timber folded surface structures. Additionally, the influence

of the connection detail type on the global behaviour of the folded system was studied for the first time in the context of MTSJ timber folded surface structures. The performed study gave valuable insight into the global system load bearing and failure mechanisms as well as connection local failure modes. For all tested structure types, the results show that the serviceability limit state (SLS) would be the one to govern the design of timber folded surface structures. When reaching the maximal SLS prescribed displacement, all the structures stay well within their elastic stage, by exhibiting high reserve of load bearing capacity. By further application of load, regardless of the detail type, all tested structures failed by exceeding the connection detail load bearing capacity. Tension perpendicular to the grain orientation and bending around the edges were found to be the most crucial loading cases. According to the obtained results, closed slot MTSJ structures were found to be the most advantageous concerning their ultimate load-bearing capacity and connection provided ductility. On the other hand, MTSJ open slot structures were found to be unreliable for the tested purpose, while the most stiff adhesively bonded structures showed numerous significant disadvantages concerning their potential on-site application. The large variation in the elastic range stiffness obtained from structures with different connection details, primarily demonstrated the importance of taking into consideration the exact behaviour of semi-rigid connections when evaluating timber folded surface systems for structural application.

Within this scope, in Chapter 4 a pertinent FE model for predicting the structural behaviour of integrally attached timber folded surface structures is provided. In this model the semi-rigid behaviour of the closed slot MTSJ connections is simulated. Between the two presented modelling techniques, using strip and spring elements, the strip element model indicated slightly better agreement with the experimentally obtained values. The results suggested that both linear and nonlinear analysis can be used for modelling the displacements within the structures' elastic range. However, it is essential to include geometric nonlinearities in the analysis for accurate modelling of occurring strains as well as displacements when considering higher load levels. Furthermore, the level of closed slot MTSJ semi-rigidity was established by comparing its results to the adhesively bonded systems, typically considered rigid when performing simplified structural analysis. Both experimentally and numerically obtained results were considered in this comparison, where the adhesively joined connections were modelled as completely rigid. The results suggest that structures built using any of the above considered connection types, including the adhesively joined ones, show a significantly lower stiffness when compared to the fully rigid ones. This leads to the conclusion that numerical models including the connection semi-rigidity, such as the one presented in this thesis, are necessary for appropriately analysing the structural response of timber folded surface structures.

The final investigation presented in Chapter 5 aimed to establish a correlation between the surface form foldability potential and the structural capacity of a static folded system. For this purpose the concepts of rigid foldability and foldability range were used together with methods for their evaluation adopted from the domain of origami folding and deployable structures. The study was performed on a set of comparable structures and it included the analysis of their forms' available kinematic mechanisms as well as their structural behaviour, by using previously validated numerical models. The results show that the amount of internal forces occurring in the panels, as well as those exerted on the connections of the structures with the same topological properties, correspond well to the folding transformation movement trend of the respective form. Forms with larger foldability range, notably towards the relevant flat-folded direction, exhibit higher critical tension and bending forces exerted on the connections, when used in a static system. Within this investigation, an application of the dynamic relaxation (DR) method was proposed for obtaining reduced foldability range of more complex forms, consisting of a large number of faces. Such newly obtained forms have shown to have a significant positive influence concerning the load bearing behaviour when applied in static folded systems. Additional benefit of using the DR method is recognised in the possibility of automatic inclusion of various MTSJ timber surface structures related constraints into the form finding process. Finally, it is recommended that when designing timber folded surface structures, foldability of the form should be considered in addition to previously mentioned geometric constraints arising from material, fabrication and connection details requirements. Preferably, all of these constraints should be included within a single design process, reducing the need for subsequent modifications.

In conclusion, a great structural potential is recognized in the proposed timber folded plate systems and the points discussed within this thesis have shown to be of significant influence in establishing these structures on a building scale. The validity of the presented research and its outcomes are further endorsed by the realization of the first MTSJ timber folded surface construction. During the writing of this thesis a double layer timber folded structure with closed slot multiple-tab-and-slot joints has been realized for the first time in large scale [34, 70] (see Fig. 6.1). The new adjunct building to the theater of *Vidy* in Lausanne features a doubly curved design with a roof spanning 21 m. By using two-level structural hierarchy in form of a double layer system together with bidirectional curvature introducing a three-dimensional load carrying behaviour, a structural system with enhanced robustness was obtained. The realisation of the project has been made possible through the application of same computational tools as used in the presented experimental investigations within this thesis (see Chapter 3, Section 3.2). Its construction process confirmed many advantages of using MTSJ timber folded structures presented within this thesis. The high level of prefabrication allowed for the entire



Figure 6.1 – Vidy Theater Pavilion, Lausanne, Switzerland [54]; (above) exterior view of the structure with a visible doubly curved form; (below left) the interior view with the featured closed slot MTSJ roof details; and (below right) the on-site assembly of the prefabricated roof segment.

wall and roof modules to be pre-assembled at the factory and delivered ready-made to the site (the entire structure consists of 22 wall and 11 roof segments). This considerably reduced the on-site construction process. Additionally, the manufacturing time was minimized by automated generation of the individual plate geometries with integrated MTSJs as well as the CNC machine G-code required for fabrication, making the entire project very time and cost-effective.

6.2 Outlook

Findings of this thesis provide a solid foundation for future works in the field of timber folded surface structures. From the above presented Vidy Theater project it can be seen that this research field has a large potential for prospective developments. Moreover, some of the results of this thesis have been applied within other structural contexts employing integral attachments too, opening new perspectives for future applications.

Several investigations following the research line presented in this thesis are currently ongoing within the Timber Construction Laboratory, IBOIS.

A doctoral research projectⁱ conducted by A.C. Nguyen, initiated in 2016, focuses on the application of the presented simplified numerical FE model to a newly developed construction system (more specifically, plate-shell structures built from two interconnected layers of structural wood veneer plates mutually assembled using closed slot MTSJ, both within each layer and at the interlayer). A complimentary research focusing on plate-shell systems, was initiated in 2016 as well, and is conducted by A.R. Rad. This research proposes an alternative, macro-element modelling approach for the numerical analysis of MTSJ timber plate-shell structures. For validating both of the above mentioned studies, extensive experimental testing will be necessary. For this purpose, the principles of the test setup developed in this thesis, will provide a solid base available for further customization.

Moreover, an integral part of an ongoing research conducted by S. Roche consists in establishing an analytical relation between the individual tab-and-slot connection bending moment resistance and the bending capacity of a plate edge including n number of tabs and slots. Additionally, reliable shear and tension load capacity should be established as well. Also, the influence of the timber panel material properties, varying MTSJ geometrical parameters as well as fabrication caused corner notch sizes and positions should be determined for all three critical load cases (bending, shear and tension). Continuing on the work of S. Roche and G. Mattoni, a detailed numerical 3D solid model of the MTSJ connections should be further developed and refined for this purpose. A simplified numerical analysis could then be performed on a global structure, as proposed within this thesis, where the obtained critical force values exerted on the connections could be further checked analytically against the connection resistance. This would allow for a reliable verification of the connection utilization, i.e. the percentage of use of the maximum resistance capacity, applied to any type of structural system. Also, in this way a precise connection design could be offered depending on the global requirements imposed by the structural system.

ⁱSupported by the National Centre of Competence in Research (NCCR) Digital Fabrication, funded by the Swiss National Science Foundation (NCCR Digital Fabrication Agreement #51NF40 – 141853)

Chapter 6. Conclusion and Outlook

The herein proposed numerical models have been developed but are not restricted to MTSJ timber folded surface structures, they can also be used for modelling different types of structural forms using MTSJ connections, such as plate-shell structures mentioned above. The necessary modifications regarding the used timber panel material as well as the respective connection detail resistance, could be easily integrated into the existing model.

Additionally, the methods applied to design variations of timber folded surface structures forms could be used regardless of the applied material. Even though in timber engineering the gained benefits are highly emphasized due to material characteristics and available techniques for edgewise joining of thin timber panels, reducing the actions applied on the connection details would be highly desirable for folded structures realized in any other structural material as well.

Bibliography

- [1] RhinoCommon SDK for Rhino. <https://github.com/mcneel/rhinocommon>. Accessed: 05-01-2017.
- [2] Unesco paris headquarters, the construction of the second building. <http://www.unesco.org/new/en/unesco/about-us/who-we-are/history/paris-headquarters/>, 1953. Accessed: 12-06-2017.
- [3] Saint john's abbey university church. <http://www.saintjohnsabbey.org/your-visit/abbey-church/>, 1961. Accessed: 12-06-2017.
- [4] ISO 6891:1983, Timber structures – Joints made with mechanical fasteners – General principles for the determination of strength and deformation characteristics, 1983.
- [5] Rigid-foldable gallery. <https://www.flickr.com/photos/tactom/sets/72157621419726061/with/4115805515/>, 2009. Accessed: 12-02-2017.
- [6] Abaqus documentation v6.12. <http://abaqus.software.polimi.it/v6.12/index.html>, 2012. Accessed: 05-01-2017.
- [7] The creation of the eternal miami marine stadium. <https://miami.curbed.com/2013/12/9/10169544/marine-stadium-marvin-aguilar>, 2013. Accessed: 12-026-2017.
- [8] Strain gauges technical data sheet,tml pam e-1007b. <http://www.tml.jp/e/download/catalogdownload.html>, 2016. Accessed: 02-04-2017.
- [9] Vic-3d 7 manual. <http://www.correlatedsolutions.com/supportcontent/Vic-3D-v7-Manual.pdf>, 2016. Accessed: 12-02-2017.
- [10] S. Adriaenssens and et al. *Shell Structures for Architecture*, chapter Dynamic Relaxation: design of a strained timber gridshell, pages 89–101. Routledge, 2014.
- [11] A. Asiz and I. Smith. New generation of timber design practices and code provisions linking system and connection design. In H. J. Larsen and J. Munch-Andersen, editors,

Bibliography

- CIB-W18 Timber Structures, A review of meetings 1-43, Part 2:Material properties*, pages 53–54, 2011.
- [12] A. Bagger. *Plate shell structures of glass: Studies leading to guidelines for structural design*. PhD thesis, DTU Civil Engineering, Technical University of Denmark, 2010.
- [13] C. C. Baniotopoulos and F. Wald, editors. *The Paramount Role of Joints into the Reliable Response of Structures: From the Classic Pinned and Rigid Joints to the Notion of Semi-rigidity*, volume 4 of *NATO Science Series II: Mathematics, Physics and Chemistry*. Springer Netherlands, 2000.
- [14] M. Bechthold. *Innovative Surface Structures: Technology and Applications*. Taylor and Francis, 2008.
- [15] B. S. Benjamin and Z.S. Makowski. The analysis of folded-plate structures in plastics. In *Plastics in building structures*, pages 149–163, London, June 1965. The Plastics Institute, Pergamon Press.
- [16] J. Bodig and B.A. Jayne. *Mechanics of wood and wood composites*. Van Nostrand Reinhold, New York, 1982.
- [17] M. Botsch and et al. *Polygon Mesh Processing*. AK Peters, 2010.
- [18] H. Buri. *Origami - Folded Plate Structures*. PhD thesis, Ecole Polytechnique Federale de Lausanne, 2010.
- [19] R. Chudoba and et al. Oricrete: Modeling support for design and manufacturing of folded concrete structures. *Advances in Engineering Software*, 4:119–127, 2013.
- [20] Collano AG. Semparoc Rapid V- technical sheet, 2015. https://www.collano.com/downloads/datenblaetter/fr/semparoc_rapid_v_fr.pdf. Accessed: 20-01-2017.
- [21] M. Dedijer, S. Roche, and Y. Weinand. Shear resistance and failure modes of edgewise multiple tab-and-slot joint (mts) connection with dovetail design for thin lvl spruce plywood kerto-q panels. In J. Eberhardsteiner, W. Winter, A. Fadaei, and M. Poll, editors, *Proceedings of the World Conference of Timber Engineering*, pages 1516–1523. TU Verlag, 2016.
- [22] S. Pellegrino (Ed.). *Deployable structures*. volume 412 of *CISM International Centre for Mechanical Sciences*. Springer Vienna, first edition, 2001.
- [23] G. Ehlers. Ein neues konstruktionsprinzip. *Bauingenieur*, 9, 1930.
- [24] H. Engel. *Structure Systems*. Verlag Gerd Hatje, Stuttgart, 2nd edition, 1977.

-
- [25] I. Engel. *Structural Principles*. Prentice Hall, 1984.
- [26] J. N. Richardson et al. Coupled form-finding and grid optimization approach for single layer grid shells. *Engineering Structures*, 52:230–239, 2013.
- [27] European Committee for Standardization, Brussels. *EN 1995-1-1, Eurocode 5: design of timber structures - part 1-1: general-common rules and rules for buildings*, 2004.
- [28] A. Falk and P. von Buelow. Form exploration of folded plate timber structures based on performance criteria. In D. Nethercot and S. Pellegrino, editors, *Taller, Longer, Lighter: Meeting growing demand with limited resources; Proceedings of the 35th Annual Symposium of IABSE and the 52nd Annual Symposium of IASS*, London, September 2011.
- [29] M. Farshad. *Design and Analysis of Shell Structures*, volume 16. Kluwer Academic Publishers, 1992.
- [30] J. S. Foster and R. Greeno. *Structure and fabric*. Harlow: Pearson Prentice Hall, 2007.
- [31] S. G. Foster and S. Krishnakumar. A class of transportable demountable structures. *International Journal of Space Structures*, 2(3):129–137, 1987.
- [32] C. R. Frihart and C. G. Hunt. *Wood Handbook, Wood as an Engineering Material. General Technical Report FPL-GTR-190. Centennial Edition*, chapter Adhesives with Wood Materials, Bond Formation and Performance. U.S. Department of Agriculture, Forest Service, Forest Products Laboratory, 2010.
- [33] P. Frostick. Antiprism based form possibilities for folded surface structures. *Architectural science review*, 21(3):59 – 67, 1978.
- [34] J. Gamero, C. Robeller, P.-O. Coanon, and Y. Weinand. Rotational mechanical behavior of wood-wood connections with application to double-layered folded timber plate structure. 2017. manuscript submitted for publication.
- [35] C. J. Gantes. *Deployable Structures: Analysis and design*. WIT Press, 2001.
- [36] F. Gioia and et al. Design and analysis of a foldable/unfoldable corrugated architectural curved envelop. *ASME Journal of Mechanical Design*, 134(3):031003–11, 2012.
- [37] E. Gruber. Berechnung prismatischer scheibenwerke. In *IABSE publications = Mémoires AIPC = IVBH Abhandlungen*, volume 1, pages 225–241, 1932.
- [38] S. D. Guest. *Deployable Structures: Concepts and Analysis*. PhD thesis, University of Cambridge, 1994.

Bibliography

- [39] S. D. Guest and S. Pellegrino. The folding of triangulated cylinders, part i: Geometric considerations. *ASME Journal of Applied Mechanics*, 61:773–777, 1994.
- [40] P. Haller, editor. *COST C1: Semi-Rigid Timber Joints- Structural Behaviour, Modelling and New Technologies*, Semi-Rigid Behaviour of Connections in Civil Engineering. COST, European Cooperation in the field of Scientific and Technical Reserach, 1992-1999.
- [41] H.G. Harris and G.M. Sabnis. *Structural modelling and experimental techniques*. CRC Press, 2nd edition, 1999.
- [42] H. Hosdorf. *Model analysis of structures*. Van Nostrand Reinhold Company Ltd., 1974.
- [43] P. Huybers. *See-through structuring. A method of construction for large span plastic roofs*. PhD thesis, TU Delft, 1972.
- [44] J. S. B. Iffland. Folded plate structures. *Journal of the structural division, ASCE*, 105(ST1):111–123, 1979.
- [45] M. Irle and M. C. Barbu. Wood-based panel technology. In H. Thoemen, M. Irle, and M. Sernek, editors, *Wood-Based Panels: An Introduction for Specialists*, pages 1–90. Brunel University Press, 2010.
- [46] S. Jaksch and V. Sedlak. A foldable umbrella structure- developments and experiences. *International Journal of Space Structures*, 26(1):1 – 18, 2011.
- [47] L. Jian-Min and J-Knippers. Segmental timber plate shell for the landesgartenschau exhibition hall in schwäbisch gmünd—the application of finger joints in plate structures. *International Journal of Space Structures*, 30(2):123–140, 2015.
- [48] A. Jorissen and M. Fragiaco. General notes on ductility in timber structures. *Engineering Structures*, 33(11):2987–2997, 2011.
- [49] M. Ketchum. What happened to shells? <http://www.ketchum.org/-milo/what.html>. Accessed: 07-06-2017.
- [50] A. Killian and J. Ochsendorf. Particle-spring systems for structural form finding. *Journal of the International Association for Shell and Spatial Structures (IASS)*, 46(147), 2005.
- [51] P. H. Kirkegaard, J. D. Sorensen, D. Cizmar, and V. Rajcic. System reliability of timber structures with ductile behaviour. *Engineering Structures*, 33(11):3093–3098, 2011.
- [52] J. Knippers and et al. From nature to fabrication: Biomimetic design principles for the production of complex spatial structures. In L. Hesselgren, S. Sharma, J. Wallner,

- N. Baldassini, P. Bompas, and J. Raynaud, editors, *Advances in Architectural Geometry 2012*. Springer Verlag, 2013.
- [53] L. Kollar. Some problems of static analysis of folded plate structures. *Periodica Polytechnica ser. civil eng.*, 37(3):167–202, 1993.
- [54] I. Kramer. Vidy theatre Lausanne. <http://vidy.ch/exposition-un-nouveau-pavillon-en-bois>, 2017. Accessed: 04-08-2017.
- [55] R. la Magna et al. From nature to fabrication: Biomimetic design principles for the production of complex spatial structures. *International Journal of Spatial Structures*, 28(01):27–40, 2013.
- [56] A. Lebee. From folds to structures, a review. *International Journal of Space Structures*, 30(2):55–74, 2015.
- [57] K. Leitner. *Tragkonstruktion aus plattenförmigen Holzwerkstoffen mit der TEXTILEN FUGE*. PhD thesis, RWTH Aachen University, 2014.
- [58] S. Marinitsch, C. Schranz, and M. Teich. Folded plate structures made of glass laminates: a proposal for the structural assessment. *Glass Structures & Engineering*, 1(2):451–460, 2016.
- [59] G. Mattoni. Design and analysis of woodworking joints for structural timber panels. Master’s thesis, Ecole Nationale des Ponts et Chaussées and Ecole Polytechnique Fédérale de Lausanne, 2014.
- [60] K. Miura. Proposition of pseudo-cylindrical concave polyhedral shells. Report 442, Institute of Space and Aeronautical Science, University of Tokyo, 1969.
- [61] K. Miura. Concepts of deployable space structures. *International Journal of Space Structures*, 8(1 and 2):3–16, 1993.
- [62] K. Miura. The science of miura-ori: A review. In R. J. Lang, editor, *Origami 4, Fourth International Meeting of Origami Science, Mathematics, and Education*, pages 97–99. A K Peters, 2009.
- [63] F. Moussavi. *The function of form*. Actar and Harvard University Graduate School of Design, 2009.
- [64] Task Committee on Folded Plate Construction. Phase i report on folded plate construction. *Journal of the Structural Division, ASCE*, 89(ST6):365–406, December 1963.

Bibliography

- [65] E. Onate. *Structural Analysis with the Finite Element Method. Linear Statics*, volume 2. Beams, plates and shells of *Lecture Notes on Numerical Methods in Engineering and Sciences*. Springer, first edition, 2013.
- [66] D. Piker. Kangaroo Physics. <http://www.food4rhino.com/app/kangaroo-physics>. Accessed: 07-04-2016.
- [67] E. Pizzi. *Renzo Piano*. Birkhauser, 2003.
- [68] C. Robeller. *Integral Mechanical Attachment for Timber Folded Plate Structures*. PhD thesis, Ecole Polytechnique Federale de Lausanne, 2015.
- [69] C. Robeller and et al. A double-layered timber plate shell computational methods for assembly, prefabrication, and structural design. In S. Adriaenssens, F. Gramazio, M. Kohler, A. Menges, and M. Pauly, editors, *Advances in Architectural Geometry 2016*, Advances in Architectural Geometry, pages 104–122. vdf Hochschulverlag AG, 2016.
- [70] C. Robeller, J. Gamero, and Y. Weinand. Theatre vidy lausanne – a double-layered timber folded plate structure. 2017. manuscript submitted for publication.
- [71] C. Robeller, S. Nabaei, and Y. Weinand. Design and fabrication of robot-manufactured joints for a curved-folded thin-shell structure made from clt. *Robotic Fabrication in Architecture, Art and Design*, pages 67–81, 2014.
- [72] C. Robeller, A. Stitic, P. Mayencourt, and Y. Weinand. Interlocking folded plate - integrated mechanical attachment for structural timber panels. In P. Block, J. Knippers, N. J. Mitra, and W. Wang, editors, *Advances in Architectural Geometry 2014*, volume 4 of *Advances in Architectural Geometry*, pages 281–294. Springer Verlag, 2014.
- [73] C. Robeller and Y. Weinand. A 3d cutting method for integral 1dof multiple-tab-and-slot joints for timber plates, using 5-axis cnc cutting technology. In J. Eberhardsteiner, W. Winter, A. Fadaei, and M. Poll, editors, *Proceedings of the World Conference of Timber Engineering*, pages 2576–2584. TU Verlag, 2016.
- [74] S. Roche, J. Gamero, and Y. Weinand. Multiple tab-and-slot joint: improvement of the rotational stiffness for the connection of thin structural wood panels. In J. Eberhardsteiner, W. Winter, A. Fadaei, and M. Poll, editors, *Proceedings of the World Conference of Timber Engineering*, pages 1556–1564. TU Verlag, 2016.
- [75] S. Roche, G. Mattoni, and Y. Weinand. Rotational stiffness at ridges of timber folded-plate structures. *International Journal of Space Structures*, 30(2):153–167, 2015.

- [76] S. Roche, C. Robeller, H. Laurent, and Y. Weinand. On the semi-rigidity of dovetail joint for the joinery of lvl panels. *European Journal of Wood and Wood Products*, 73(5):667–675, 2015.
- [77] M. Schenk. *Folded Shell Structures*. PhD thesis, University of Cambridge, 2011.
- [78] V. Sedlak. Folded surface structures. *Architectural science review*, 21(3):58–59, 1978.
- [79] C. Siegel. *Strukturformen der modernen Architektur*. Georg D.W. Callwey, Munchen, 1960.
- [80] M. Simek and V. Sebera. Traditional furniture joinery from the point of view of advanced technologies. In *Proceedings of the International Convention of Society of Wood Science and Technology and United Nations Economic Commission for Europe, Geneva, Switzerland*, 2010.
- [81] S. W. Smith. *The Scientist and Engineer's Guide to Digital Signal Processing*. California Technical Publishing, San Diego, California, second edition, 1999.
- [82] B. Specht. System überzeugt - investition in den holzbau. In *Proceedings of the 18th International Timber Construction Forum*, Garmisch Partenkirchen, Germany, 2013.
- [83] H. Stehling, F. Scheurer, and J. Roulier. Bridging the gap from cad to cam: concepts, caveats and a new grasshopper plug-in. In *Proceedings of the FABRICATE conference*, Zurich, 2014.
- [84] M.A. Sutton, J.J. Orteu, and H.W. Schreier. *Image correlation for shape, motion and deformation measurements*. Springer, 2010.
- [85] T. Tachi. Generalization of rigid foldable quadrilateral mesh origami. In A. Domingo and C. Lazaro, editors, *International Association for Shell and Spatial Structures: Proceedings of the IASS Symposium on Evolution and Trends in Design, Analysis and Construction of Shell and Spatial Structures*, Valencia, 2009.
- [86] T. Tachi. Freeform origami. <http://www.tsg.ne.jp/TT/software/>, 2013.
- [87] N. De Temmerman. *Deployable folded plate structures – folding patterns based on 4-fold-mechanism using stiff plates*. PhD thesis, Vrije Universiteit Brussel, 2007.
- [88] S. Timoshenko and S. Woinowsky Krieger. *Theory of plates and shells*. McGraw-Hill Book Company, 1959.
- [89] O. L. Tonon. Geometry of spatial folded forms. *International Journal of Space Structures*, 6(3):227–240, 1991.

Bibliography

- [90] M. Trautz and R. Herkrath. The application of folded plate principles on spatial structures with regular, irregular and free-form geometries. In A. Domingo and C. Lazaro, editors, *International Association for Shell and Spatial Structures: Proceedings of the IASS Symposium on Evolution and Trends in Design, Analysis and Construction of Shell and Spatial Structures*, Valencia, 2009.
- [91] S. Trometer and M. Krupna. Development and design of glass folded plate structures. *Journal of the International Association for Shell Structures and Spatial Structures IASS*, 47(3):253–260, 2006.
- [92] P. Vejrum. A generative gridshell form finding tool. Master’s thesis, Faculty of Civil Engineering, Aarhus University, 2013.
- [93] E. Ventsel and T. Krauthammer. *Thin Plates and Shells, Theory, Analysis and Applications*. Marcel Dekker, New York, 2001.
- [94] VTT Technical Research Centre of Finland, certification body (S017, EN 45011) accredited by FINAS. Certificate for structural laminated veneer lumber, 2009.
- [95] N. Watanabe and K. Kawaguchi. The method for judging rigid foldability. In R. J. Lang, editor, *Origami 4: Fourth International Meeting of Origami Science, Mathematics and Education*, pages 165–174. A K Peters, 2009.
- [96] T. Wester. *Structural Order in Space: the plate-lattice dualism*. Smed Grafik, Copenhagen, 1984.
- [97] C. B. Wilby. *Concrete folded plate roofs*. Elsevier, 1998.
- [98] A. Zingoni. *Shell Structures in Civil and Mechanical Engineering: Theory and Closed-form*. Thomas Telford, London, 1997.



Andrea Štitić | MSc

Rue des Terreaux 21 – 1003, Lausanne, Switzerland

✉ andrea.stitic@gmail.com • 🌐 <https://ch.linkedin.com/in/andreastitic>

Education

Phd in Civil Engineering

IBOIS, EPFL

Thesis: Integrally Attached Timber Folded Surface Structures:
Geometrical, Experimental and Numerical Study

Lausanne, Switzerland

1/2014–9/2017

MSc in Structural Engineering

University of Rijeka, Faculty of Civil Engineering, Summa cum Laude

Rijeka, Croatia

9/2010–9/2012

BSc in Civil Engineering

University of Rijeka, Faculty of Civil Engineering

Rijeka, Croatia

9/2007–9/2010

Languages

Croatian: Mother tongue

English: Full professional proficiency

French: Limited working proficiency

Italian: Limited working proficiency

Softwares

- Rhinoceros 3D
- Grasshopper
- Abaqus
- Matlab
- VIC3D
- LaTeX

Honors and awards

- Dean's Award for the best student of the generation 2011/2012, Faculty of Civil Engineering, University of Rijeka, June 2012

- Rector's Award for the best student of the Faculty of Civil Engineering in academic year 2011/2012, University of Rijeka, May 2012
- Fellowship grant for the best final year student in academic year 2011/2012, University of Rijeka, January 2012
- Fellowship grant for the best final year student in academic year 2009/2010, University of Rijeka, January 2010

Journal Publications

- Stitic A., Nguyen A.C. and Weinand Y. (2017). "Numerical Modelling of Semi-Rigidity of Timber Folded Surface Structures with Multiple Tab and Slot Joints", manuscript submitted for publication.
- Stitic A., Robeller C. and Weinand Y. (2017). "Experimental Investigation of the Influence of Integral Mechanical Attachments on Structural Behaviour of Timber Folded Surface Structures". In: *Thin-Walled Structures* xx, pp. xx-xx.
- Stitic A. and Weinand Y. (2015). "Timber Folded Plate Structures Topological and Structural Considerations". In: *International Journal of Space Structures* 30.2, pp. 169-177.

Conference Publications

- Stitic A., Robeller C. and Weinand Y. (2015). "Timber Folded Plate Structures- Folded Form Analysis". In: *IABSE Symposium Report*. IABSE Conference Nara, 2015: Elegance in Structures, 1-8(8).
- Robeller C., Stitic A., Mayencourt P. and Weinand Y. (2014). "Interlocking Folded Plate - Integrated Mechanical Attachment for Structural Timber Panels". In: *Advances in Architectural Geometry 2014*. Ed. by P. Block, J. Knippers, N. J. Mitra, and W. Wang. Vol. 4. Springer Verlag, pp. 281-294.

